Aircraft Design 1 – Fall 2025

Assignment 6, Conceptual Design Report

Student Names and USCIDs:
Om Manish Patel, B85143996
Om Prathmesh Patel, C96881852

Instance 1
Hours spent on assignment: 310h

Figure 1.1: CAD modelling of Aircraft

UNIVERSITY OF SOUTH CAROLINA

Aircraft type: General Aviation
Aircraft number: 101

Table 1: Requirements Table

Requirement type	Value	Unit
Maximum Passengers	4	Passengers (including Pilot)
Range	1600	km
Cruise altitude	2440	m
Cruise speed	77.2	m/s
Take-off distance	410	m
Design Empty Weight	925	Kg
Maximum Take-off Weight	1361	Kg

Figure 1.2: CAD modelling of Aircraft Configuration

Table of Contents

1. Introduction

This Conceptual Design Report presents the complete development of our aircraft, a four-seat general aviation aircraft. The report consolidates all major design stages including mission definition, requirements analysis, fuselage and cabin layout, preliminary weight and propulsion sizing, wing and airfoil design, stability and control evaluation, and refined drag estimation — into a unified and coherent conceptual aircraft configuration. Each design decision is supported by comparative data, analytical methods, and performance verification aligned with FAR Part 23 standards. The purpose of this report is to document how the aircraft's configuration evolved through iterative analysis, demonstrate compliance with key requirements and constraints, and present a validated conceptual design ready for future preliminary design development. The resulting aircraft configuration reflects a balanced optimization of aerodynamic efficiency, structural feasibility, stability, manufacturability, and mission performance.

2. Requirements and Fuselage

2.1 Introduction

This presents the initial design process for a medium-size general aviation aircraft meant to carry up to four passengers and one crew/pilot. The objective of this assignment is to define the typical mission profile for this type of aircraft, analyze the given set of requirements, and identify the main drivers that will guide the later stages of the design process including fuselage layout, concept generation, etc. Initially, in chapter 2, the analysis begins with defining the representative mission, which details each phase of the operation from aircraft startup to landing and shutdown. Then, an evaluation of the given requirements like payload, performance, and operation constraints follows. In chapter 3, comparable aircrafts will be used as a reference for every stage in the design process. Chapter 4 entails the concept generation for our aircraft, creating multiple different concept aircrafts that meet the requirements and deciding which design is the most ideal. Then chapter 5 concludes with the creation of the entire fuselage layout of the ideal concept including the cabin, tail, cockpit, wings, etc. Finally, the appendix will showcase the technical drawings, full list of reference aircraft, and concept designs that were used earlier.

2.2 Mission Definition and Analysis of Requirements

This chapter establishes the foundation for the design of the aircraft. It begins by defining a representative mission profile, detailing each segment of a typical flight from boarding through shutdown. By doing so, the operational context of the aircraft is made clear. Following this, the chapter examines the requirements that govern the design, such as payload, propulsion, certification, and performance criteria. These requirements are analyzed to determine their completeness and impact on the design, with assumptions added where data is missing. The combination of mission definition and requirement analysis sets the stage for selecting appropriate reference aircraft and generating initial design concepts.

2.2.1 Mission Profile

The mission of typical general aviation aircraft is to provide regional transport for small groups of passengers using smaller airports with limited or no ground support infrastructure. The aircrafts are designed for short to medium-range flights of 500–900 nm with a cruise speed of around 140-160 knots true airspeed (KTAS). Its mission profile is broken down into the following key segments:

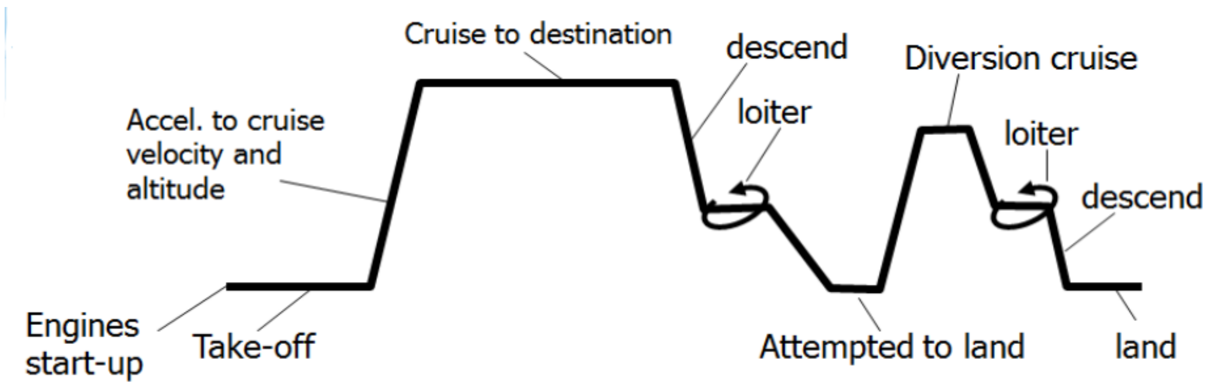

Figure 2.1: Typical Mission Profile for General Aviation Aircraft

1. **Boarding and Startup:**
   Passengers (4) and baggage (~20–25 kg each) are loaded through a cabin side door. The pilot (and optional copilot) performs a preflight inspection (fuel, oil, control surfaces, tires, and avionics). The engine is started using onboard systems, with no external power required, ensuring independence at small regional airports. Avionics, navigation, and communication systems are powered on and checked before taxi.

2. **Taxi**
   The aircraft taxis for approximately 10-15 minutes to the active runaway. During taxi, brakes, nosewheel steering, and flight controls are tested. At the run-up area, the engine is advanced to ~1,700 RPM to check magnetos, propeller governor, and system responses. Fuel reserves are planned to cover this phase, so extended ground delays do not affect flight safety.

3. **Take-off**
   At full power, the aircraft accelerates along the runway, rotates at ~65 KIAS, and clears a 50 ft obstacle within the 1,340 ft takeoff distance at MTOW. A 10 degrees flap setting may be used for short-field performance, allowing operation from regional runways between 800-1,200 meters. Engine and flight instruments are monitored throughout take-off to confirm maximum performance.

4. **Climb**
   After liftoff, the aircraft climbs at 80-90 KIAS towards the selected cruise altitude, typically 8,000-12,000 ft. Power is reduced from takeoff to climb settings (~75%) to protect the engine and optimize fuel use. Avionics are configured for enroute navigation, and engine parameters are monitored for temperature and pressure stability.

5. **Cruise**
At cruise altitude, the aircraft maintains 150 KTAS at fuel-efficient power settings. The expected range is ~865 nm with reserves, providing 3-5 hours of endurance. Fuel mixture is leaned for efficiency, with consumption averaging 9-12 gallons per hour. The cabin accommodates four passengers comfortably for medium-range flights, while navigation is managed via GPS and VOR systems.

6. **Descent**
The descent is initiated in advance of the destination airport, typically 80–100 nm away, depending on altitude. Power is gradually reduced and mixture enriched to prevent shock cooling of the engine. The pilot coordinates with ATC or follows VFR procedures while reviewing approach charts, weather, and runway conditions. This phase ensures the aircraft is stabilized and properly configured for approach.

7. **Loiter**
If conditions at the destination require a delay—such as congestion, weather, or air traffic sequencing—the aircraft enters a holding pattern. Aircraft 101 must sustain loitering for an adequate period while maintaining safe fuel reserves. Loiter flight occurs at reduced power settings and lower altitudes to minimize fuel burn. Cabin comfort must be preserved during this time, and avionics systems support accurate navigation in racetrack or circular holding patterns.

8. **Approach**
Following clearance from ATC, the pilot exits the loiter and aligns for approach. Configuration changes such as extending gear and deploying initial flap settings are made. Speeds are reduced to ensure stable approach profiles, and avionics systems such as GPS and ILS (if available) aid in precise alignment with the runway centerline.

9. **Missed Approach/Diversion**
If a landing cannot be completed, the aircraft executes a go-around. Full power is applied, climb attitude established, and flaps are retracted in stages. Reserve fuel ensures capability to divert to an alternate airport up to ~100 nm away and maintain 30 minutes of loiter, meeting FAA reserve requirements. This provides operational flexibility under poor weather or traffic delays.

10. **Landing**
The aircraft deploys flaps as needed and establishes final approach at 65-70 KIAS. Touchdown occurs within the specified landing performance, with landing rolls typically between 1,300-1,600 ft depending on conditions. Safe braking margins are maintained even on wet or contaminated runways. After landing, flaps are retracted, and braking is applied to bring the aircraft to taxi speed.

11. **Taxi-in and Shutdown**
After exiting the runaway, the aircraft taxis to parking. Systems and brakes are monitored during taxi-in. The engine idles briefly to cool before shutdown. Avionics and electrical systems are switched off in sequence, and fuel and ignition systems are secured. Passengers disembark safely, baggage is unloaded, and the aircraft is tied down or stored in a hanger.

2.2.2 Requirement Analysis

This section looks at the main requirements for the aircraft and how they affect the design. Each part, such as payload, engine choice, certification, and performance, is reviewed to see if the given values are reasonable and complete. Assumptions are added where needed, and the most important requirements are identified since they will guide the rest of the design process.

2.2.2.1 Payload Analysis

The aircraft is designed to carry a maximum of four passengers plus one pilot. Using the given weights, the maximum take-off weight (MTOW) is 3,000 lbs, and the design empty weight is 2,040 lbs. This leaves a useful load of about 960 lbs. Assuming an average passenger weight of 175 lbs and baggage allowance of 40 lbs each, the total payload for four passengers is ~860 lbs. This leaves only a small margin for fuel when all seats are occupied, meaning payload and range will trade off depending on the mission.

To compare, similar General Aviation aircraft such as the Cessna 182 Skylane, Cirrus SR20, and Diamond DA40 NG have useful loads between 900-1,100 lbs, showing that the chosen configuration is reasonable. Table 2.1 summarizes the payload capacities and cabin arrangements.

Reference Data	Cessna 182 Skylane	Cirrus SR20	Diamond DA40 NG	Aircraft 101 (our aircraft)
Max Payload (lbs)	1,100	1,025	904	960
# of Passengers	4	5	4	4
# of Crew	1	1	1	1
Baggage Volume (ft^3)	~18	~17	~15	~15

Table 2.1 Reference Payload Data

This comparison shows that the design payload capacity is realistic and in line with existing General Aviation aircraft.

2.2.2.2 Propulsion Analysis

The cruise requirement is 150 KTAS at 8,000 ft. To meet this, a single front-mounted piston engine in the 200-230 horsepower range with a constant-speed propeller is suitable. Comparable aircraft (Cessna 182, Cirrus SR20, Diamond DA40) all use engines in this class. A constant-speed propeller is preferred over a fixed-pitch propeller since it allows the pilot to optimize performance during take-off, climb, and cruise, improving both fuel efficiency and climb rate. A constant-speed propeller adjusts the blades' pitch angle to maintain a constant RPM. A fixed-pitch propeller is simpler and less efficient, but it’s more cost-effective and has a blade angle that cannot be adjusted during flight. At cruise, fuel consumption is expected to be around 9-12 gallons per hour, giving an endurance of 3-5 hours depending on payload and reserves. The selected propulsion system must also allow for safe climb performance at MTOW, ensuring obstacle clearance after take-off. Reliability and maintainability are key considerations since this aircraft will operate from smaller airports with limited support. Alternate propulsion technologies (diesel piston or hybrid-electric) could be explored for efficiency or sustainability, but for initial design, a proven piston engine provides the best balance of performance, cost, and certification feasibility.

Figure 2.2: Cessna 350 Corvalis Constant-Speed Propeller

Figure 2.3: Morane-Saulnier Type G Fixed-Pitch Propeller

2.2.2.3 Certification Analysis

With a maximum take-off weight of 3,000 lbs, this aircraft falls under FAR (Federal Aviation Regulations) Part 23 – Normal Category Airplanes, which regulates small aircraft under 12,500 lbs. These standards cover flight performance (stall speeds, controllability), structural design (strength and fatigue), and occupant safety (seat crash loads, restraints, emergency exits). For a four-seat unpressurized aircraft, certification focuses on ensuring safe stall characteristics, adequate visibility, and compliance with door and baggage access rules. Since the aircraft Is unpressurized and will typically cruise below 12,500 ft, no oxygen systems are required, which simplifies systems design. Still, FAR Part 23 requires that the aircraft be stable and controllable in all normal and emergency conditions, meaning that the fuselage and cockpit layout must support good pilot visibility and quick egress in emergencies. Meeting these standards will be essential for the aircraft to be accepted for private, training, and small commercial use worldwide.

2.2.2.4 Performance Analysis

The target performance values shape much of the design. The aircraft must achieve a range of 865 nm, which will be reached through careful balanced of fuel capacity, engine efficiency, and aerodynamic design. A cruise speed of 150 KTAS at 8,000 ft places the design in line with established General Aviation aircraft while keeping fuel use at manageable levels. The required take-off distance of 1,340 ft at sea level and MTOW ensures the aircraft can operate from smaller regional or grass runways, a key capability for private and training operations. To achieve this, wing loading and flap design must provide sufficient lift at low speeds. The landing distance is expected to be between 1,200-1,400 ft, ensuring safe operations even on shorter airstrips. These requirements directly influence the wing geometry, high-lift devices, and power-to-weight ratio chosen in the design.

2.2.2.5 Additional Requirements

In addition to the stated numbers, several operational factors must be included. The cockpit must provide excellent pilot visibility to allow safe operation in VFR conditions. Cabin layout must provide adequate comfort for flights of up to 4-5 hours, with ergonomic seating and basic environment controls such as ventilation and heating. Baggage space must be sufficient for at least four small suitcases or equivalent cargo, with secure stowage to meet safety standards. The aircraft must be able to start and operate without external ground support equipment, which is important for smaller airports. Regulatory fuel reserves require at least 30 minutes of extra flight at cruise power, and provision for a diversion of ~100 nm must be built into fuel capacity. While noise and vibration are less regulated than in commercial jets, they remain important for comfort and acceptance in General Aviation markets, so design attention to propeller noise and cabin insulation is needed.

2.2.2.6 Driving Requirements

From the analysis, the most critical requirements driving the design are useful load, cruise performance, and short-field capability. The useful load of 960 lbs means payload and fuel must be carefully balanced for each mission, and the cabin must be optimized to make the best use of limited weight allowance. The cruise speed of 150 KTAS ensures competitiveness in the General Aviation market, requiring a clean aerodynamic layout and efficient engine/propeller selection. Finally, the short take-off distance requirement of 1,340 ft makes low-speed handling, wing loading, and flap design central to the configuration. Secondary but important drivers include pilot visibility, comfort on flights for several hours, and compliance with FAR Part 23 standards. These requirements together will strongly influence fuselage dimensions, wing geometry, engine choice, and cabin layout in the later stages of design.

2.3 Reference Aircraft Data Collection

Manufacturer	Type	Crew	Passengers	Range (nm)	Cruise Altitude (ft)	Cruise Speed (KTAS)	Take-off Distance (ft, clear 50 ft)	Design Empty Weight (lbs)	Max. Take-off Weight (lbs)
Cessna	182 Skylane	1	3	930	8000-12000	145-155	1514	2000	3100
Cirrus	SR20	1	4	920	8000-12000	155	1685	2122	3150
Mooney	M20J (201)	1	3	1000	7500-12000	155	1550	1671	2740
Diamond	DA40 NG	1	3	940	>12000	154	1214	1984	2888

Cessna	172 Skyhawk	1	3	650	3000-10000	122	1630	1670	2550
Piper	Archer LX	1	3	520	5000-10000	128	1853	1660	2550
Beechcraft	Bonanza G36	1	5	920	6000-12000	174	1913	2650	3650
Diamond	DA42 Twin Star	1	3	950	6000-12000	156	2267	3131	4407
Piper	PA-28R Arrow	1	3	875	5000-10000	141	1600	1380	2500

Table 3.1: Sample Aircraft Reference Data

2.4 Concept Generation and Selection

2.4.1 Concept Generation

In order to explore possible layouts for the aircraft, three different design concepts were compared. Two of these concepts follow conventional configurations commonly used in general aviation, while the third represents a more unconventional approach. The concepts considered include a high-wing configuration, a low-wing configuration, and a rear-mounted pusher-prop configuration. Each option was evaluated for its advantages and disadvantages in relation to the mission requirements of carrying four passengers, achieving a cruise speed of 150 KTAS at 8,000 ft, maintaining a useful load of approximately 960 lbs, and operating from a 1,340 ft runway.

- **High-Wing Conventional Configuration**
  - Wing Configuration: High-wing, strut-braced
  - Engine Configuration: Nose-mounted piston
  - Tail Plane Configuration: Conventional low-mounted horizontal stabilizer and vertical fin

- **Low-Wing Conventional Configuration**
  - Wing Configuration: Low-wing, cantilever with winglets
  - Engine Configuration: Nose-mounted piston

- Tail Plane Configuration: Conventional T-tail

- **Pusher-Prop Unconventional Configuration**

  - Wing Configuration: Low, swept wings with forward canard
  - Engine Configuration: Twin pusher turboprops on aft of fuselage
  - Tail Plane Configuration: No conventional tailplane; uses canards and twin vertical fins

2.4.1.1 High-Wing Conventional Configuration

This design places the wing above the fuselage and a tractor propeller engine at the nose, similar to the Cessna 182 Skylane. The configuration is well established in general aviation and

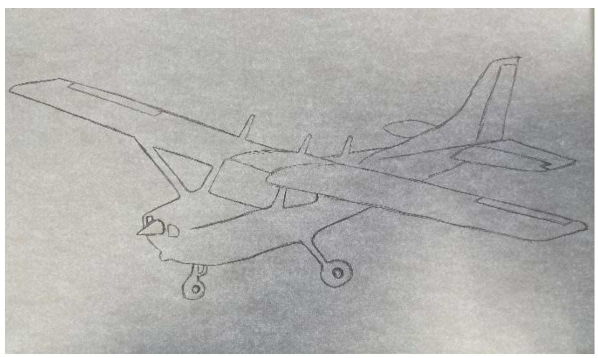

emphasizes stability, safety, and ease of operation. One of the main benefits of the high-wing layout is the strong downward visibility it provides for pilots and passengers, which is especially valuable in VFR operations. The high wing also creates greater clearance between the propeller and wing and the ground, making the aircraft more suitable for grass strips or unpaved runways. In addition, the position of the wing above the fuselage contributes to stable flight characteristics due to the pendulum effect of the fuselage hanging below the wing. Passenger access is also easier since the fuselage sits lower to the ground, reducing the need for steps or ladders.

Figure 4.1.1: Hand-Drawn Picture of Cessna 182 Skylane

However, this configuration also has drawbacks. High-wing aircraft generally experience more drag than low-wing designs, which can reduce cruise efficiency. The placement of the wing spar across the cabin roof may limit interior space and make the cabin feel more cramped compared to a low-wing alternative. Finally, while the high-wing design is reliable at moderate speeds, its aerodynamic efficiency is lower at higher speeds, which may make it difficult for the aircraft to consistently reach the target cruise speed of 150 KTAS.

2.4.1.2 Low-Wing Conventional Configuration

This layout uses a wing mounted below the fuselage with a nose-mounted piston engine and tricycle landing gear. The configuration is comparable to the Cirrus SR20 and Diamond DA40, and is frequently chosen for modern general aviation aircraft where performance and cabin comfort are priorities. A low-wing design provides lower drag and better aerodynamic efficiency at cruise, which helps the aircraft achieve the 150 KTAS requirement. With the wing spar positioned below the cabin floor, the interior is more spacious and comfortable, giving passengers more room. Refuelling and wing inspections are also easier at ground level, and the overall design is proven and widely certified in general aviation, offering strong reference data for continued development.

Despite these benefits, the configuration has some limitations. Downward visibility from the cockpit is restricted compared to a high-wing aircraft, which can be a disadvantage during approaches and landings. Ground clearance is also reduced, meaning the propeller and wingtips are more exposed to potential damage on rough or unpaved fields. Finally, the design requires longer and heavier landing gear to maintain safe propeller clearance, which can increase weight and complexity.

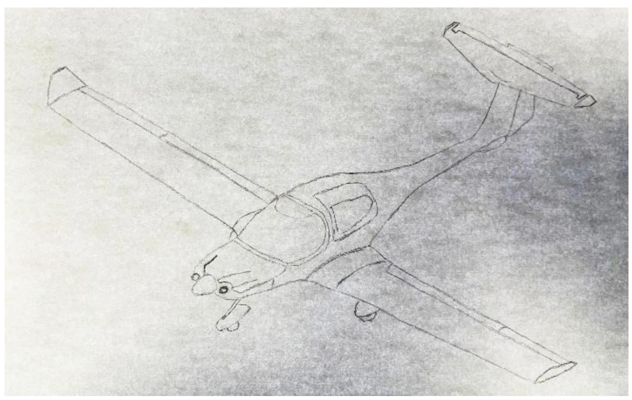

Figure 4.1.2: Hand-Drawn Picture of Diamond DA40

2.4.1.3 Pusher-Prop Unconventional Configuration

This configuration places the engine at the rear of the fuselage with a pusher propeller. Though less common in certified general aviation aircraft, it has been tested in designs such as the Rutan Long-EZ and Beechcraft Starship. The layout offers unique aerodynamic and visibility benefits but also introduces design challenges. One of the main advantages is the unobstructed forward

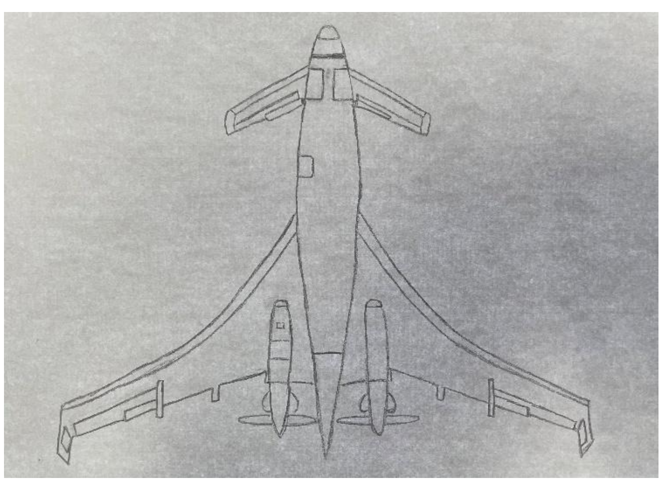

visibility for both the pilot and passengers, since there is no engine or propeller in front of the cockpit. The rear-mounted engine can also make the cabin quieter by placing the main noise source behind the fuselage. In addition, the airflow over the wings remains clean and uninterrupted by propeller wash, which can improve efficiency in some conditions.

Figure 4.1.3: Hand-Drawn Picture of Beechcraft Starship

On the other hand, this configuration faces several disadvantages. Cooling the engine is more difficult when is it mounted at the rear, often requiring additional ducting and design complexity. The tail structure must also be reinforced to support the weight and loads from the engine and propeller, adding structural weight. Passenger safety during boarding is another concern, as the rear-mounted spinning propeller poses a hazard close to the entry area. Finally, because pusher designs are less common in general aviation and rarely certified under FAR Part 23, they face additional certification hurdles compared to more conventional layouts.

2.4.2 Concept Selection

After comparing the three proposed concepts, the low-wing configuration with a T-tail has been selected as the most suitable layout for the design. While the high-wing arrangement provides good stability and visibility, its higher drag and more constrained cabin space make it less efficient for reaching the 150 KTAS cruise target as a 5-seater. The pusher-prop configuration offers unique aerodynamic advantages, but the added complexity, cooling challenges, and certification difficulties make it less practical under FAR Part 23 standards.

The low-wing T-tail design has the best balance between performance, comfort, and feasibility. A low-mounted wing reduces drag and improves cruise efficiency, making it easier to achieve the required cruise speed while keeping fuel consumption within reasonable limits. With the wing spar located right below the cabin floor, interior space can be optimized for a more comfortable five-seat layout. At the same time, the T-tail arrangement ensures that the horizontal stabilizer operates in clean airflow, improving stability during take-off, climb, and landing. This configuration also reduces the risk of elevator effectiveness loss from propeller slipstream or wing turbulence.

A strong reference for this configuration is the Diamond DA40, a proven low-wing general aviation aircraft that shares similar weight, performance, and mission requirements. The DA40 demonstrates how a low-wing aircraft with modern aerodynamic design can provide efficiency, passenger comfort, and performance. Using this as a benchmark helps validate the feasibility of our concept and provides useful performance data for comparison.

2.5 Study and Generation of Complete Fuselage Layout

2.5.1 Cabin Configuration

2.5.1.1 Cabin Cross-Section Development

The cabin cross section is based on seating five people: two in the front (pilot and one passenger) and three in the back on a single bench. This layout makes good use of the available space while keeping the fuselage compact.

To fit three passengers across the rear row, the cabin width is set about 48-50 inches, slightly wider than typical four-seat general aviation aircraft. Each seat is around 17-18 inches wide, which is standard for light aircraft. Cabin height is about 50 inches, giving enough headroom for most people. The fuselage walls are about 1.5-2 inches thick to allow for structure and interior panels.

The fuselage cross section is nearly circular, which is simple to build and provides good strength. The wing spar runs below the cabin floor to support the wings without taking away much passenger space. A baggage compartment of about 15 ft^3 is located behind the rear bench, similar to other general aviation aircraft in this class. This cross-section design provides space for five people with enough comfort for flights for several hours while staying light and efficient.

2.5.1.2 Cabin Layout Measurements

The cabin dimensions were sized to seat five occupants in a 2+3 layout. Reference data from the Cessna 182 Skylane, Cirrus SR20, and Diamond DA40 NG was used to guide the selected values. Table 5.1 shows the main cross-section measurements for the reference aircraft compared to our design.

Measurement	Cessna 182 Skylane	Cirrus SR20	Diamond DA40	Our Aircraft
Cabin Width (m)	1.07	1.24	1.12	1.27
Cabin Height (m)	1.22	1.27	1.24	1.27
Seat Width (m)	0.43	0.46	0.43	0.44
Seat Pitch (m)	0.76	0.79	0.79	0.77
Seats per Row	2	2 (front), 3 (rear)	2	2 (front), 3 (rear)
Baggage Volume (ft^3)	20	17	15	15

Table 5.1: Cabin Cross-Section Measurements

The final cross-section provides slightly more cabin width than most four-seat general aviation aircraft, allowing three passengers to be seated in the rear row. Headroom and seat dimensions remain in line with existing designs to ensure comfort and feasibility. The baggage space of approximately 15 ft^3 is consistent with this class of aircraft.

2.5.1.3 Cabin Entry and Emergency Provisions

For a small general aviation aircraft with seating for five occupants, cabin access and emergency egress must be kept simple, reliable, and complaint with FAR Part 23 requirements. The primary access to the cabin is provided by a single side door located on the left side of the fuselage, adjacent to the front seats. This door is sized to allow both the pilot and passenger to enter easily and provides direct access to the rear bench for the remaining three passengers. A step and handhold will be incorporated below the door sill to assist boarding, which is common practice in aircraft such as the Cessna 182 and Cirrus SR20.

In addition to the main cabin door, an emergency exit is required to meet certification standards. This is planned as a secondary door or window hatch on the opposite side of the fuselage, located near the rear bench. The emergency exit will meet minimum Part 23 requirements, which specify an unobstructed opening of at least 19 inches by 26 inches (Type IV exit). The location ensures that all passengers can evacuate the aircraft in case of an accident or fire, even if the primary door is blocked.

Both the main door and emergency exit will be designed with quick-release latches operable from inside and outside the aircraft. Door placement also considers clearance from the wing and landing gear to ensure accessibility on the ground. Together, these provisions provide safe and efficient entry and exit under normal operations, as well as rapid evacuation under emergency conditions.

2.5.1.4 Interior Layout

The aircraft uses a 2+3 seating arrangement. The pilot and one passenger sit side-by-side in the front row, each with a width of about 0.44 meters. Behind them, a three-seat bench spans the cabin, providing seating across a total cabin width of approximately 1.27 meters. Seat pitch between the rows is about 0.77 meters, which balances comfort with the compact overall fuselage length. A baggage compartment of roughly 15 ft^3 is located directly aft of the bench, giving adequate space for small suitcases or personal items. The floor also carries the wing spar structure, which runs beneath the front row without significantly reducing legroom.

2.5.1.5 Design Flexibility

While the main mission of the aircraft is to carry five occupants in a 2+3 seating arrangement, the cabin layout can be adapted for other uses without major changes to the fuselage. One option is to remove the rear bench seat to create a larger baggage area. This would allow the aircraft to carry bulkier cargo to recreational equipment such as camping gear or tools, while still seating the pilot and one passenger in the front row. Another possible arrangement is a training configuration, where the front passenger seat is replaced with dual controls. This setup would allow the aircraft to be used for flight instruction, with the rear bench still available for student passengers or observers.

These flexible options show that the cabin design can support more than one role, increasing the aircraft's usefulness while maintaining its primary function.

2.5.2 Cockpit/Nose Design

2.5.2.1 Pilot Visibility

Pilot visibility is an important factor for light general aviation aircraft operating under VFR conditions. In our design, the pilot's eye reference point is set at about 1.13 meters above the cabin floor, consistent with comparable aircraft such as the Diamond DA40 and Cessna 182. From this position, the estimated visibility angles were compared with the minimum values required by FAR Part 23.

The over-the-nose angle is approximately 12°, within the acceptable 11°-20° range and giving a clear forward view during taxi, take-off, and landing. To the sides, the overside angle is about 36°, exceeding the 35° minimum, while the grazing angle is around 32°, above the 30° requirement. The upward angle measures 18°, close to the 20° guideline. Together, these values confirm that the cockpit and nose geometry provide adequate all-around visibility for safe operations.

Visibility Angle	Our Aircraft	Acceptable Values (FAR Part 23)
Over-nose	12°	11-20°
Overside	36°	≥35°
Grazing	32°	≥30°
Upward	18°	20°

Table 5.2: Pilot Visibility Angles

2.5.2.2 Nose Design

The nose of the aircraft houses the piston engine and propeller and is shaped to provide a balance between internal space and aerodynamic efficiency. Its design must also allow for adequate cooling airflow and engine mounting while keeping drag low.

To determine the nose length, a fineness ratio is applied. This ratio is the nose length divided by the fuselage diameter. For small general aviation aircraft, typical nose fineness ratios range between 1.8 and 2.2. With our fuselage cross-section diameter set at about 1.27 meters, a ratio of 2.0 gives a nose length of approximately 2.54 meters. This provides sufficient space for the piston engine, mount, and accessories while keeping the external profile streamlined.

The chosen slope of the nose not only improves aerodynamics but also enhances pilot visibility by reducing blind spots over the cowling. The combination of length, slope, and cooling inlets ensures the nose design meets both structural and operational requirements.

2.5.3 Tail Design

The aircraft uses a T-tail configuration to keep the horizontal stabilizer in clean airflow above the propeller slipstream and wing wake. This improves elevator effectiveness during take-off and landing and follows the example of aircraft like the Diamond DA40.

The tail cone length was estimated using a fineness ratio of 2.5, with the fuselage diameter of 1.27 meters. This gives a tail length of about 3.18 meters, which provides enough space for the empennage structure and control linkages. The rotation angle is 14.3°, above the 14° minimum to avoid tail strikes, and the divergence angle is kept at ~17°, below the 24° aerodynamic limit. This design keeps the tail compact, stable, and efficient while meeting handling and clearance requirements for a 3,000 lbs general aviation aircraft.

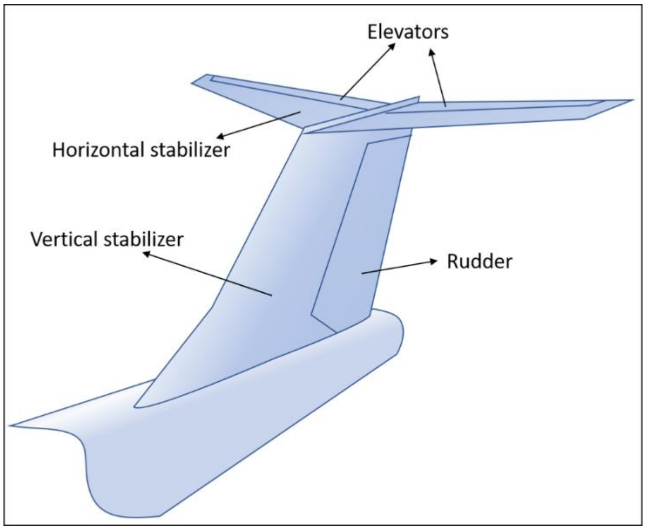

Figure 5.3: T-Tail Configuration

2.5.4 Landing Gear Design

The aircraft uses a tricycle landing gear configuration with a steerable nose wheel and two main gear units under the wings. This setup is common in general aviation and provides stable ground handling, better forward visibility, and reduced risk of ground looping.

The nose gear is placed just behind the engine compartment, while the main gear is located slightly aft of the center of gravity to allow safe rotation on take-off. The geometry provides enough clearance for the propeller and maintains a rotation angle of about 18° to prevent tail strikes.

For simplicity and reliability, the design assumes fixed gear with fairings to reduce drag, similar to other general aviation aircraft in this weight class. The gear legs are sized to handle operations from both paved and grass runways. The tricycle layout provides a strong balance of safety, clearance, and ease of operation for a light 3,000 lbs aircraft.

2.5.5 Tail Plane and Wings

The aircraft uses a low-wing design to improve cruise efficiency and allow the wing spar to pass beneath the cabin floor without limiting passenger space. Wing size and loading are chosen to support a 3,000 lbs MTOW while meeting the 1,340 ft take-off requirement. A slight sweep of about 15° balances performance and manufacturability.
A T-tail configuration was selected for the horizontal stabilizer to keep it clear of wing turbulence and propeller slipstream, improving elevator effectiveness. The vertical stabilizer provides directional stability and supports the T-tail. Together, the wing and tailplane provide stable handling, efficient cruise, and compliance with FAR Part 23 stability standards.

3 Preliminary and Propulsion Sizing

3.1 Introduction

This presents the second stage in the conceptual design of a four-seat general aviation aircraft developed in the first stage. The focus here is on preliminary sizing and propulsion system selection. The first part of the stage establishes an estimate of the maximum take-off weight by combining payload, fuel, and operational empty weight. The methodology follows a standard fuel fraction analysis, supported by statistical relationships derived from reference aircraft. Based on this weight estimate, a weight-to-power versus wing-loading (W/P–W/S) diagram will be constructed to identify an optimum design point. The second part of the stage examines propulsion options for the aircraft. Several piston engines will be compared in terms of power, weight, fuel efficiency, and suitability for the mission requirements. The most suitable engine will then be scaled, checked against the sizing results, and evaluated for improvements in fuel consumption.

3.2 **Estimation of Take-off Weight**

The maximum take-off weight (W_{TO}) consists of three contributions: payload weight (W_{PL}), fuel weight (W_F), and operational empty weight (W_{OE}). This relationship is expressed in Eq. (2.1).

$$W_{TO} = W_{PL} + W_F + W_{OE} \quad Eq.(2.1)$$

3.2.1 Payload

The payload includes one pilot and three passengers. Each occupant is assumed to have a body weight of 75 kg with an additional 15 kg of baggage allowance. The payload weight is therefore:

$$W_{PL} = (75 + 15)kg \times 4 = 360 \text{ kg}$$
$$W_{PL} = m_{PL}g = 360 \times 9.81 = 3531.6 \text{ N}$$

This corresponds to approximately 792 lb. The breakdown of the payload calculation is shown in Table 2.1.

Item	Mass (kg)	Quantity	Weight (N)	Total Weight (N)
Occupant	75	4	736	2943
Baggage allowance	15	4	147	589
Total Payload	90	4	883	3532

Table 2.1: Payload Calculation

3.2.2 Fuel

3.2.2.1 Normal Flight Fraction

The normal flight fuel fraction accounts for engine start, taxi, take-off, climb, descent, and landing. Typical values for small piston-engine aircraft are given in Table 2.2.

Flight Phase	Fraction
Engine start and warm-up	0.995
Taxi	0.997
Take-off	0.998
Climb	0.992
Descent	0.993
Landing, taxi, shutdown	0.993

Table 2.2: Normal Flight Fuel Fractions

Multiplying these yields a total normal flight fraction of 0.968, meaning the aircraft retains 96.8% of its weight after normal operations.

In addition to these normal phases, extra fuel is allocated for one go-around, and a 30-minute reserve loiter at cruise power. These segments typically require approximately 1% of the total take-off weight, which corresponds to a remaining weight fraction of 0.99. Incorporating this allowance gives the adjusted normal flight fuel fraction:

$$M_{ff,normal} = 0.968 \times 0.99 = 0.958$$

This adjusted value is used in subsequent mission fuel-fraction calculations to ensure sufficient fuel for diversion, holding, and missed-approach operations.

3.2.2.2 Cruise Fraction

The cruise fuel fraction is determined using the Breguet range equation for propeller-driven aircraft:

$$\frac{W_i}{W_{i+1}} = \exp\left(-\frac{Rgc_p}{\eta_p\left(\frac{L}{D}\right)}\right) \quad Eq.(2.2)$$

where the mission distance is 1600 km (1.6×10^6 m), the gravitational acceleration is 9.81 m/s², the specific fuel consumption is $c_p = 8.448 \times 10^{-8}$ kg/J , and the lift-to-drag ratio in cruise is taken as 10 with an efficiency of 0.8. Substitution of these values gives a cruise fuel fraction of 0.847.

3.2.2.3 Loiter Fraction

The loiter fraction is evaluated using the endurance form of the Breguet equation:

$$\frac{W_2}{W_1} = \exp\left(-\frac{EVgc_p}{\eta_p\left(\frac{L}{D}\right)}\right) \quad Eq.(2.3)$$

with a loiter time of 1800 s (0.5 h), a specific fuel consumption of 8.448 x 10^{-8} kg/J, and a lift-to-drag ratio of 12 with efficiency of 0.7 and speed generally slower than the speed for max range, therefore about 70 m/s. Substitution gives a loiter fuel fraction of 0.988.

3.2.2.4 Total Fuel

The overall mission fuel fraction is obtained by multiplying the results of the previous subsections:

$$M_{ff,total} = M_{ff,normal} \times M_{ff,cruise} \times M_{ff,loiter} \quad Eq. (2.4)$$

$$M_{ff,total} = 0.958 \times 0.847 \times 0.988 = 0.802$$

The fuel weight fraction therefore becomes

$$\frac{W_F}{W_{TO}} = 1 - M_{ff,total} \quad Eq. (2.5)$$

$$\frac{W_F}{W_{TO}} = 1 - 0.802 = 0.198$$

This means that approximately 19.8% of the maximum ramp weight is allocated to fuel. Because engine start, taxi, and run-up consume a small amount of fuel before take-off, the maximum take-off weight (MTOW) at brake release is slightly lower, typically by about 1-2% of the ramp weight.

3.2.3 Operational Empty Weight

Reference aircraft including the Cessna 172, Mooney M20J, Diamond DA40, Cessna 182, Cirrus SR20, Beechcraft Bonanza G36, etc. were used to establish the relationship between empty weight and maximum take-off weight. A regression of the data indicates an average empty weight fraction of about 0.5791. From Figure 2.2 below the formula for operational empty weight as a function of take-off weight is:

$$W_{OE} = 0.5791 \times W_{TO} + 503.47 \quad Eq. (2.6)$$

The regression trend is also shown in Figure 2.2, where blue points represent the general aviation aircraft, while the dashed line is the linear regression fit through those data.

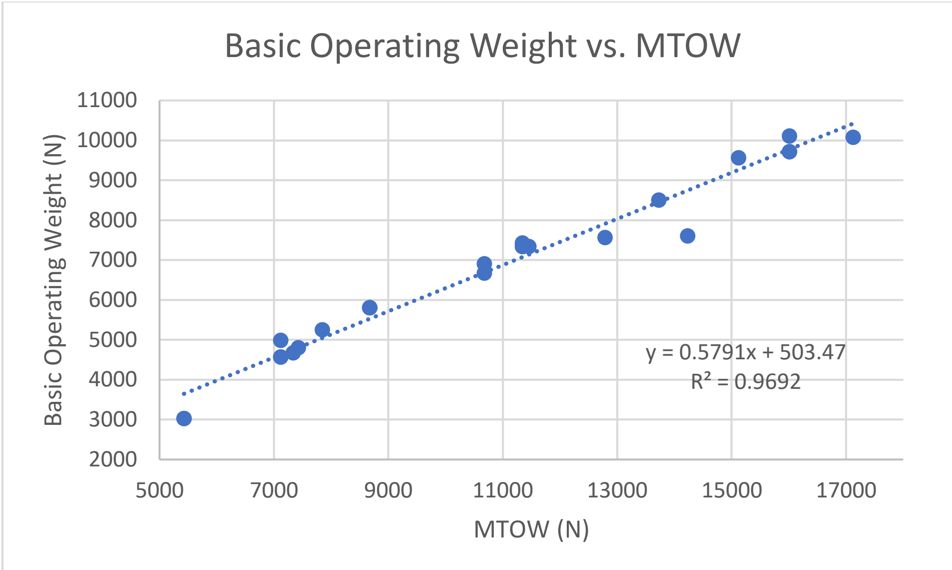

Figure 2.2: Basic Operating Weight vs MTOW for GA aircraft

3.2.4 Preliminary Take-off Weight Estimate

The three contributions are now combined, including the effects of trapped fuel and oil. The complete weight balance is given by

$$W_{TO} = W_{PL} + W_F + W_{OE} + W_{TFO}$$

Substituting the regression from Figure 2.2, $W_{OE} = 0.579W_{TO} + 503.47$, the fuel-weight fraction $W_F = 0.199W_{TO}$, and the trapped fuel and oil term $W_{TFO} = 0.005W_{TO}$, yields

$$W_{TO} = W_{PL} + 0.198W_{TO} + 0.579W_{TO} + 503.47 + 0.005W_{TO}$$

which simplifies to

$$W_{TO}(1 - 0.782) = 3532 + 503.47$$

For the full-payload case of $W_{PL} = 3532\ N$,

$$W_{TO} = \frac{3532 + 503.47}{0.218} = 18511.3\ N = 1887\ kg$$

This corresponds to approximately 18,500 N, which greatly exceeds the design maximum take-off weight of 1361 kg (~13354 N). The implication is that the full payload and the full range cannot be achieved simultaneously. A payload–range trade analysis is therefore necessary. The full payload can be carried only at a reduced range, while achieving the full design range requires a reduction in payload or MTOW.

To maintain the full four-occupant payload without exceeding the design MTOW, the range must be reduced until the mass-balance equation satisfies $W_{TO} = 1361$ kg. The required range is determined by iterating the Breguet range equation for a propeller-driven aircraft,

$$R = \frac{\eta_p}{gc_p}\frac{L}{D}\ln(\frac{W_i}{W_f}) \qquad Eq. (2.7)$$

where $\frac{W_i}{W_f} = \frac{1}{M_{ff,cruise}}$.

For a fixed payload and MTOW, $W_F = W_{TO} - (W_{PL} + W_{OE} + W_{TFO})$, which gives the available fuel mass and hence $\frac{W_i}{W_f}$. By substituting the known parameters ($\eta_p = 0.8, \frac{L}{D} = 10, c_p = 8.448 * 10^{-8}$ kg/J), the new cruise fuel fraction corresponding to $W_{TO} = 1361$ kg and $W_{PL} = 360$ kg yields a range of approximately 630 km.

Since this range is not a reasonable balance between payload and range, to maintain the design take-off weight of 1361 kg while improving range performance, the payload was reduced from four to three occupants. Each occupant is assumed to weigh 90 kg, giving a new payload of 270 kg. The operational empty weight was updated using the refined regression

$$W_{OE} = 0.5791\, W_{TO} + 503.47\, N$$

with $W_{TO} = 13{,}345$ N, which yields $W_{OE} = 8{,}235$ N or 839.5 kg. Accounting for a trapped-fuel allowance of 0.5 % of MTOW, the available fuel increases from approximately 155 kg in the four-seat configuration to 245 kg in the three-seat configuration. Applying the same propeller Breguet parameter, the mission fractions used in the previous analysis gives a realistic cruise range of about 634 km for the full four-passenger case and 1,382 km for the three-passenger case. This demonstrates that by reducing the payload to three occupants while keeping the MTOW constant, the aircraft can achieve much closer to the original design-range objective without exceeding the structural or performance limits.

3.3 Determining the W/P – W/S Diagram

To identify the design point, the aircraft must satisfy performance requirements for stall speed, take-off, landing, and climb. These constraints are combined on a weight-to-power versus wing loading (W/P–W/S) diagram. Because our design uses a piston–propeller engine, the thrust-to-weight relations developed in the previous equations are converted into power loading using the propeller power–thrust relation.

For a propeller, the shaft power, thrust and speed are related by $T = \eta_p P/V$, where η_p is propeller efficiency and V is the representative flight speed for the constraint under consideration. Rearranging gives

$$\frac{W}{P} = \frac{\eta_p}{V}\frac{1}{(\frac{T}{W})}.$$

This form allows any T/W constraint (e.g., the climb thrust requirement $T/W = C_D/C_L + c$) to be expressed consistently in W/P–W/S space. For example, substituting the drag-based climb expression yields

$$\frac{W}{P} = \frac{\eta_p}{V}\left(\frac{C_D}{C_L} + c\right)^{-1} = \frac{\eta_p}{V}\left(\frac{C_{D0}}{C_L} + \frac{C_L}{\pi Ae} + c\right)^{-1},$$

which is the relation plotted as the climb constraint on the W/P–W/S diagram (with V chosen appropriate to climb speed, η_p set for climb, and C_{D0}, e from Section 3.4). Likewise, take-off and landing T/W constraints are converted using the same formula but with the relevant representative speeds and propeller efficiencies for those phases.

3.3.1 Stall Sizing

The stall-speed requirement makes sure that the aircraft can safely operate within certification standards. The maximum wing loading is found using the lift equation at the stall condition:

$$\frac{W}{S} = \frac{1}{2}\rho V_s^2 C_{L_{max}} \qquad Eq. (3.1)$$

where ρ is air density (sea level), V_s is the stall speed, and $C_{L,max}$ is the maximum lift coefficient in the relevant configuration (clean for cruise/clean sizing, take-off/landing for altered-flaps cases).

Based on comparable four-seat GA aircraft (e.g. Cessna 182, Mooney M20J, Cirrus SR20), typical values of stall speed and maximum lift coefficient are:

- Clean Configuration: $V_s \approx 29$ m/s, $C_{L,max} \approx 1.7$
  - $(W/S)_{clean} \approx 876$ N/m^2
- Take-off Configuration: $V_s \approx 28$ m/s, $C_{L,max} \approx 2.1$
  - $(W/S)_{TO} \approx 1008$ N/m^2
- Landing Configuration: $V_s \approx 25$ m/s, $C_{L,max} \approx 2.5$
  - $(W/S)_{landing} \approx 957$ N/m^2

Taking the average of these cases gives an average stall-limited wing loading of approximately 947 N/m², which is lower than the selected design point of 950 N/m² and satisfies the stall limits.

3.3.2 Take-off Sizing

The take-off requirement is expressed in terms of the take-off parameter (TOP). For propeller aircraft, TOP is defined as

$$TOP = \frac{\left(\frac{W}{S}\right)\left(\frac{W}{P}\right)}{\sigma C_{L_{max,TO}}} \qquad Eq.(3.2)$$

where σ ≈ 1.0 (sea level), $C_{Lmax,TO}$ is the maximum lift coefficient in take-off configuration, and P/W is the power loading used for propeller aircraft. Using a $C_{Lmax,TO}$ of 1.8 and calculated W/S and P/W values, figure 3.1 displays the TOP values of our reference aircraft:

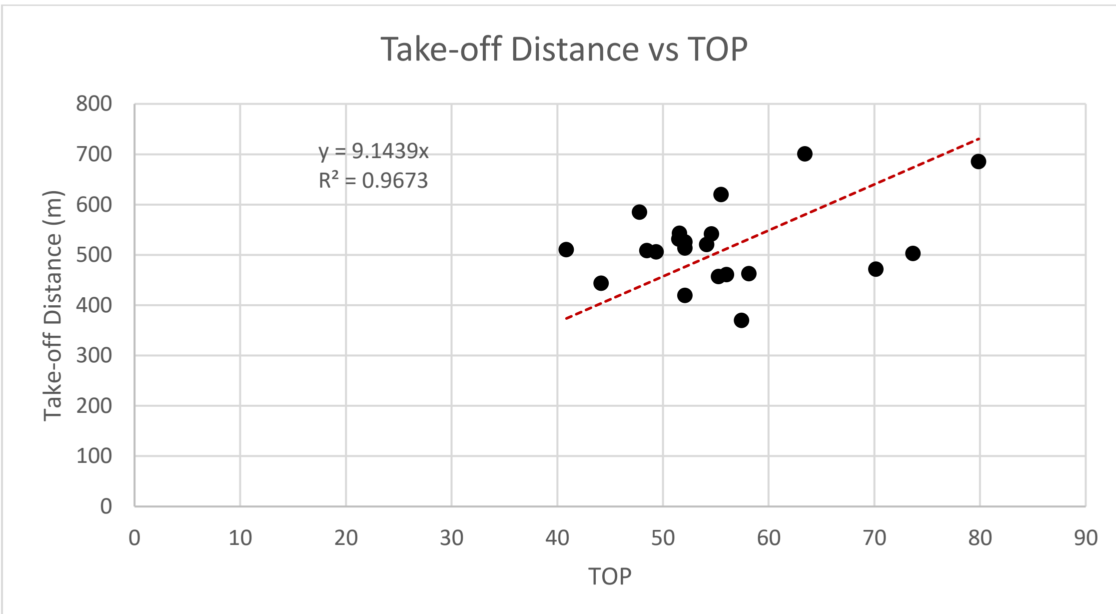

Figure 3.1: Reference Aircraft Take-Off Parameter vs Take-Off Distance

The TOP values of the reference aircraft were compared against their published take-off distances to clear a 50 ft obstacle. A linear regression fit was applied to the dataset, producing the trend line shown above. This correlation provides a practical method to translate the design TOP into a required take-off distance. Using the regression equation, our calculated take-off parameter is approximately 45. This result confirms that the selected design parameters fall within the feasible region defined by comparable general aviation aircraft, and the derived regression will be used as part of the overall W/P–W/S sizing diagram with varying $C_{Lmax,TO}$ values of 1.6, 1.8, 2.0, and 2.2.

3.3.3 Landing Sizing

Landing distance can be related to stall speed by

$$S_L = 0.592V_s^2 \qquad Eq.(3.3)$$

where S_L is the ground distance required to clear a 50 ft (15.24 m) obstacle and V_s is the stall speed in m/s.

For a required landing distance of 410 m, the corresponding stall speed is

$$V_s = \sqrt{\frac{S_L}{0.5915}} = \sqrt{\frac{410}{0.5915}} \approx 26.3 \text{ m/s}.$$

Using Eq. (3.1) with $C_{L_{\max,L}} = 2.6$ (typical for flapped general-aviation wings) and sea-level air density $\rho = 1.225 \text{ kg/m}^3$, the maximum allowable wing loading is

$$\frac{W}{S} = \frac{C_{L,max,land}\rho V_s^2}{2} = \frac{(2.6)(1.225)26.3^2}{2} = 1{,}102 \ \frac{\text{N}}{\text{m}^2}.$$

This results in a vertical constraint line at W/S ≈ 1102 N/m^2 on the W/P – W/S diagram; all feasible design points must lie to the left of this line to meet the landing/stall requirements. The C_{Lmax} will vary using the values of 2.0, 2.2, 2.4, and 2.6 and displayed on the W/P – W/S diagram.

3.3.4 Drag Polar

The drag polar is modeled as

$$C_D = C_{D0} + \frac{C_L^2}{\pi A e} \qquad Eq. (3.4)$$

where C_{D0} is the zero-lift drag coefficient, A is the wing aspect ratio, and e is the Oswald efficiency factor. The first term accounts for parasite drag from the airframe (fuselage, wing, tail, and exposed surfaces) that exists even when no lift is produced. The second term captures induced drag, which grows with the square of lift and is inversely related to both aspect ratio and efficiency. A higher aspect ratio or efficiency factor reduces induced drag and flattens the drag polar.

Separate polars were constructed for the key operating configurations of the aircraft: clean (cruise), take-off, approach, and landing. Each configuration was assigned representative values based on published data for comparable four-seat general aviation aircraft. Values were selected from Raymer (2012) and Torenbeek (1982), and compared with manufacturer data for the Cessna 172, Cirrus SR20, and Mooney M20J. Typical ranges for light GA aircraft are:

- Clean: $C_{D0} = 0.025$–$0.035, e = 0.80 - 0.85$
- Take-off: $C_{D0} = 0.035$–$0.045, e = 0.75 - 0.80$
- Approach: $C_{D0} = 0.050$–$0.065, e = 0.72 - 0.75$
- Landing: $C_{D0} = 0.075$–$0.081, e = 0.68 - 0.72$

The adopted coefficients C_{D0} = 0.030, 0.040, 0.060, and 0.08 together with e = 0.80, 0.75, 0.73, and 0.70 fall near the midpoint of the published ranges and are consistent with values for modern low-wing, single-engine piston aircraft.

The approach configuration represents flight during the final descent to landing with partial flap deflection (≈ 20-25°) and landing gear extended, providing additional lift and moderate drag for a stabilized approach path. The landing configuration corresponds to the condition immediately prior to touchdown, with full flap deflection (≈ 30-40°) and gear extended.

This produces the highest parasite drag and the lowest Oswald efficiency, due to flow separation and strong interference effects around the flaps and landing gear. Consequently, C_{D0} and $k = \frac{1}{\pi A e}$ are largest in landing configuration.

To evaluate sensitivity to wing geometry, aspect ratio was varied across A = 3, 6, 9, 12, and 15. For each combination of configuration and aspect ratio, the induced drag term was calculated, resulting in a total of 20 drag polars created in a plot of C_L vs C_D, shown as figure 3.2.

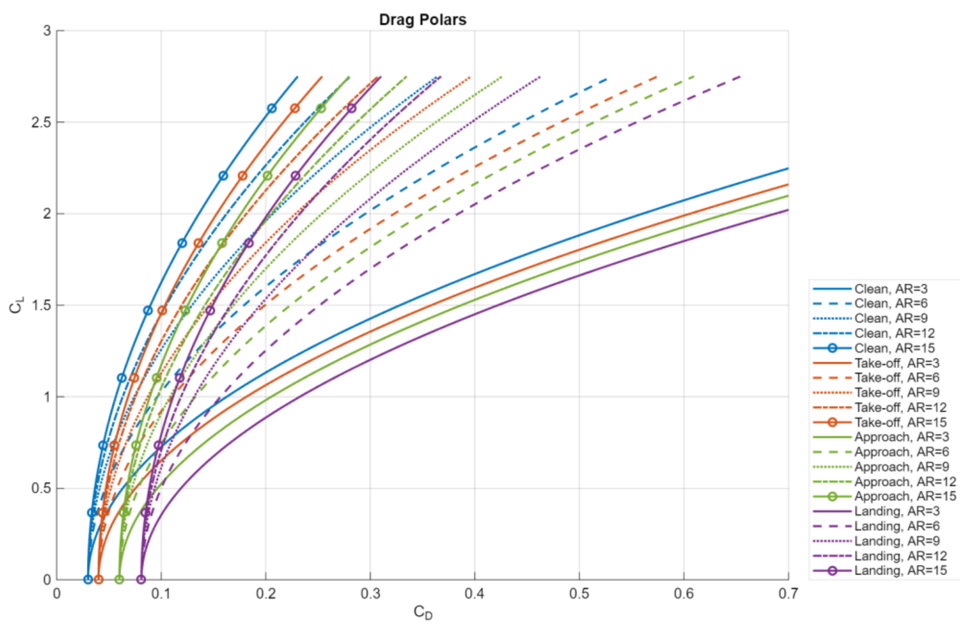

Figure 3.2: Drag Polars for Configurations of Various Aspect Ratios of Different Flight Phases

The plot illustrates several important trends. As expected, the clean configuration consistently shows the lowest drag, while the landing configuration lies highest due to large flap deflections and gear. Increasing aspect ratio systematically reduces the induced drag slope, shifting the curves leftward and producing higher lift-to-drag ratios.

This improvement more than doubles the maximum L/D, increasing it from roughly 7.6 at AR = 3 to about 16 at AR = 15. Similar patterns are observed for the other three configurations, although the higher C_{D0} values for take-off, approach, and landing result in greater overall drag and lower efficiency.

3.3.5 Climb Performance

Climb performance ensures that the aircraft has sufficient power not only for take-off but also to maintain an adequate rate of climb after departure. The requirement is typically expressed in terms of power loading (W/P), since for propeller-driven aircraft thrust is produced from engine shaft power through propeller efficiency η_p.

Using the drag polar from Section 3.4,

$$C_D = C_{D0} + \frac{C_L^2}{\pi A e}$$

the power-loading relation can be written as

$$\frac{W}{P_R} = \frac{\eta_p}{c + \sqrt{\frac{W}{S}} \times \sqrt{\frac{2}{\rho}} \times \frac{1}{1.345 \times \frac{(Ae)^{3/4}}{{C_{D_0}}^{1/4}}}} \qquad Eq. (3.5)$$

where $c = V_v/V$ is the climb rate. This form is used to plot the climb performance constraint on the W/P–W/S diagram.

For this analysis, the clean-configuration aerodynamic coefficients from Section 3.4 are applied:

$$C_{D0} = 0.030, \qquad e = 0.70$$

and the climb rate of 4 m/s was used in accordance to FAR 23.65 and representative of similar reference aircraft. Propeller efficiency and representative climb speed are selected per the performance case when plotting the curves.

To evaluate sensitivity to wing geometry, aspect ratios $A = 6,\ 9,\ 12,\ 15$ were examined. The resulting climb curves for these aspect ratios are plotted in the $W/P–W/S$ diagram; the design point must lie under these curves to satisfy climb performance requirements.

3.3.6 Climb Gradient

The climb gradient requirement is imposed by certification regulations and ensures that the aircraft can maintain a safe climb profile after take-off. According to FAA regulation 14 CFR 23.65, single-engine airplanes must be able to maintain a positive climb gradient after take-off, typically around 6.25%, at a speed not less than 1.2 times the stall speed in take-off configuration (approximately 33.6 m/s), we will use 36 m/s for a margin.

For propeller-driven aircraft, it is more convenient to express the climb requirement in terms of power loading rather than thrust loading, since the propeller converts engine shaft power into thrust with efficiency η_p. Using the drag polar

$$C_D = C_{D0} + \frac{C_L^2}{\pi A e},$$

the power-loading relation becomes

$$\frac{W}{P_{br}} = \frac{\eta_p}{\sqrt{\frac{W}{S}}\left(\frac{c}{V} + \frac{C_D}{C_L}\right)\sqrt{\frac{2}{\rho}\frac{1}{C_L}}}, \qquad Eq. (3.6)$$

where $\frac{c}{V}$ is the climb gradient. Substituting in the definitions of the coefficients of lift and drag, we get:

$$\frac{W}{P_{br}} = \frac{\eta_p}{\sqrt{\frac{W}{S}}\left(\frac{c}{V} + \frac{4C_{D_0}}{\sqrt{3C_{D_0}\pi A e}}\right)\sqrt{\frac{2}{\rho} \times \frac{1}{\sqrt{3C_{D_0}\pi A e}}}}, \qquad Eq. (3.6)$$

At the condition of maximum climb gradient, the optimum lift coefficient is

$$C_{L,opt} = \sqrt{C_{D0}\pi A e},$$

and substituting into the equation below gives the minimum power loading required for climb:

$$\left(\frac{W}{P}\right)_{min} = \frac{2V}{\eta_p}\sqrt{\frac{C_{D0}}{\pi A e}}. \qquad Eq. (3.7)$$

For this analysis, the clean-configuration coefficients from Section 3.4 are used:

$$C_{D0} = 0.030, \qquad e = 0.80$$

The climb gradient is taken as *c/V* = 0.10 (10%), resulting in almost double the 6.25% minimum required by FAR 23.65 and typical of comparable general-aviation aircraft such as the Cessna 172 and Cirrus SR20. Propeller efficiency is assumed to be $\eta_p = 0.80$.

This requirement appears as horizontal lines in the W/P – W/S diagram and varies with AR as 6, 9, 12, and 15 and, as expected, this requirement has little effect on the final design point but is included for completeness to satisfy FAA regulations.

3.3.7 W/P – W/S Diagram

The constraints from stall, take-off, landing, cruise and climb are combined in the W/P–W/S diagram (Appendix 1). The stall and landing constraints appear as vertical lines that limit the allowable wing loading (W/S). The take-off and power-required constraints appear as downward-sloping families in W/P–W/S space (since required power-per-weight decreases with increasing wing area for a fixed TOP or drag-based requirement), while the climb-gradient constraints appear approximately as horizontal lines for the specified aspect ratios.

From the optimal design region of this diagram, we selected

$$\frac{W}{P} = 0.093\ \frac{\mathrm{N}}{\mathrm{W}}, \qquad \frac{W}{S} = 950\ \frac{N}{m^2}$$

where W/P is the weight-to-shaft-power ratio (N per W) and W/S is the wing loading. Using $W = m_{TO}g$ with $m_{TO} = 1{,}361$ kg gives

$$W = 1{,}361 \times 9.81 \approx 13{,}354\ \mathrm{N},$$

so the selected wing area is

$$S = \frac{W}{(W/S)} = \frac{13{,}354}{950} \approx\ 14.06\ \mathrm{m}^2.$$

The corresponding shaft power requirement is

$$P_{\mathrm{shaft}} = \frac{W}{(W/P)} = \frac{13{,}354}{0.093} \approx\ 143{,}600\ \mathrm{W} \approx\ 144\ \mathrm{kW},$$

which is approximately 193 hp. This shaft-power figure is the required power at the propeller shaft; the installed engine rating and propeller/gearbox matching should include the usual margins and efficiency assumptions (propeller efficiency η_p and any installation losses).

The selected design point lies within the feasible envelope defined by the plotted constraints and is consistent with the mission and performance targets. The W/P–W/S diagram therefore forms the basis for the subsequent propulsion and weight-budget decisions.

3.4 Propulsion Design

With the preliminary sizing completed, the next step is to establish the power requirements for the aircraft. For piston-propeller aircraft, thrust requirements are most conveniently expressed in terms of shaft power, with the propeller efficiency η_p relating the engine power to the effective thrust power.

3.4.1 Take-off Power Requirement

From the W/P sizing in Section 3, a thrust-to-weight ratio of approximately 0.21 was required to satisfy climb performance. Using the design take-off weight of W = 13,342 N, the corresponding thrust is

$$T_{TO} = \left(\frac{T}{W}\right) \times W$$

$$T_{TO} = 0.21 \times 13{,}342 = 2{,}802\ N \qquad Eq.\ (4.1)$$

In this stage, T/W constraints are converted to W/P using

$$\frac{W}{P} = \frac{\eta_p}{V}\left(\frac{W}{T}\right)$$

where η_p is the propeller efficiency and V is the representative take-off speed.

Accordingly, the shaft power required for take-off is

$$P_{TO} = \frac{T_{TO}V}{\eta_p} \qquad Eq.\ (4.2)$$

Assuming a take-off speed of $V = 40$ m/s and a propeller efficiency of $\eta_p = 0.80$,

$$P_{TO} = \frac{2{,}802 \times 40}{0.80} = 140{,}100\ \mathrm{W} = 140.1\ \mathrm{kW} \approx 188\ \mathrm{hp}.$$

This result indicates that an installed engine rated at approximately 210 hp is sufficient to meet the take-off power requirement. This includes roughly a 10 % margin to account for installation losses, temperature effects, and manufacturing tolerances.

3.4.2 Cruise Power Requirement

The cruise drag calculation is obtained from the drag polar in Section 3.4. At cruise, the aircraft operates with a lift-to-drag ratio of L/D = 11 as assumed in Section 2.2.2.

Using the design parameters

$$W = 13354\ \mathrm{N}, \qquad \mathrm{V} = 77.2\,\frac{\mathrm{m}}{\mathrm{s}}, \qquad \rho = 1.225\,\frac{\mathrm{kg}}{\mathrm{m}^3}, \qquad S = 14.06\ \mathrm{m}^2,$$

The required lift coefficient is

$$C_L = \frac{2W}{\rho V^2 S} \approx 0.260$$

From the relation $C_D = \frac{C_L}{\frac{L}{D}}$, the corresponding cruise drag coefficient is

$$C_D = \frac{0.260}{11} = 0.024$$

Substituting this into the drag equation,

$$D = \frac{1}{2}\rho V^2 S C_D,$$

gives a total drag of approximately 1,231.8 N, which corresponds to a shaft-power requirement of about 95.1 kW (127.5 hp) to maintain level flight.

Accounting for propeller efficiency, the installed engine power required for cruise is

$$P_{cruise} = \frac{95.1}{0.8} = 118.9 \text{ kW} \approx 158 \text{ hp} \quad \text{Eq. (4.3)}$$

Thus, the cruise power requirement of approximately 158 hp is below the take-off power requirement (≈190 hp) from Section 4.1, providing a healthy margin for climb and transient power demands while reinforcing the selection of an engine in the ~210 hp class.

3.4.3 Climb Power Requirement

For a climb rate of 5 m/s at climb speed V_{climb} = 40 m/s, Section 3.5 showed a required thrust-to-weight ratio of 0.21. Using the design weight W = 13,354 N, the thrust needed is again about 2,802 N. The corresponding shaft power is

$$P_{climb} = \frac{T \times V_{climb}}{\eta_p} \quad Eq. (4.4)$$

$$P_{climb} = \frac{2800 \times 40}{0.80} \approx 140{,}000 \text{ W} = 188 \text{ hp}$$

This required climb power of approximately 188 hp closely matches the take-off power requirement from Section 4.1 and remains higher than the cruise requirement of 158 hp. Consequently, both the take-off and climb conditions are power-critical, confirming that an installed engine in the 210 hp class provides an adequate margin for all phases of flight.

3.4.4 Summary of Power Requirements

Table 4.1 summarizes the propulsion requirements determined from take-off, cruise, and climb conditions.

Flight Condition	Required Power (kW)	Required Power (hp)
Take-off (35-40 m/s)	140	188
Cruise (77 m/s)	119	158
Climb (5 m/s ROC, 40 m/s)	140	188

Table 4.1: Required engine power at key conditions

Since this is a single-engine GA aircraft, the required per-engine power equals the total values shown in Table 4.1.

The results confirm that an engine in the 210 hp class is appropriate for the design of the aircraft. This is consistent with typical general aviation aircraft such as the Cessna 182 Skylane or Cirrus SR20.

3.5 Engine Selection

The propulsion requirements from Section 4 indicated that the design aircraft requires an installed shaft power of approximately 200–220 hp. Several piston engines in this power class were reviewed to determine a suitable candidate for the design. Table 5.1 summarizes the main specifications of representative engines.

Engine Model	Lycoming IO-360-M1A	Lycoming IO-390-A	Continental IO-360-ES	Continental IO-520	Rotax 915 iS
Max Power (hp)	180-200	210	210	285	141
Max Power (kW)	134-149	157	147	213	105
Weight (kg)	128	147	150	190	85
Cylinders / Layout	4-cyl, horiz. opp.	4-cyl, horiz. opp.	6-cyl, horiz. opp.	6-cyl, horiz. opp.	4-cyl, inline
Cooling	Air-cooled	Air-cooled	Air-cooled	Air-cooled	Liquid-cooled (turbo)
Typical SFC (lb/hp*hr)	0.42-0.45	0.42-0.44	0.43-0.45	0.42-0.46	0.38-0.40
Dimensions (L x W x H, mm)	1120x560x740	1150x580x760	1130x600x780	1240x620x800	850x570x590
Applications	C172SP, Piper Archer	Cirrus SR20, RV-14	Cirrus SR20 (early models)	Bonanza, Cessna 210	LSA / experimental
Certification	FAA/EASA Part 33	FAA/EASA Part 33	FAA/EASA Part 33	FAA/EASA Part 33	ASTM/CS-E
Typical Fuel	Avgas 100LL	Avgas 100LL	Avgas 100LL	Avgas 100LL	Avgas/Mogas
Rated RPM	2700	2700	2700	2700	5800

Table 5.1: Candidate piston engines for the design aircraft

3.5.1 Evaluation of Candidates

3.5.1.1 Lycoming IO-360-M1A

The Lycoming IO-360 is a widely used, reliable four-cylinder engine that produces between 180–200 hp depending on configuration. At a dry weight of approximately 128 kg, it is relatively light and compact. However, at the lower end of the design’s required power range, it provides little margin for hot-and-high operations or maximum payload missions. It is best suited for lighter four-seat trainers such as the Piper Archer or Cessna 172SP, but it is marginal for this design's performance requirements.

3.5.1.2 Lycoming IO-390-A

The Lycoming IO-390 is a modern development of the IO-360 series, producing 210 hp with only a modest weight increase (147 kg). It offers the required power for the design while remaining compact, fuel efficient, and widely available. The engine is used in the Cirrus SR20 and several experimental aircraft such as the Van's RV-14, demonstrating strong operational performance. Given its balance of power, weight, and certification, it is an excellent candidate for this aircraft.

3.5.1.3 Continental IO-360-ES

The Continental IO-360-ES also produces 210 hp, but unlike the Lycoming IO-390 it employs a six-cylinder configuration. This makes it heavier (≈150 kg) and more complex in terms of maintenance. Although it has been used successfully in earlier Cirrus SR20 models, the extra weight and bulk make it less efficient for a four-seat design where power-to-weight ratio is critical.

3.5.1.4 Continental IO-520

The Continental IO-520 is a high-power six-cylinder engine producing 285 hp at a dry weight of about 190 kg. It has a long track record in aircraft such as the Beechcraft Bonanza and Cessna 210. While proven and robust, its output significantly exceeds the design requirement of ~210 hp. The associated weight penalty and fuel consumption would reduce the efficiency of this aircraft, making it more appropriate for larger, heavier GA designs.

3.5.1.5 Rotax 915 iS

The Rotax 915 iS is a lightweight, turbocharged four-cylinder engine producing 141 hp at only 85 kg. It is liquid-cooled and has one of the lowest specific fuel consumptions in its class. However, the maximum power falls well below the required 200–220 hp for this design, meaning it cannot provide sufficient climb or cruise performance at MTOW. While attractive for light sport aircraft and experimental designs, it is unsuitable for a four-seat general aviation aircraft.

3.5.2 Engine Selection

Among the surveyed engines, only the Lycoming IO-390-A and Continental IO-360-ES deliver the required 210 hp. The Continental option is heavier due to its six-cylinder layout, while the Lycoming provides the same output with a lighter four-cylinder configuration. Engines below the target range (Lycoming IO-360 and Rotax 915 iS) do not offer enough margin for safe climb and cruise performance at MTOW. Conversely, the Continental IO-520 provides far more power than needed, with a significant weight and efficiency penalty.

The Lycoming IO-390-A therefore offers the best match to the design requirements. At 210 hp and ~147 kg with a max power of 157 kW (leaving a larger margin of error that rules out the

Continental), it balances power and weight effectively, is already certified, and is in service on comparable modern GA aircraft such as the Cirrus SR20. It is selected as the baseline engine for the design aircraft.

3.6 Engine Scaling

Once the Lycoming IO-390-A was selected as the baseline powerplant, its specifications were compared with the design requirements to determine if any power scaling was necessary. The IO-390-A produces 190 hp (144 kW) at take-off and a continuous rating of approximately 160 hp (120 kW), closely matching the required power estimated in Section 4 (take-off ≈ 188 hp, cruise ≈ 158 hp).

For piston engines, scaling relationships are less straightforward than for turbofans. However, approximate adjustments can be expressed using empirical relations, where engine weight and dimensions scale with power according to:

$$W_{eng} = W_{ref}\left(\frac{P}{P_{ref}}\right)^{a} \qquad Eq.(6.1)$$

$$L = L_{ref}\left(\frac{P}{P_{ref}}\right)^{b} \qquad Eq.(6.2)$$

where $a \approx 0.7$ and $b \approx 0.3$ are typical exponents for piston engines. Here, P_{ref} and W_{ref} correspond to the rated power and weight of the reference engine.

Using the IO-390-A data:

$$P_{ref} = 210 \text{ hp}, \qquad W_{ref} = 147 \text{ kg}.$$

Substituting into the scaling equation:

$$W_{eng} = 147 \times \left(\frac{210}{210}\right)^{0.7} = 147 \text{ kg}$$

Thus, scaling the engine isn't needed because it already produces the power required with a margin of 10% for safety. In practice, the certified IO-390-A already meets the design power without modification, so no rescaling is necessary. The off-the-shelf engine can be installed directly, ensuring compatibility with certification standards and minimizing development costs.

Parameter	IO-390-A Reference	Required (scaled)	Difference
Power (hp)	210	210	0
Weight (kg)	147	147	0
Length (mm)	1150	1150	0
SFC (lb/hp*hr)	0.42-0.44	~0.43	≈0

Propeller Diameter (m/in)	1.96/76	1.96/76	-
Propeller Type	3-blade constant-speed composite	same	-
Propeller Efficiency ($\boldsymbol{\eta_p}$)	0.78-0.82 (TO) / 0.84-0.86 (Cruise)	0.80 (TO) / 0.85 (Cruise)	-

Table 6.1: Engine scaling comparison

3.7 Required Checks and Engine Improvements

3.7.1 Fuel Weight Check

The mission analysis in Section 2 estimated a fuel fraction of 19%, corresponding to a fuel mass of approximately 258kg at MTOW (1361 kg). The IO-390-A has a typical cruise SFC of 0.3 kg/kW*hr. At a cruise power of 119 kW (158 hp), the fuel flow rate is:

$$\dot{m}_f = P \times c_j \qquad Eq.(7.1)$$

$$\dot{m}_f = 119 \times 0.3 = 36 \text{ kg/hr}$$

For the revised mission range of 1382 km, the cruise speed of 77.2 m/s (278 km/h) gives a cruise time of

$$t_{cruise} = \frac{R}{V} = \frac{1382}{278} = 5 \text{ hr}$$

The fuel consumed during cruise is therefore

$$m_{f,cruise} = 36 \times 5 = 180 \text{ kg}$$

Including reserves and one go-around, equivalent to approximately 30 minutes of reserve plus 5 minutes for go-around (0.6 hr total), the additional fuel required is

$$m_{f,res} = 36 \times 0.6 = 22 \text{ kg.}$$

The total usable fuel required for the mission becomes

$$m_{f,total} = 180 + 22 = 202 \text{ kg.}$$

This value is consistent with the earlier estimate and lies within the available 258 kg fuel budget, confirming the adequacy of the sizing.

Parameter	Value (kg)
Available fuel mass	258
Fuel required (cruise + reserves)	202

Margin	+56

Table 7.1: Fuel Weight Verification for 1382 km Mission

Reducing the design range to 1368 km therefore provides a realistic mission endurance of about 5 hour + reserves while maintaining the full payload at MTOW.

3.7.2 Engine Weight Check

The selected Lycoming IO-390-A engine has a dry weight of approximately 147 kg, representing about 17 % of the aircraft's operational empty weight (840 kg). This fraction falls squarely within the typical range for four-seat general-aviation aircraft, where the engine accounts for 15–18 % of OEW. For reference, the Cirrus SR20, which employs the IO-360-ES, has an engine weight fraction of roughly 17 % OEW, while the Diamond DA40 averages around 15 % OEW. The IO-390-A installation therefore aligns with established aircraft in its category and fits comfortably within the expected mass distribution without requiring any structural redesign or reinforcement of the airframe.

3.7.3 Payload Check

With MTOW = 1361 kg, an empty weight of 840 kg, and fuel mass of 258 kg, the available payload is:

$$W_{TO} = W_{PL} + W_F + W_{OE} \quad Eq. (2.1)$$

$$W_{PL} = 1361 - 840 - 258 = 263 \text{ kg}$$

This corresponds to three occupants with reduced baggage, which is almost half of the nominal 400 kg payload defined in Assignment 1. The result indicates that the aircraft cannot carry full fuel and the full four-person payload simultaneously, which is a trade-off typical for four-seat general aviation aircraft. From the payload–range relationship (Section 2.4 and Figure 2.3), carrying the full 400 kg payload reduces the achievable range from 1600 km (full-fuel case) to roughly 600 km, depending on cruise power setting and reserve policy. Conversely, when carrying full fuel (258 kg), the available payload is limited to about 263 kg, supporting three occupants with light baggage. This trade-off behavior aligns with comparable aircraft such as the Cirrus SR20, which similarly cannot carry full fuel and four passengers simultaneously, requiring the operator to adjust payload or fuel load depending on mission range.

Configuration	Payload (kg)	Fuel (kg)	Estimated Range (km)	Notes
Full fuel, limited payload	263	258	1382	three occupants + baggage
Full payload, reduced fuel	400	≈ 130	550-600	Four occupants + baggage, reduced range

Table 7.2: Payload-Range Trade Summary

3.7.4 Improvements in Specific Fuel Consumption

Although the Lycoming IO-390-A adequately meets the current performance and range requirements, further reductions in specific fuel consumption (SFC) would directly enhance both range and payload capacity. Several improvement strategies could be considered for future development or engine optimization:

- Higher compression ratio to improve thermal efficiency and reduce brake-specific fuel consumption under cruise conditions.
- Full Authority Digital Engine Control (FADEC) and refined electronic fuel injection to maintain an optimal fuel–air ratio across all power settings and flight phases.
- Enhanced cooling and lubrication systems to minimize parasitic power losses and improve durability under continuous operation.
- Propeller–engine integration optimization, including the use of modern composite constant-speed propellers with advanced blade airfoils, to increase propulsive efficiency and reduce fuel burn.
- Lean-of-peak operation techniques (where applicable) to decrease fuel flow during cruise without compromising engine longevity.

These refinements could reduce SFC by 3–5 %, extending the aircraft's endurance and range while lowering operating costs and emissions—all without requiring significant changes to the existing airframe or propulsion layout.

4 Wing Design

4.1 Introduction

This presents the third stage in the design of our aircraft, focusing on the development of the wing configuration. Using the requirements and fuselage layout from Assignment 1 and the preliminary sizing and propulsion results from Assignment 2, the objective of this stage is to determine the wing geometry, airfoil selection, and lift characteristics that meet the aircraft's performance targets. The clean wing is first analyzed to define its aerodynamic properties, followed by the sizing of high-lift devices to ensure proper take-off and landing performance. Finally, the available fuel-tank volume in the wing is checked against the mission fuel requirements established earlier.

4.2 Clean Wing Design

To design the wing, the aerodynamic properties are first determined for the clean configuration before considering any high-lift devices or fuel integration. The process begins by evaluating the required lift characteristics based on the aircraft's performance during cruise and loiter, followed by the selection of an appropriate airfoil and the sizing of the finite wing geometry.

4.2.1 The Infinite Wing

The starting point of the wing design is to determine the total lift that must be produced during steady, level flight. In normal cruise conditions, the lift equals the aircraft's total weight; however, it is common practice to include a margin to account for small maneuvers and atmospheric gusts that temporarily increase the effective load on the wing. A 10 % load factor is therefore applied. The required total lift is expressed as

$$L_{TOT} = 1.1\,W = 1.1\,(m \times g) \qquad (2.1)$$

Substituting the design mass of $m = 1361$ kg the gravitational acceleration $g = 9.81\ \mathrm{m/s^2}$ gives

$$L_{TOT} = 1.1(1361)(9.81) = 14{,}687\ \mathrm{N} \qquad (2.2)$$

This value represents the total lift that the wing must generate in nominal cruise conditions, ensuring a small margin for operational disturbances.

The next step is to determine the wing area required to sustain this load. Although the performance sizing analysis initially selected a design wing loading of W/S = 950 N/m², our original detailed wing-design work showed that this value pushed the aircraft too far to the right on the W/S–W/P diagram. At W/S = 950, the landing configuration required a C_{Lmax} of approximately 2.4 which, after applying the 5% safety margin to reach 2.52, exceeded our allowable stall limit of 2.5. To restore adequate stall margin, the design point was shifted slightly left to a lower wing loading. The updated wing loading of W/S = 920 N/m² reduces the required landing C_{Lmax} to approximately 2.2, bringing the aircraft back within acceptable limits. The change in wing loading also keeps the engine and its scaling consistent to the results found in the propulsion sizing. A higher wing loading would result in a smaller wing area and therefore higher cruise speed, but it would also increase stall speed and take-off distance. Conversely, a lower wing loading would provide better low-speed characteristics but higher induced drag during cruise. Using the chosen value, the total reference wing area becomes

$$S = \frac{W}{(W/S)} = \frac{13354}{920} = 14.52\ \mathrm{m^2} \qquad (2.3)$$

At the nominal cruise altitude of 2440 m, the standard-atmosphere density is approximately $\rho = 1.006\ \mathrm{kg/m^3}$. The corresponding cruise velocity is $V_\infty = 77.2\ \mathrm{m/s}$. Under steady flight conditions, the lift force can be expressed as

$$L = \frac{1}{2}\rho V_\infty^2 S C_L \qquad (2.4)$$

Rearranging for the lift coefficient yields

$$C_L = \frac{2L}{\rho V_\infty^2 S} \qquad (2.5)$$

This relation allows the required coefficient of lift to be evaluated at any flight point once weight, speed, and altitude are known.

Because fuel is consumed throughout the flight, the aircraft weight and the required lift decreases slightly from the start to the end of cruise. The updated mission analysis determined a 19.8% fuel fraction including reserves and go-around, giving start and end of cruise weight fractions of $0.958\ W_{TO}$ and $0.811\ W_{TO}$, respectively. Substituting these values gives

$$C_{L,sc} = \frac{2(0.958\ W_{TO})}{\rho V_\infty^2 S} = 0.293, \qquad C_{L,ec} = \frac{2(0.811\ W_{TO})}{\rho V_\infty^2 S} = 0.249 \qquad (2.6)$$

These results show that the required lift coefficient decreases slightly as the aircraft becomes lighter during the cruise segment.

During the loiter phase, the aircraft operates at a reduced airspeed to improve endurance. For propeller-driven aircraft, loiter speed is typically about 80-85% of cruise speed, corresponding to the condition of minimum power required. Using the cruise velocity of $V_\infty = 77.2\ \mathrm{m/s}$ and applying a 0.84 ratio gives

$$V_{loiter} = 0.84 V_\infty = 0.84(77.2) \approx 65\,\frac{\mathrm{m}}{\mathrm{s}} \qquad (2.7)$$

At this speed, the aircraft operates near its best endurance condition while maintain ample margin above the stall speed of approximately 29 m/s. The corresponding lift coefficient for loiter is therefore

$$C_{L,loiter} = \frac{2W_{loiter}}{\rho V_{loiter}^2 S} \approx 0.358 \qquad (2.7)$$

The variation of lift coefficient through the principal mission phase is summarized below.

Flight Segment	**Weight Fraction**	**Speed (m/s)**	$\boldsymbol{C_L}$
Start of Cruise	0.958	77.2	0.293
End of Cruise	0.811	77.2	0.249
Loiter	0.802	65.0	0.347

Table 2.1 Variation of lift coefficient during cruise and loiter

To define a representative design condition for the airfoil, the mean cruise lift coefficient is averaged and multiplied by the same 10% safety factor used earlier. The design lift coefficient is thus

$$C_{L,des} = 1.1\left(\frac{C_{L,sc} + C_{L,ec}}{2}\right) = 1.1\left(\frac{0.293 + 0.249}{2}\right) = 0.298 \qquad (2.8)$$

The chosen $C_{L,design}$ represents the target lift coefficient for the airfoil and will be used moving forward to select a suitable profile. This value ensures efficient cruise performance while maintaining adequate margin for climb, maneuver, and gust loading. It provides the foundation for determining the wing's geometric and aerodynamic characteristics in the finite-wing analysis that follows.

4.2.2 Finite Wing and Mean Aerodynamic Chord

The finite-wing geometry is developed using the design lift coefficient and wing-loading results obtained in the previous section. The objective of this step is to determine the main geometric parameters of the wing like its span, aspect ratio, taper ratio, and mean aerodynamic chord (MAC), which define the aerodynamic and structural characteristics of the aircraft.

The aspect ratio, AR, plays a crucial role in determining induced drag. Increasing the aspect ratio reduces induced drag, improving cruise efficiency, but can also increase structural bending moments and wing weight. For this design, an aspect ratio of $AR = 7.5$ is selected as a compromise between aerodynamic efficiency and structural feasibility. This value provides improved cruise performance compared to lower aspect ratios without imposing excessive structural penalties, which aligns with the weight and load distribution constraints associated with the Lycoming IO-390-A installation.

With the aspect ratio known, the wingspan can be found from the relationship between span, aspect ratio, and wing area:

$$b = \sqrt{AR \times S} = \sqrt{7.5 \times 14.52} = 10.43 \text{ m} \qquad (2.9)$$

This span remains practical for a four-seater general aviation aircraft, improving the lift-to-drag ratio and overall range efficiency without compromising ground handling or hangar requirements.

A trapezoidal wing planform is selected for manufacturability and aerodynamic efficiency. The taper ratio, defined as the ratio of the tip chord to the root chord can be found as:

$$\lambda = \frac{c_t}{c_r} = 0.40 \qquad (2.10)$$

The taper ratio was determined based on aerodynamic, structural, and manufacturability considerations. A moderate taper ratio between 0.35 and 0.45 is typical for light general-aviation aircraft and provides a good balance between induced-drag reduction, favorable stall behavior, and structural simplicity. This range closely matches reference aircraft such as the Cessna 182 (0.44), Cirrus SR20 (0.42), and Mooney M20J (0.38). Selecting a value of $\lambda = 0.40$ places the design near the midpoint of this range, offering a smooth aerodynamic lift distribution with sufficient tip chord for aileron installation and adequate internal depth for spars and fuel tanks.

The wing area for a trapezoidal planform is expressed as

$$S = \frac{b}{2}(c_r + c_t) = \frac{b}{2} c_r (1 + \lambda) \qquad (2.11)$$

and rearranging for the root chord gives:

$$c_r = \frac{2S}{b(1+\lambda)} = \frac{2(14.52)}{10.43(1+0.40)} = 1.99\ \text{m} \qquad (2.12)$$

The corresponding tip chord is

$$c_t = \lambda c_r = 0.40(1.99) = 0.80\ \ \text{m}$$

These chord values provide sufficient structural depth for the main and rear spars, while also allowing adequate internal volume for the required 258 kg of mission fuel stored within the wing tanks.

The mean aerodynamic chord (MAC) is the chord length that produces the same aerodynamic moment as the entire wing. For a tapered wing, the MAC is found by:

$$\bar{c} = \frac{2}{3} c_r \left(\frac{1+\lambda+\lambda^2}{1+\lambda} \right) = \frac{2}{3}(1.99) \left(\frac{1+0.40+0.40^2}{1+0.40} \right) = 1.48\ \text{m} \qquad (2.13)$$

The spanwise location of the MAC from the root along the semispan is:

$$\bar{y} = \frac{b}{6} \left(\frac{1+2\lambda}{1+\lambda} \right) = \frac{10.43}{6} \left(\frac{1+2(0.40)}{1+0.40} \right) = 2.23\ \text{m} \qquad (2.14)$$

This location represents the point along the span where the resultant aerodynamic force acts and will be used later for the longitudinal-stability analysis.

The refined wing design increases the aspect ratio from earlier estimates while maintaining a similar total area. This adjustment reduces induced drag by approximately 10–12 %, improving cruise efficiency and endurance while keeping structural loads within acceptable limits. The modest increase in span can be easily accommodated by local reinforcement around the wing-fuselage attachment and the engine mount structure. The resulting configuration achieves a balanced design that enhances aerodynamic performance, structural feasibility, and manufacturability for the aircraft's mission profile.

In summary the final wing geometry parameters are:

- Wing area, $S = 14.52\ \text{m}^2$
- Aspect ratio, $AR = 7.5$
- Wingspan, $b = 10.43$ m
- Taper ratio, $\lambda = 0.40$
- Root chord, $c_r = 1.99$ m
- Tip chord, $c_t = 0.80$ m
- Mean aerodynamic chord, MAC = 1.48 m
- Spanwise MAC location, $\bar{y} = 2.23$ m

The refined geometry achieves a well-balanced configuration that improves aerodynamic efficiency and range capability while remaining structurally practical for the selected engine and mission requirements.

4.2.3 Airfoil Selection

To determine a suitable airfoil for our aircraft, the design requirements from Assignments 1 and 2 were used as a foundation. The aircraft is a three-seat general aviation (GA) airplane designed for a cruise speed of 150 KTAS (77.2 m/s), a cruise altitude of 8,000 ft (2,440 m), and a maximum takeoff weight (MTOW) of 1,361 kg. With a range of 1382 km and a payload of 270 kg, the aircraft within the low subsonic regime (Mach ≈ 0.23), where compressibility effects are negligible. Therefore, a conventional cambered GA airfoil with high lift and stable low-speed behavior is appropriate.

The selection aims to ensure efficient cruise performance while providing adequate low-speed lift capability to meet the stall and takeoff distance requirements defined earlier.
The characteristic Reynolds number for the design was computed using:

$$Re = \frac{\rho V c}{\mu} \qquad (2.15)$$

At cruise conditions, where $\rho = 1.006\ \text{kg/m}^3$, V = 77.2 m/s and assuming a mean aerodynamic chord of 1.48 m, the Reynolds number becomes:

$$Re = \frac{(1.006)(77.2)(1.41)}{1.75 \times 10^{-5}} \approx 6.56 \times 10^6 \qquad (2.16)$$

This value lies in the typical range for light-aircraft wings (10^6–10^7), confirming that viscous effects are moderate and compressibility remains negligible at Mach 0.23. The aerodynamic data can therefore be treated under incompressible low-speed conditions.

According to the lecture notes on airfoil selection, general-aviation aircraft typically use NACA 4- or 5-series airfoils, which offer favorable lift and drag characteristics at low Reynolds numbers. The NACA 4-series (e.g., 2412, 4412) provide gentle stall characteristics and low drag, ideal for low-speed GA aircraft. The NACA 5-series (e.g., 23012, 23015) yield higher maximum lift and greater camber near the leading edge, though with a slightly sharper stall.

Given the mission of our aircraft, a light, three-seat piston aircraft with short-field capability and low-subsonic cruise, a 5-series airfoil with moderate camber, higher maximum lift, and medium thickness provides the best compromise between lift, drag, and stall behavior. The NACA 23012 airfoil satisfies these design goals. It features a 12% thickness-to-chord ratio (t/c = 0.12), offering sufficient structural depth for spars and fuel volume without having excessive drag. As one of the 23-series, it is designed around a theoretical lift coefficient of approximately 0.30, placing the aircraft's required cruise lift coefficient ($C_L \approx 0.298$) right within its efficient operating range. It also features a max-lift coefficient of $C_{L,max} \approx 1.4$–1.8 at Reynolds numbers typical of our wing ($Re \approx 3 \times 10^6$), ensuring strong low-speed lift capability and reducing the flapped-area required for takeoff and landing. These characteristics make NACA 23012 a strong candidate for modern general-aviation configurations seeking robust short-field performance alongside efficient cruise.

Using the average cruise lift coefficient from Section 2.1, $C_{L,des} = 0.298$, the corresponding airfoil design-lift coefficient can be obtained using the finite-to-infinite-wing correction:

$$C_{l,des} = \frac{C_{L,des}}{cos^2\,(\Lambda)} \qquad (2.17)$$

Assuming a straight, unswept wing ($\Lambda_{LE} = 0°$), the airfoil design-lift coefficient becomes approximately $C_{l,des} \approx 0.298$. An unswept wing was selected because the aircraft cruises at a low Mach number (M ≈ 0.23), where sweep provides no compressibility-related benefits and would instead reduce low-speed lift and raise stall speed. This design-lift coefficient falls near the intended operating range of the NACA 23012 airfoil, which exhibits low drag around its theoretical design-lift coefficient and provides stable, predictable behavior while maintaining adequate lift margin for takeoff and landing.

The NACA 23012 airfoil provides a well-balanced aerodynamic performance appropriate for our aircraft's mission and operating conditions. Its moderate camber and 12% thickness-to-chord ratio offer a good compromise between structural efficiency, internal wing volume, and favorable lift characteristics across the full flight envelope. At the design operating point of $C_{L,max} = 0.298$, the airfoil performs within its low-drag region, supporting efficient cruise performance and contributing to improved range and fuel economy.

At low speeds, the NACA 23012 produces a max-lift coefficient of approximately $C_{L,max} \approx 1.4$–1.8 at Reynolds numbers representative of our wing, enabling the aircraft to meet the stall and takeoff performance requirements established in the previous stage with the necessary high-lift devices.

In summary, the NACA 23012 was selected because it provides efficient cruise lift, predictable low-speed behavior, strong maximum-lift capability, and structurally practical geometry. These qualities align well with the performance objectives of a three-seat general-aviation aircraft designed for a 1382 km range and short-field capability.

To confirm the aerodynamic suitability of the chosen NACA 23012 airfoil, a detailed viscous analysis was conducted in JavaFoil at two representative operating conditions, both at low-speed (takeoff and landing) conditions.

- Cruise: $Re = 6.6 \times 10^6$, Mach = 0.10
- Low-Speed: $Re = 3.6 \times 10^6$, Mach = 0.10

Each case was analyzed for angles of attack between −4° and +16°, covering the full linear region and post-stall behavior. The objective was to verify that the airfoil delivers efficient cruise performance near the design lift coefficient ($C_{l,des} = 0.298$) while maintaining sufficient low-speed lift margin with only a minimal flap system.

At Re = 6.6 × 10^6, the JavaFoil results show a smooth and nearly linear lift curve up to approximately 10°, with a slope of 0.1163 per degree (6.66 per radian). The zero-lift angle is near -1.2°, consistent with published NACA 23012 data. The maximum lift coefficient for the clean configuration is $C_{l,max}$ ≈ 1.381, while the design lift coefficient for cruise ($C_{l,des}$ = 0.298) occurs at an angle of attack of roughly 1.3°. This places the cruise point well inside the linear region and far from stall. The minimum drag coefficient at cruise is $C_{d,min}$ ≈ 0.0094, while, similarly, the drag at the design point is C_d ≈ 0.0098.

At the lower Reynolds number (Re = 3.6 × 10^6), representing approach and take-off conditions, the airfoil maintains favorable performance with a similar lift-curve slope of 0.1161 per degree (6.65 per radian) and a $C_{l,max}$ ≈ 1.361. The zero-lift angle remains approximately –1.2°, indicating consistent behavior between regimes. The minimum drag is also similar, with $C_{d,min}$ ≈ 0.0091, and the stall angle occurs near 13°, confirming low-speed behavior without harsh flow separation.

These results demonstrate that the NACA 23012 maintains strong lift capability, stable stall progression, and efficient low-drag behavior near the design lift coefficient. This makes it well suited for a general-aviation aircraft with simple high-lift devices. The lift curves and drag polars for Re = 6.6 × 10^6 and Re = 3.6 × 10^6 are presented in Figures 2.3.1 and 2.3.2, respectively, are almost visually indistinguishable, and key parameters are summarized in Table 2.3.

Overall, the analysis confirms that the NACA 23012 provides a practical combination of low drag at the design point and strong maximum-lift capability at low speeds. This supports both the cruise and short-field requirements of our aircraft without the need for complex high-lift systems.

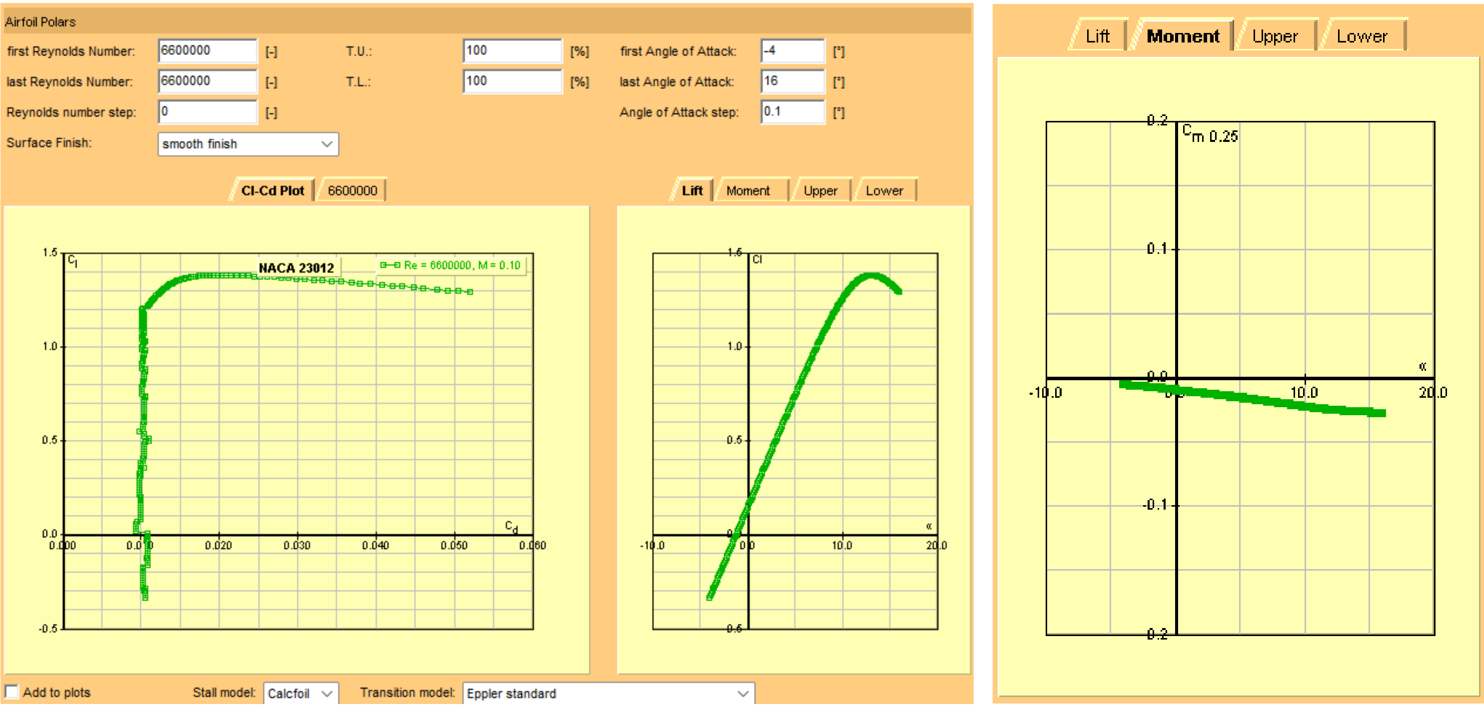

Figure 2.3.1: C_L-C_D plot and Lift curve (C_l vs α) for NACA 23012 for Re=3.6e6

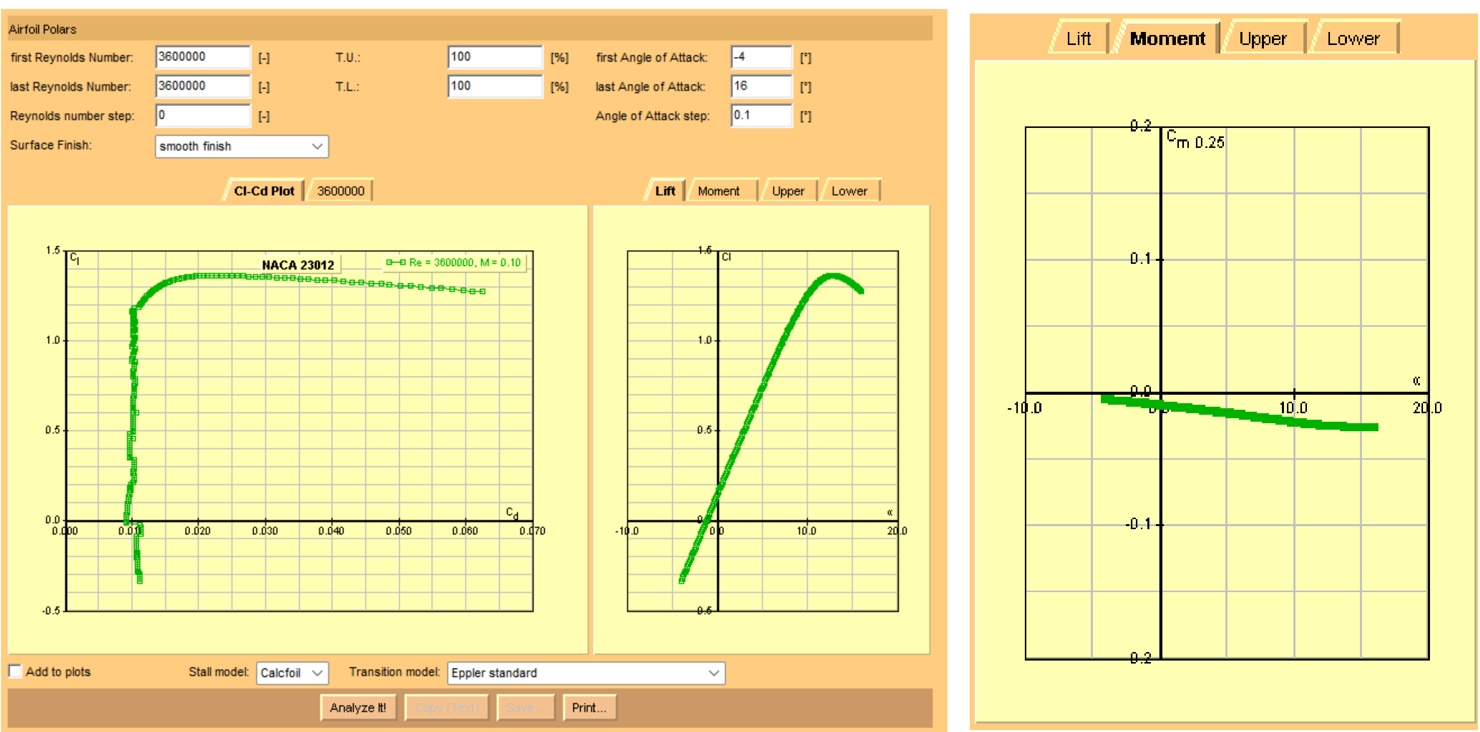

Figure 2.3.2: C_L-C_D plot and Lift curve (C_l vs α) for NACA 23012 for Re=6.6e6

The NACA 23012's aerodynamic parameters are summarized below:

Parameter	Re = 3.6 x 10^6	Re = 6.6 x 10^6	Unit
Zero Cl Angle	-1.2	-1.2	degrees
Zero Angle Cl	0.143	0.143	
Max Cl	1.361	1.381	
Stall Angle	13.0	13.1	degrees
Min Cd	0.00914	0.00936	
Cl at Min Cd	0.010	0.034	
Angle at Min Cd	-1.1	-0.9	degrees

Table 2.3: NACA 23012 parameters

The figures and table above show that the aerodynamic parameters of the NACA 23012 airfoil remain remarkably consistent across the relevant Reynolds number range for both cruise and takeoff/landing conditions. Parameters such as zero-lift angle, maximum lift coefficient, stall angle, and minimum drag vary only marginally, indicating stable and predictable behavior throughout the operating envelope.

4.2.4 Validity and Sanity Checks

The following section performs a series of validity and sanity checks to ensure that the calculated wing geometry parameters fall within realistic limits when compared to historical data and reference aircraft. These comparisons confirm that the selected wing configuration for our aircraft is both aerodynamically and structurally acceptable.

4.2.4.1 Pitch-Up Tendency

The pitch-up tendency of the wing was evaluated using the NASA TN 1093 pitch-up risk chart provided in the notes. This chart relates the quarter-chord sweep angle to the aspect ratio to identify configurations that are susceptible to pitch-up at high angles of attack. For our aircraft, the calculated aspect ratio is 7.5, and the leading-edge sweep angle is 0°, corresponding to an unswept, straight-wing configuration typical of propeller-driven general-aviation aircraft. A quarter chord sweep angle can be found using equation 2.18:

$$\Lambda_{x/c} = \arctan[\tan(\Lambda_{LE}) - \frac{x}{c}\frac{2c_r}{b}(1-\lambda)], \qquad (2.18)$$

For our aircraft, the wing parameters are:

$$\Lambda_{LE} = 0°, \quad c_r = 1.99\,m, \quad b = 10.43\,m, \quad \lambda = 0.40.$$

Substituting these into Equation (2.18) for the quarter-chord line (x/c=0.25) gives:

$$\Lambda_{0.25c} = \arctan[\tan(0) - 0.25\frac{2(1.99)}{10.43}(1 - 0.40)] \approx -3.3°.$$

When plotted on the NASA TN 1093 chart, the design point (AR = 7.5, $\Lambda_{0.25}$ = -3.3°) lies within the "Increased Stability at High Angle of Attack" region, indicating no pitch-up risk for the clean-wing configuration. The moderate aspect ratio and absence of sweep ensure that stall will initiate inboard at the wing root rather than at the wingtips, providing predictable and stable nose-down behavior during stall recovery.

A reproduction of the chart is shown in Figure 2.4.1, where a vertical line at $\Lambda_{0.25}$ = -3.3° and a horizontal line at AR = 7.5 identify the intersection point for our aircraft. The position of this point within the stable subsonic region confirms that the selected wing geometry exhibits no significant pitch-up tendency and will maintain satisfactory longitudinal stability.

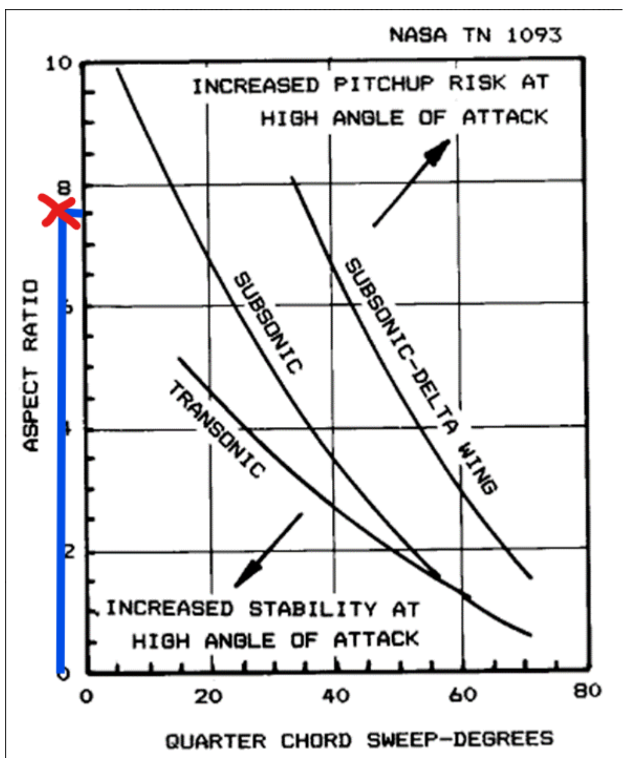

Figure 2.4.1: Pitch-Up Risk Chart

4.2.4.2 Sweep Angle

For propeller-driven, low-subsonic aircraft, leading edge sweep provides no aerodynamic benefit since compressibility effects are negligible below Mach ≈ 0.3. At such speeds, sweep would only increase structural weight and complexity. Thus, the straight-wing design of our aircraft is optimal for its general-aviation mission, offering predictable stall characteristics, good low-speed lift, and simplified manufacturing.

To validate the choice of sweep angle, the design point was compared against the historical trend of leading-edge sweep versus maximum Mach number, shown in Figure 2.4.2. This chart, from the NASA trend data, illustrates that higher leading edge sweep angles are used primarily by transonic and supersonic aircraft to delay compressibility effects. When plotted on the graph, our aircraft design point (M = 0.23, Λ_{LE} = 0°) lies at the far-left end of the subsonic region, exactly where the historical data shows no sweep is necessary. This confirms that the straight-wing configuration is entirely appropriate for the aircraft's low-speed, propeller-driven operation.

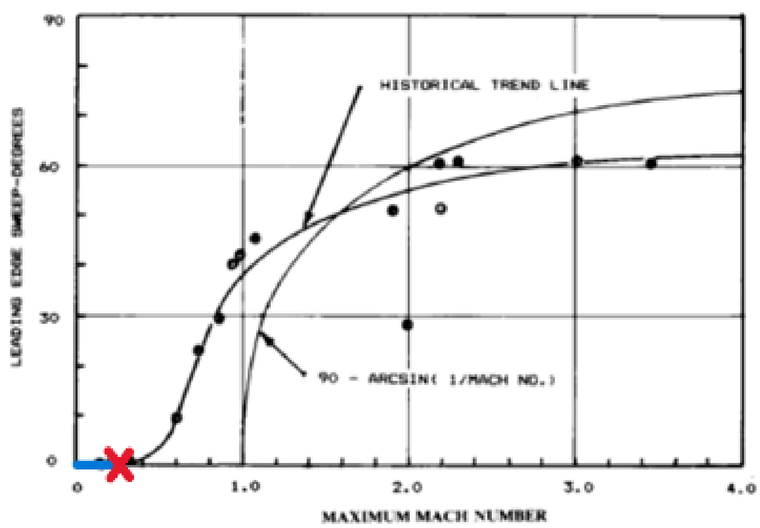

Figure 2.4.2: Historical Trend of Leading-edge Sweep angle vs. Max Mach Number

We can also calculate the trailing edge sweep angle using equation 2.18:

$$\Lambda_c = \arctan[\tan(0) - 1.0\frac{2(1.99)}{10.43}(1 - 0.40)] \approx -12.9°.$$

Aerodynamically, this does not introduce any stability penalties for our aircraft; instead, it simply reflects the geometric shaping required to achieve the selected taper ratio and chord distribution.

A dihedral angle +3° provides a small positive dihedral and is selected to provide modest passive lateral (roll) stability for our low-wing aircraft. This value lies in the common 2°–5° range used on light GA designs and preserves adequate aileron authority while improving hands-off rolling trim when there are gusts and sideslip.

With the sweep characteristics fully defined, including leading-edge, quarter-chord, and trailing-edge sweep, we can now evaluate how these choices relate to the wing's aspect ratio, which governs induced drag and strongly influences both cruise efficiency and low-speed performance.

4.2.4.3 Aspect Ratio

The aspect ratio (AR) is a key geometric parameter that influences both the aerodynamic and structural performance of the wing. A higher aspect ratio reduces induced drag and improves lift-to-drag efficiency, but it also increases structural weight and bending stresses at the wing root.

Conversely, a low aspect ratio provides a stiffer and stronger structure but causes higher induced drag, lowering cruise performance.

An aspect ratio of 7.5 was selected as a balanced value that provides low induced drag during cruise while maintaining acceptable structural weight. This value is typical for single-engine, low-subsonic general-aviation aircraft such as the Cessna 182 (A ≈ 7.5), Cirrus SR20 (A ≈ 9.1), and Diamond DA40 (A ≈ 11), confirming that it falls within the historical trend range for similar configurations.

To assess the structural feasibility of the chosen span and thickness, the cantilever ratio (R_c) was computed using the following expression:

$$R_c = \frac{\left(\frac{b}{2}\right)}{t_r \cos(\Lambda_{0.5c})} \qquad (2.19)$$

where t_r is the root thickness, given by $t_r = (\frac{t}{c})_{max} \times c_r$. Using $b = 10.43\ m$, $\frac{t}{c} = 0.12$, $c_r = 1.99\ m$, and a calculated $\Lambda_{0.5c} = -6.5°$,

$$t_r = 0.12(1.99) = 0.24\ m$$

$$R_c = \frac{(\frac{10.43}{2})}{0.24\cos(-6.5°)} = 21.9$$

The computed cantilever ratio falls within the recommended range of 18–22, indicating that the wing's structural slenderness is appropriate for a cantilever configuration. This confirms that the selected aspect ratio provides a suitable balance between aerodynamic efficiency and structural feasibility.

4.2.4.4 Taper Ratio

Taper ratio influences the lift distribution, structural weight, and stall behavior of the wing. A taper ratio closer to an elliptical distribution reduces induced drag and improves aerodynamic efficiency. Designers often select moderate taper ratios to achieve a balance between efficient lift distribution, structural simplicity, and predictable stall progression. Raymer provides a historical reference chart that relates taper ratio to quarter-chord sweep angle and identifies regions associated with near-elliptical lift distributions.

For our aircraft, the selected taper ratio is $\lambda = 0.40$ and the quarter-chord sweep angle is $\Lambda_{0.25c} = -3.3°$. Using Raymer's chart, the optimal taper ratio at this sweep angle is approximately $\lambda \approx 0.45$. The chosen value of 0.40 lies slightly below this optimal range, meaning our wing is more tapered. This deviation is small and remains consistent with the design trends of comparable general-aviation aircraft.

Although λ = 0.40 produces a more tapered wing than the theoretical optimum, it remains a practical and well-justified choice. A slightly lower taper ratio reduces structural weight, improves induced-drag efficiency, and is widely used in GA aircraft to balance performance with manufacturability. The tip chord remains sufficiently large to accommodate ailerons and maintain acceptable stall characteristics, ensuring that the aerodynamic and structural penalties of the increased taper are minimal.

Figure 2.11 illustrates the optimal taper ratio region for various sweep angles. When the design point ($\Lambda_{0.25c} = -3.3°$, $\lambda = 0.40$) is placed on the chart, it sits slightly below the optimal taper ratio curve for this sweep angle. This indicates that our wing is tapered a bit more than the ideal elliptical distribution. The deviation is small and remains consistent with the trend shown by other light aircraft. The selected taper ratio still provides acceptable aerodynamic efficiency and predictable stall behavior, so it is suitable for the clean-wing configuration of our aircraft.

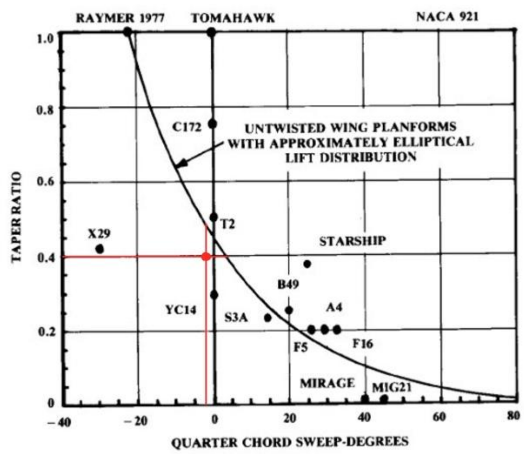

Figure 2.4.3: Historical trend of taper ratio relative to quarter-chord sweep angle

4.2.4.5 Mach Drag Divergence

To verify that the wing does not encounter drag divergence within the aircraft's operating envelope, the suction peak of the selected airfoil (NACA 23012, $t/c = 0.12$) was evaluated at the cruise condition. A viscous, incompressible JavaFoil analysis at $Re \approx 6.6 \times 10^6$ and the operating cruise angle of attack ($\alpha \approx 1.2°$) produced a minimum pressure coefficient of $C_{p,\min} \approx -0.909$. This value represents the strongest suction on the airfoil and is the key input in determining the onset of local sonic flow.

To convert this incompressible suction peak into a corresponding freestream Mach number at which the local surface Mach reaches unity, the isentropic sonic-point relation from the lecture notes is used:

$$C_{p,cr}(M) = \frac{2}{\gamma {M_{cr}}^2}\left[\left(\frac{1 + \frac{\gamma - 1}{2}{M_{cr}}^2}{1 + \frac{\gamma - 1}{2}}\right)^{\frac{\gamma}{\gamma - 1}} - 1\right] \qquad Eq. (2.20)$$

The critical Mach number M_{cr} is obtained by solving

$$C_{p,cr}(M_{cr}) = C_{p,min} \qquad Eq. (2.21)$$

Using $\gamma = 1.4$, solving for M_{cr} yields

$$M_{cr} \approx 0.63$$

For conventional unswept, moderate-thickness general-aviation airfoils, the drag-divergence Mach number is typically 2–4% above the critical value. Applying this engineering offset gives

$$M_{DD} \approx M_{cr}\ (1.02 + 0.08(1 - \cos\Lambda_{0.25c})) \approx \ 0.643$$

This result provides a substantial margin relative to the aircraft's actual operating Mach numbers. The cruise condition is only $M \approx 0.23$, and typical FAR-23 design-dive/certification speeds for similar GA aircraft fall in the range $M \approx 0.40$–0.45. Both values lie far below even conservative estimates of $M_{cr}$and M_{DD}, indicating that no transonic effects are approached in service.

Because the wing uses no sweep ($\Lambda_{LE} = 0°$), a moderate thickness ratio ($t/c = 0.12$), and an airfoil whose suction peak remains mild at the cruise design-lift coefficient, the pressure distribution remains well within the subcritical regime. Therefore, the chosen combination of airfoil, thickness ratio, and geometry ensures that the wing will not approach Mach drag divergence anywhere within the operational envelope, fully satisfying the design requirement.

4.2.5 Clean Wing Lift Curve

With the airfoil selected and the wing geometry defined, the next step is to determine the clean-wing lift curve for our aircraft. This requires evaluating several key aerodynamic angles, including the lift-curve slope, the trim angle, and the stall angle. Once these quantities are established, the complete lift curve for both cruise and low-speed operation can be constructed. These results verify that the wing meets the required aerodynamic performance without relying on high-lift devices and confirm that the clean-wing behavior aligns with the aircraft's mission and design conditions.

4.2.5.1 Curve Slope Angle

The lift-curve slope of the clean wing was evaluated at both cruise and low-speed conditions. The Prandtl–Glauert compressibility factor is first determined for each flight regime. Since our leading-edge sweep angle is 0, the compressibility factor at cruise for Mach = 0.23 is:

$$\beta_{\text{cruise}} = \sqrt{1 - M^2} \qquad Eq. (2.22)$$

$$\beta_{\text{cruise}} = \sqrt{1 - 0.23^2} = 0.973$$

At low speed, the aircraft operates near Mach 0.10, resulting in

$$\beta_{\text{landing}} = \sqrt{1 - 0.10^2} = 0.995$$

The finite-wing lift-curve slope is computed using the DATCOM expression, which accounts for aspect ratio, compressibility effects, and the sweep angle at the half-chord line:

$$C_{L\alpha} = \frac{2\pi A}{2 + \sqrt{4 + (\frac{A\beta}{\eta})^2 (1 + \frac{\tan^2 \Lambda_{0.5c}}{\beta^2})}} \qquad Eq.(2.23)$$

The wing parameters are $A = 7.5$, $\eta = 0.95$, $\Lambda_{0.5c} = -6.5°$.

Using the cruise compressibility factor $\beta_{\text{cruise}} = 0.973$, the lift-curve slope is

$$C_{L\alpha,\text{cruise}} = 4.72 \text{ rad}^{-1}$$

$$C_{L\alpha,\text{cruise}} = 0.082 \text{ deg}^{-1}$$

Repeating the calculation for the low-speed case ($\beta_{\text{landing}} = 0.995$) gives

$$C_{L\alpha,\text{landing}} = 4.64 \text{ rad}^{-1}$$

$$C_{L\alpha,\text{landing}} = 0.081 \text{ deg}^{-1}$$

These values remain below the infinite-wing theoretical limit of $2\pi = 6.283 \text{ rad}^{-1}$, as expected for a finite-span wing. The results confirm that the selected wing geometry produces a realistic and well-behaved lift response across the full operating envelope. The lift-curve slopes at both cruise and low speed fall within the expected range for a low-subsonic general-aviation aircraft, indicating that the wing provides stable and predictable aerodynamic performance under the required mission conditions.

4.2.5.2 Trim Angle

The trim angle of attack is the angle at which the wing must operate to produce the design lift coefficient during steady, level cruise. Using the calculated lift-curve slope from Section 2.5.1, the trim angle is found by

$$\alpha_{\text{trim}} = \alpha_{0L} + \frac{C_{L,\text{des}}}{C_{L\alpha}} \qquad Eq.(2.24)$$

The zero-lift angle of the NACA 23012 airfoil at the cruise Reynolds number is approximately $\alpha_{0L} = -1.2°$. The design lift coefficient for the wing is $C_{L,\text{des}} = 0.298$, and the clean-wing lift-curve slope at cruise is $C_{L\alpha,\text{cruise}} = 4.72\ \text{rad}^{-1} = 0.082\ \text{deg}^{-1}$. Substituting these values gives

$$\alpha_{\text{trim}} = -1.2° + \frac{0.298}{0.082} = -1.2° + 3.62° = 2.42°$$

The resulting trim angle of approximately 2.42° indicates that the wing operates at a modest positive angle of attack in cruise, which is typical for low-subsonic general-aviation aircraft. This trim point lies well within the linear portion of the lift curve and below the airfoil's drag-rise region, confirming that the wing is appropriately sized and that the aircraft will maintain efficient cruise performance. The trim angle is also not critical for M_{DD} or M_{cr}, therefore no sonic conditions will appear at this angle. This also means that to maintain almost level fuselage attitude in cruise of about 0.5°, a wing incidence angle of 2.0° is required to ensure the wing operates at the required lift coefficient. This value is also consistent with typical 1-3° incidence range for other general-aviation aircraft.

4.2.5.3 Stall Angle

To determine the stall angle, the planform must first satisfy the condition for the high aspect ratio stall method. Using,

$$A > \frac{4}{(C_1 + 1)\cos\ \Lambda_{LE}} \qquad Eq.(2.25)$$

The coefficient C_1 is found from the taper-ratio chart in figure 2.5.1, giving $C_1 = 0.40$ for a taper ratio of 0.40. With $\Lambda_{LE} = 0°$, the right-hand side becomes 2.86. Since the aircraft uses an aspect ratio of 7.5, the high-aspect-ratio method is valid.

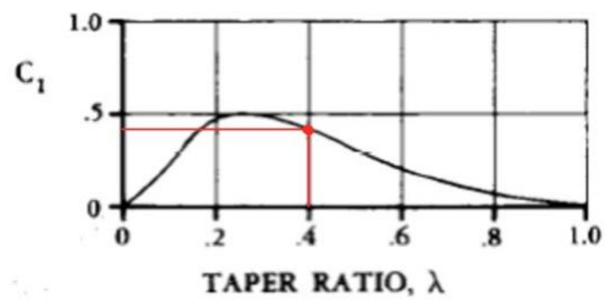

Figure 2.5.1: Historic data relating taper ratio to the C_1 coefficient

Next, the sharpness of the leading edge is computed. The general rule to determine the ΔY for common NACA 5-series airfoils is by multiplying the thickness of the airfoil by 26. Since our airfoil thickness is 12%, the sharpness of the leading edge, ΔY, for our wing is approximately 3.

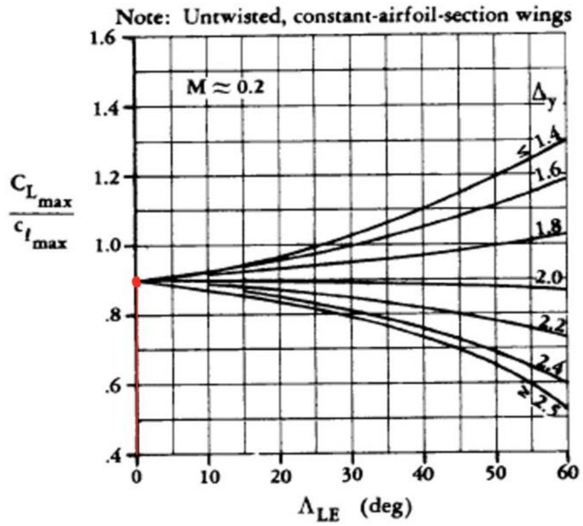

Figure 2.5.2: Ratio of wing $C_{L,max}$ to airfoil $c_{l,max}$ as a function of leading-edge sweep angle for untwisted wings

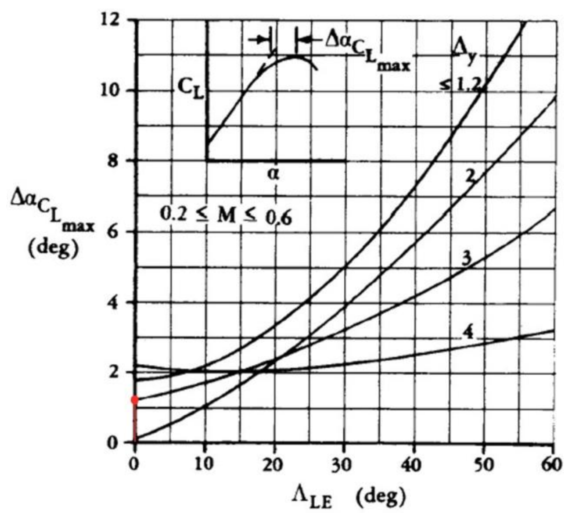

Figure 2.5.3: Stall-angle correction $\Delta\alpha_{C_{Lmax}}$ as a function of leading-edge sweep angle

For low-speed flight, the charts for $C_{L\max}/C_{l\max}$ and $\Delta\alpha_{C_{L\max}}$ at $M \approx 0.10$ are used. The ratio $C_{L\max}/C_{l\max}$ is read as 0.9, and the stall-angle correction is $\Delta\alpha_{C_{L\max}} = 1.2° = 0.021$ rad.
Using the NACA 23012 airfoil data, the low-speed maximum lift coefficient is

$$C_{l\max} = 1.361$$

The wing maximum lift coefficient is then found using the equation below,

$$C_{L\max} = \left[\frac{C_{L\max}}{C_{l\max}}\right] C_{l\max} + \Delta C_{L\max} \qquad Eq. (2.26)$$

Since this is a low-speed condition ($M < 0.2$), $\Delta C_{L\max} = 0$. Substituting,

$$C_{L\max} = 0.9(1.361) = 1.23$$

Now, using the equation below, the stall angle is calculated:

$$\alpha_s = \frac{C_{L\max}}{C_{L\alpha}} + \alpha_{0L} + \Delta\alpha_{C_{L\max}} \qquad Eq. (2.27)$$

With $C_{L\alpha} = 4.64 \text{ rad}^{-1}$, $\alpha_{0L} = -1.2° = -0.021$ rad,

$$\frac{C_{L\max}}{C_{L\alpha}} = \frac{1.23}{4.64} = 0.265 \text{ rad}$$

The stall angle becomes

$$\alpha_s = 0.265 + -0.021 + 0.021 = 0.265 \text{ rad} = 15.2°$$

This result shows that the wing stalls near 15°, which is consistent with the expected behavior of the NACA 23012 airfoil and provides adequate margin above the trim and cruise operating angles.

4.2.5.4 The Lift Curve

With the calculated values from the previous sections, the complete C_L–α curve for the clean wing can be assembled, as shown in figure 2.5.4:

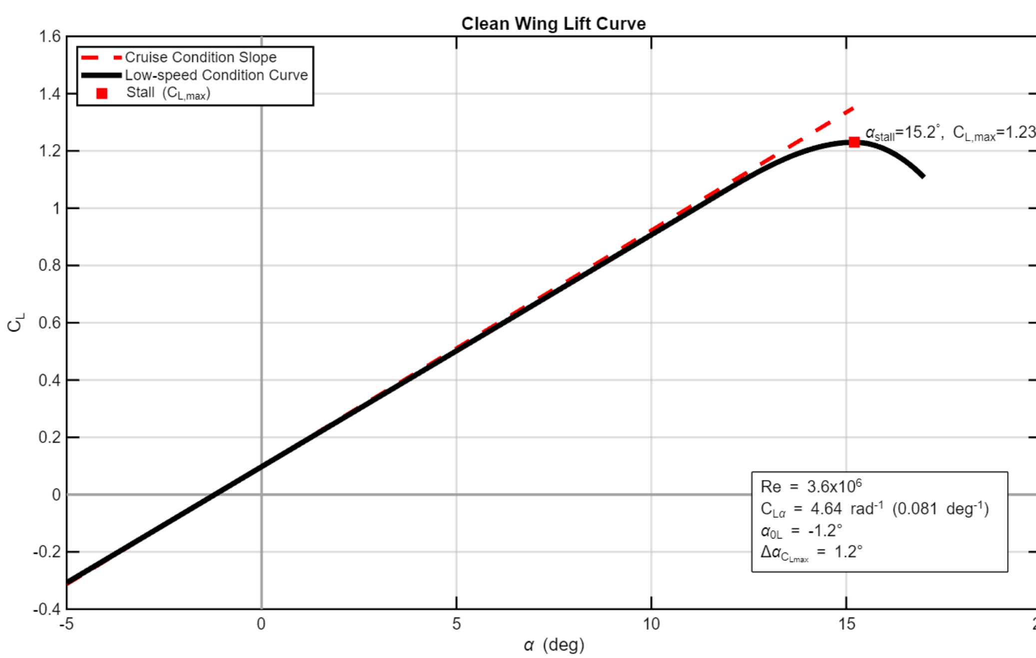

Figure 2.5.4: Complete $C_L - \alpha$ Lift Curve Slope for Proposed Clean Wing

4.3 High Lift Device

The clean-wing analysis in the previous section showed that the maximum lift coefficient of the wing is $C_{L\max} = 1.23$, which is below the lift levels required for both landing and take-off. Assignment 2 specifies a required landing lift coefficient of approximately $C_{L,land} = 2.2$ and a take-off requirement of $C_{L,TO} = 2.0$. The deficit between the clean-wing performance and these operational needs confirms that dedicated high-lift devices are required. These devices must increase the maximum lift coefficient of the wing while maintaining suitable stall margins and controllability throughout the low-speed envelope.

To meet these performance objectives, the high-lift system must generate a $\Delta C_{L\max}$ sufficient enough to raise the total lift capability to the levels needed for safe approach, rotation, and obstacle-clearance requirements. Trailing-edge flaps and leading-edge devices provide the most effective means of supplying the additional lift. Their use addresses the shortfall in clean-wing $C_{L\max}$ and ensures the aircraft can satisfy regulatory stall-speed, take-off-distance, and landing-distance criteria with adequate safety margin.

In the following subsections, the required lift increments for take-off and landing are quantified, and suitable high-lift device configurations are selected based on their aerodynamic effectiveness, mechanical simplicity, and compatibility with our wing structure.

4.3.1 Take-off and Landing Conditions

Based on the required landing lift coefficient of $C_{L,land} = 2.2$ and the clean-wing maximum lift coefficient of $C_{L\max} = 1.23$, the high-lift devices must provide an increment of

$$\Delta C_{L\max,land} = 2.2 - 1.23 = 0.97$$

A margin of 10% should also be added to avoid reaching the required $C_{L,max}$ on the verge of stalling, therefore the high-lift devices should provide an increment of 1.06 during landing. This increase ensures the aircraft can achieve the stall-speed and approach-speed requirements established in Assignment 2 while maintaining adequate stall margin during landing. For take-off, the required lift coefficient is assumed to be $C_{L,TO} = 2.0$, which gives

$$\Delta C_{L\max,TO} = 2.0 - 1.23 = 0.73$$

Because flaps are typically deployed only partially during take-off to limit drag, the full $\Delta C_{L\max}$ generated at landing will not be available. A partial-deflection configuration must therefore still supply at least 0.73 of lift increment for safe rotation and obstacle-clearance performance, and with a 10% margin, the partial-deflection must supply at least 0.8 of lift increment for added safety and necessary performance.

These required values confirm that the clean wing alone cannot meet the take-off and landing performance objectives. The high-lift system must provide most of the lift augmentation, with trailing-edge devices contributing the majority of the $\Delta C_{L\max}$. Leading-edge devices may also be used to improve stall margins and delay flow separation near the root, ensuring predictable handling during low-speed operations, but for mechanical simplicity and the use of a thin wing, only trailing-edge devices will be utilized.

4.3.2 High-Lift Device Selection

To obtain the required increase in maximum lift coefficient, the high-lift system must be selected to generate most of the total $\Delta C_{L\max}$ identified in the previous section. Trailing-edge devices provide the primary lift enhancement, and for this aircraft, single-slotted Fowler flaps have been chosen. Fowler flaps are widely used on general-aviation aircraft due to their ability to deliver a large $\Delta C_{L\max}$ while operating effectively over a broader angle-of-attack range than simple plain flaps.

At landing, the required lift increment is $\Delta C_{L\max,land} = 1.06.$ A single-slotted Fowler flap system is potentially capable of providing lift increments in this range when fully deployed, while maintaining favorable stall progression and predictable handling characteristics near the low-speed limits. For take-off, the flaps will be deployed only partially to reduce drag. Even at partial deflection, Fowler flaps typically provide 60–80% of their full $\Delta C_{L\max}$, which should be sufficient to reach the required $\Delta C_{L\max,TO} = 0.80$.

In the next section, only trailing-edge high-lift devices are assumed. A single-slotted Fowler flap system might prove the required increases in maximum lift for both landing and take-off without the need for additional leading-edge treatments. Fowler flaps are well suited for general-aviation aircraft because they significantly increase camber while also translating aft to enlarge the effective wing area, yielding large lift increments with predictable stall behavior. When properly sized, they provide the full landing lift increment and 60–80% of that benefit at partial deflection for take-off. By relying solely on trailing-edge Fowler flaps and together with appropriate flap span, chord ratio, and moderate wing washout, the aircraft maintains stable aileron effectiveness and a root-first stall progression without the added complexity, weight, or maintenance of slats or other leading-edge devices.

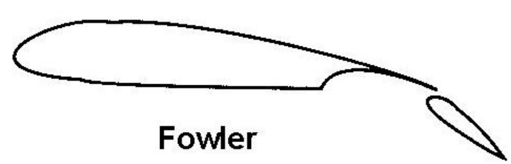

Figure 3.2.1: Example of a single-slotted Fowler flap system

4.3.3 Device Sizing

The required increase in maximum lift coefficient provided by the high-lift system is determined using Equation 3.1:

$$\Delta C_{Lmax} = 0.9\, \Delta C_{lmax} \left(\frac{S_{wf}}{S}\right) \cos\left(\Lambda_{hinge}\right) \qquad Eq.\ (3.1)$$

Here, ΔC_{Lmax} is the required wing lift increment from Section 3.1, ΔC_{lmax} is the sectional lift increment created by the devices, S_{wf}/S is the ratio of flapped wing area to total wing area, and Λ_{hinge} is the sweep angle of the hinge line. It should be clarified that S_{wf} is the flapped wing area, the portion of the wing's trapezoidal surface that is covered by the high-lift device. It is not the area of the flap itself, but the wing surface area over which the flap operates. Figure 3.3.1 visualizes the definition of S_{wf}.

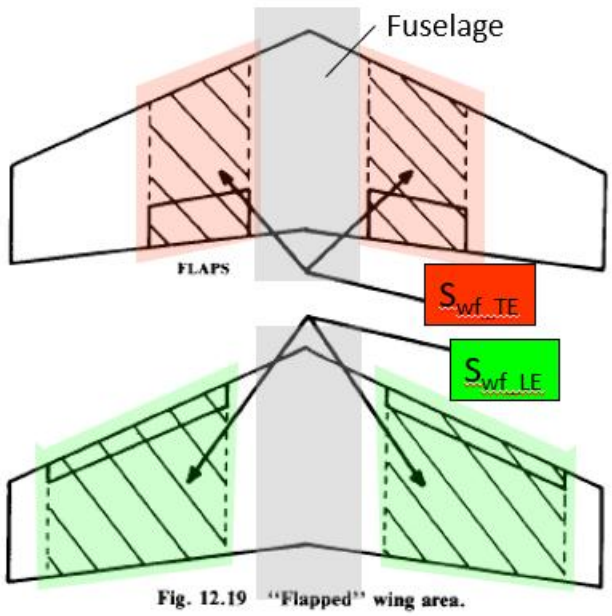

Figure 3.3.1: Visualization of S_{wf}

The hinge-line sweep is computed based on the flap actuation point. Using a typical rear spar location for general aviation aircraft at 0.60c and placing the hinge at 0.65c for mechanism clearance gives a hinge sweep of approximately $\Lambda_{hinge} \approx -8.5°$.

The Fowler flap sectional lift increment, $\Delta C_{l_{max}}$ is defined by the value of c'/c, the ratio of the extended flap chord to the clean wing chord. This ratio is obtained from Figure 3.3.2:

High lift device	ΔC_{lmax} **(fully deployed)**
TE devices (flaps)	
Plain and split	0.9
slotted	1.3
fowler	1.3 c'/c
Double slotted	1.6 c'/c
Triple slotted	1.9 c'/c
LE devices	
Fixed slot	0.2
Leading edge flap	0.3
Kruger flap	0.3
Slat	0.4 c'/c

Figure 3.3.2: Lift Contributions of High-Lift Devices

The values of $\frac{\Delta c}{c_f}$ can be estimated with figure 3.3.3, which estimates change in chord length per flap length based on deflection for multiple different types of flaps:

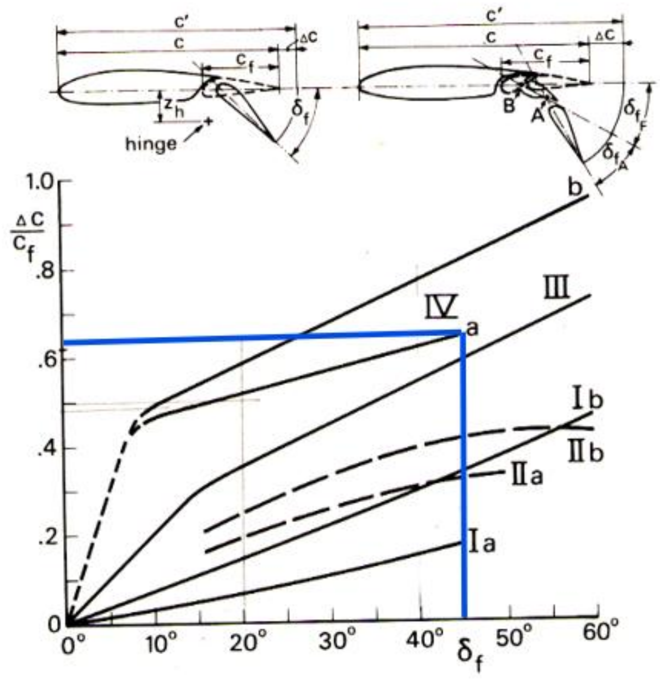

Figure 3.3.3: $\frac{\Delta c}{c_f}$ Estimation Based on Flap Deflection and Types

For a flap deflection of 40°, curve IV_a corresponds to a single Fowler flap and gives

$$\frac{\Delta c}{c_f} = 0.64$$

Using a flap chord fraction of $c_f = 0.35c$, the dimensional increase becomes

$$\Delta c = 0.64(0.35c) = 0.22c$$

Adding the baseline chord gives

$$\frac{c'}{c} = 1 + \Delta c = 1.22$$

Using Figure 3.3.2, a value of

$$\Delta C_{lmax} = 1.6$$

is obtained for a single-slotted Fowler flap at this chord-ratio and deflection. Substituting into Equation 3.1 and solving for S_{wf},

$$S_{wf} = S\left(\frac{\Delta C_{Lmax}}{0.9\,\Delta C_{lmax}\cos\left(\Lambda_{hinge}\right)}\right) \qquad Eq.\ (3.2)$$

Using $\Delta C_{Lmax,land} = 1.06$, $\Delta C_{lmax} = 1.6$, $\Lambda_{hinge} = -8.5°$, and $S = 14.52\ \text{m}^2$,

$$S_{wf} = 14.52\left(\frac{1.06}{(0.9)(1.6)\cos(-8.5°)}\right) = 10.81\ \text{m}^2$$

This corresponds to roughly 74% of the wing area, which is not feasible on aircraft due to the existence of the fuselage and ailerons. Therefore, trailing-edge flaps alone cannot supply the required increase in maximum lift coefficient, and additional lift must come from the leading edge. Suitable leading-edge high-lift devices are introduced to offload the trailing-edge system and bring the total ΔC_{Lmax} to the required value.

A slat is implemented into the leading edge. But since most of the leading edge will have slats on it (0.75 $\frac{S_{wf}}{S}$), we much calculate the slats effect on the ΔC_{Lmax} and plan the trailing edge devices accordingly. At 30° and a c_f value of 0.15c to allow for the front spar, the $\frac{c'}{c}$ can be found using curve III as 1.07, and therefore, the value of $\Delta C_{lmax} = 0.426$. This leads to a ΔC_{Lmax} value of approximately 0.287, which is normally significantly less than the effect of the trailing edge high-lift devices. This means that for landing, the trailing edge devices must supply a ΔC_{Lmax} value of approximately 0.773 for landing configuration and safety margin.

Working backwards from equation 3.1, if $\Delta C_{Lmax} = 0.773$, the required value for $\Delta C_{lmax} * \frac{S_{wf}}{S} = 0.87$. We can then assume a reasonable and feasible value of 55% for $\frac{S_{wf}}{S}$ leading to a required

ΔC_{lmax} value of 1.57. Utilizing Fowler flaps and a c_f of 0.35c, a $\frac{\Delta c}{c_f}$ value of 0.6 must be achieved. This is possible by having a reasonable flap deflection angle of approximately 40°.

This means that incorporating Fowler flaps at a 40° deflection angle, along with a c_f of 0.35c to make room for the rear spar and a 55% ratio of flapped wing area to overall wing area, leads to a ΔC_{Lmax} of approximately 0.773, while a leading-edge slat with a 30° deflection angle, c_f of 0.15, and 75% ratio of flapped to overall wing area leads to a ΔC_{Lmax} of approximately 0.287. Together, they provide the necessary ΔC_{Lmax} of 1.06 at landing. At take-off the Fowler flaps are partially deployed meaning a 70% value of ΔC_{Lmax} to reduce drag, which equates to about 0.541. Combined with the slats, this number jumps to approximately 0.83, which is higher than the necessary ΔC_{Lmax} for take-off, 0.80, and provides a larger safety margin than previously applied exceeding expectations. In the next section, the complete $C_{L\alpha}$ curve for flapped wings during take-off and landing will be constructed.

4.3.4 CL-a Curve

With the high-lift devices sized in the previous section, the next step is to determine how flap deployment modifies the aerodynamic characteristics of the wing. The installation of trailing-edge Fowler flaps and leading-edge slats alters both the zero-lift angle of attack and the lift-curve slope, and these modified parameters must be evaluated before generating the full flapped CL–α curves for take-off and landing. The change in zero-lift angle occurs because the flaps increase the effective camber of the airfoil, shifting the airfoil's α_0L to more negative values. The zero-lift shift is computed as

$$\Delta\alpha_{0L} = \Delta\alpha_{0L,\text{airfoil}}\left(\frac{S_{wf}}{S}\right)\cos\Lambda_{\text{hinge}} \qquad Eq. (3.3)$$

where $\Delta\alpha_{0L,\text{airfoil}}$ is taken from standard values (−10° for take-off and −15° for landing), S_{wf}/S is the ratio of flapped area to reference wing area, and Λ_{hinge} is the hinge-line sweep angle determined earlier. The resulting flapped zero-lift angle is then

$$\alpha_{0L,\text{flapped}} = \alpha_{0L,\text{clean}} + \Delta\alpha_{0L} \qquad Eq. (3.4)$$

which defines the horizontal shift of the CL–α curve when the flaps are deployed.

In addition to modifying α_0L, the deployment of Fowler flaps also alters the lift-curve slope because the flaps increase the effective wing area through chord extension. This change must be accounted for when constructing the linear portion of the flapped lift curve. The corrected flapped lift-curve slope is given by

$$C_{L\alpha,\text{flapped}} = C_{L\alpha,\text{clean}}\left(\frac{S'}{S}\right) \qquad Eq. (3.5)$$

where the ratio S'/S represents the increase in wing surface due to the extended chord and is computed as

$$\frac{S'}{S} = 1 + \left(\frac{S_{wf}}{S}\right)\left(\frac{c'}{c} - 1\right) \qquad Eq. (3.6)$$

with c'/c obtained from the flap-type chord-extension chart used during the high-lift device sizing. This formulation ensures that any increase in effective wing area is properly carried into the lift-curve slope calculation. Slats primarily increase C_{Lmax} and do not significantly influence the zero-lift angle, but they may contribute to S′/S if they extend the local chord, which is not the case for our configuration.

Together, these expressions provide the modified aerodynamic parameters necessary to generate the take-off and landing flapped CL–α curves. The adjusted zero-lift angle determines the horizontal placement of each curve, while the increased lift-curve slope governs the steepness of the linear portion. Using these corrected values, we can now construct the complete flapped lift-curve diagrams and identify the resulting C_{Lmax}, α_{stall}, and operational margins for both high-lift configurations, as shown in figure 3.5.1:

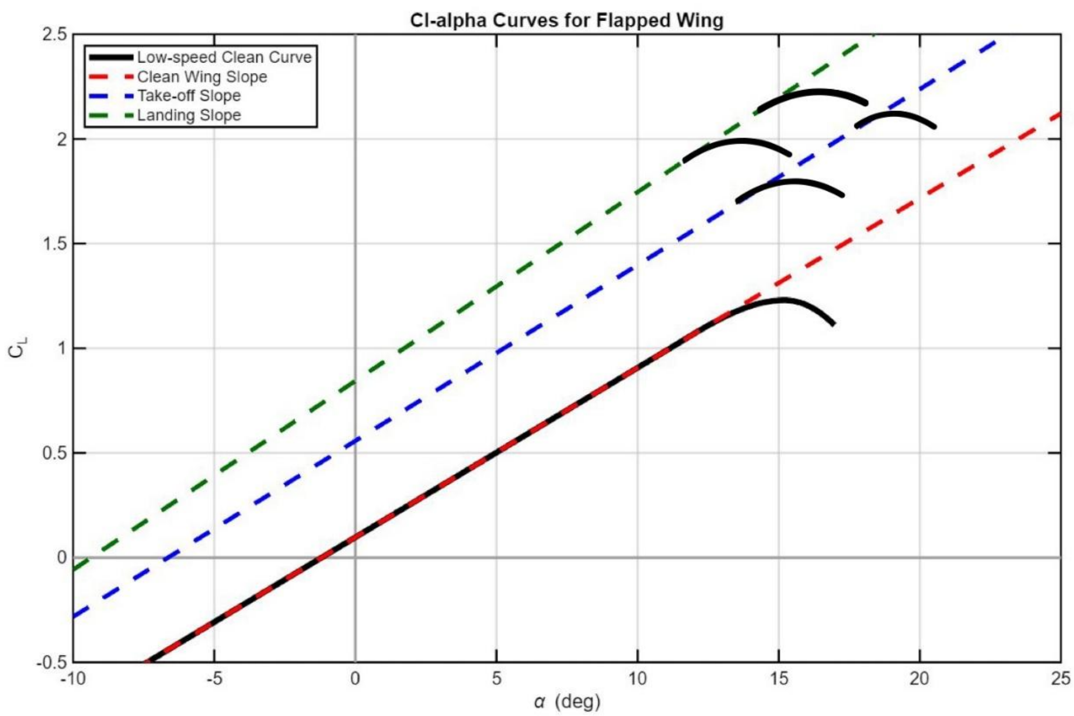

Figure 3.4.1: Flapped Wing C_L-α Curves

Parameter	Takeoff TE	Takeoff TE and LE	Landing TE	Landing TE and LE	Clean Wing	Unit
α_{0L}	-6.64	-6.64	-9.36	-9.36	-1.2	degrees
$C_{L\alpha}$	0.084	0.084	0.0902	0.0902	0.081	CL/degree
C_{Lmax}	1.77	2.06	2.0	2.3	1.23	-
$a\ stall$	15.6	19.1	14.0	17.3	15.2	degrees

Table 3.4.1: Flapped wing parameters

4.4 Fuel Storage

The final step of the wing design is to verify that the internal structure provides sufficient volume to accommodate the required mission fuel without compromising strength or aerodynamic efficiency. From the mission sizing in Assignment 2, the total usable fuel mass required to achieve the maximum design range is approximately 258 kg, which corresponds to a fuel weight of 2,531 N or a total volume of ≈ 0.36 m^3, assuming an aviation-gasoline density of 0.72 kg/L for Avgas 100LL.

The selected wing geometry provides ample internal space for fuel integration. Each half-wing has a semispan of 5.22 m and a trapezoidal planform with a root chord of 1.99 m, a tip chord of 0.80 m, and a mean aerodynamic chord of 1.48 m. With a maximum thickness ratio of t/c = 0.12, the structural box height at the root is approximately 0.26 m and 0.10 m near the tip. The enclosed torque box—bounded by the front and rear spars positioned at 20% and 60% of the chord—extends along the majority of the span, forming the main integral fuel tank volume. Integrating this geometry yields an available volume per wing of roughly 0.21 m^3, or 0.42 m^3 total, which exceeds the required mission-fuel volume by about 6% even after allowing for structure, expansion, systems, and unusable sump fuel.

This configuration allows all fuel to be stored within the wings, eliminating the need for external or fuselage tanks. Locating the fuel outboard of the fuselage provides multiple benefits: it reduces the fuselage bending moment, improves structural load balance, and minimizes trim changes as fuel is consumed. The fuel weight distribution along the span also increases torsional rigidity and dampens gust response, contributing to improved handling characteristics during cruise and descent. Standard wing-integral tanks of this type are easily accessible through removable panels on the upper wing surface for inspection and maintenance, ensuring compliance with FAR 23.963 fuel-system accessibility and sealing requirements.

To maintain a positive head to the engine-driven fuel pump under all flight attitudes, the tanks incorporate a small collector bay near the wing root. This bay includes anti-splash baffles and venting lines to the opposite tank, ensuring consistent fuel feed during coordinated turns or climbing and descent maneuvers. Venting outlets are positioned on the underside of each wingtip to balance pressure and prevent vapor lock. Drain points and fuel-quantity senders are installed at the lowest points of the tank cells, with provisions for fuel sampling during preflight inspection.

The structural weight impact of the integral tanks is minimal because the main spars already define the load path required for the wing bending moment. Only local reinforcement around access panels and rib openings is necessary. The added mass of sealing compound and fittings is estimated at less than 1% of the wing structural weight, a negligible penalty relative to the simplicity and aerodynamic cleanliness of the configuration.

In summary, the designed NACA 23012 wing possesses more than adequate internal capacity to store the entire mission fuel load within the main structural box. The integral wing-tank arrangement ensures proper weight distribution, simplifies refueling and maintenance, and avoids the drag and complexity associated with external pods or fuselage bladders. Therefore, the existing wing geometry fully satisfies the fuel-storage requirement for our aircraft without modification.

5 Center of Gravity and Tail Design

5.1 Introduction

In this stage, the stability, control, weight, and balance of the designed general aviation aircraft are analyzed. The tail surfaces are first sized using the V-bar method based on reference data from comparable light aircraft. The resulting tail geometry is then used to calculate the load factors from the combined maneuver and gust V-n diagram, which defines the ultimate design load factor for the structure. Using this load factor, the aircraft's operational empty weight and center of gravity are refined through a Class II weight estimation. The center of gravity travel is evaluated through loading diagrams for various payload and fuel conditions, and the effect of wing position on stability limits is examined. Finally, the scissor plot is generated to assess the longitudinal stability and controllability of the configuration, ensuring that the design satisfies the static margin and control requirements for safe operation.

5.2 Load Factor

The load factor (n) defines the ratio of the total lift acting on an aircraft to its weight, and it quantifies the structural stresses experienced during flight. Because aircraft regularly undergo accelerations greater or less than 1G during maneuvers, gusts, or turbulence, determining these load factors is essential for ensuring structural integrity and compliance with airworthiness standards. According to CS-23/CS-25 regulations, the limits of these loads are expressed through the V–n diagram, which outlines the operational envelope of the aircraft. The upper and lower boundaries of this diagram represent the maximum positive and negative limit load factors, while the intersections with the stall curves define the boundaries of safe flight. The greater of the maneuvering or gust loads, multiplied by a safety factor of 1.5, yields the ultimate load factor ($n_{(ult)}$) used in the Class II structural weight estimation and component sizing. Constructing the V–n diagram therefore establishes the critical input for determining structural weight groups and validating that the aircraft can safely sustain all expected aerodynamic loads throughout its mission.

5.2.1 Maneuver Loading

The maneuver loading defines the portion of the V–n diagram produced by pilot-controlled accelerations. It represents the range of aerodynamic loads that the structure must withstand during normal flight maneuvers such as pull-ups and push-overs. The load factor in this region is determined from the stall-limited relation

$$n(V) = \frac{q\, C_{L,max}}{\frac{W}{S}}, \qquad Eq. (2.1)$$

where q is the dynamic pressure defined as $\frac{1}{2}\rho V^2$, V is the true airspeed, $C_{L,\max}$ is the maximum lift coefficient, and W/S is the wing loading. This relation defines the curved boundaries of the maneuver envelope where the wing reaches its maximum lift capability and stalls.

For our aircraft, a wing loading of 920 $\frac{N}{m^2}$, a maximum lift coefficient of 2.4, and a standard sea-level density of 1.225 $\frac{kg}{m^3}$ are used. These parameters define the positive stall-limited curve of the V–n diagram. The negative maximum loading is taken as –0.4 times the corresponding positive value, which gives a realistic representation of the negative stall boundary for a conventional light aircraft.

The structural limit load factors for a normal-category airplane are +3.8 g for positive loading and −1.52 g for negative loading. Since the calculated positive value slightly exceeds the certification maximum, the regulatory limit of +3.8 g is used as the upper boundary of the envelope.

These positive and negative limits define the maneuver envelope that will later be combined with the gust loading to generate the complete operational V–n diagram. This combined diagram establishes the total load factors used in the subsequent structural weight estimation and stability analysis.

5.2.2 Gust Loading

The gust loading defines the additional aerodynamic forces produced when the aircraft encounters a vertical gust of air. These unsteady loads act instantaneously on the wing and can significantly increase or decrease the overall load factor experienced by the structure. Unlike the maneuver loads, which are generated by pilot input, gust loads depend on the atmospheric turbulence intensity and the aircraft's aerodynamic characteristics. The total load factor at any flight condition is therefore the sum of the steady 1 g flight load and the incremental load caused by the gust.

The incremental load factor due to a vertical gust is determined using

$$\Delta n = \frac{\rho V C_{L_a} K \hat{u}}{2(W/S)}, \qquad Eq.(2.2)$$

where $\hat{u}$ is the gust velocity, V is the true airspeed, K is the load alleviation factor and C_{L_a} is how much the wing's lift coefficient changes with angle of attack. The variable, K, can be determined by

$$K = \frac{0.88\,\mu}{5.3 + \mu}, \text{ with } \mu = \frac{2(W/S)}{\rho\, g\bar{c}C_{L_a}}. \qquad Eq.(2.3)$$

Here μ is the mass ratio parameter, ρ is the air density, and $\bar{c}$ is the mean aerodynamic chord of the wing. These equations quantify how a sudden change in the local flow angle from a vertical gust increases or decreases the lift and consequently the load factor.

For the gust calculations, the standard statistical gust magnitudes $\hat{u}$ are used for the three design conditions: high angle of attack , level flight, and dive. These values are:

$$\hat{u}_{\text{highAoA}} = 20.1 \text{ m/s (=66 ft/s)}, \qquad \hat{u}_{\text{level}} = 15.2 \text{ m/s (=50 ft/s)}, \qquad \hat{u}_{\text{dive}} = 7.6 \text{ m/s (=25 ft/s)}.$$

These gust velocities represent typical vertical air disturbances encountered at low altitude, cruise altitude, and dive conditions, respectively, and are used to determine the incremental load factors at each flight regime.

	High AoA	Cruise	Dive	Units
V	45.63	77.2	81.06	m/s
Altitude	0	2440	1500	m
$\hat{u}$	20.1	15.2	7.6	m/s
ρ	1.225	1.006	1.058	Kg/m^3
μ	23.25	27.03	25.70	
K	0.717	0.736	0.729	
C_{L_a}	4.45	4.66	4.66	rad^{-1}
n+	3.162	3.412	2.370	Gs
n-	-1.162	-1.412	-0.370	Gs

Table 2.1: Gust Loading Analysis Values

5.2.3 Combined Loading

The maneuver and gust load analyses are integrated to develop the aircraft's complete flight envelope. The maneuver loads represent steady aerodynamic conditions that define the positive and negative structural limits, while the gust loads capture the transient effects of atmospheric disturbances. By combining these two cases, the resulting V–n diagram, shown in Figure 2.2, illustrates the operational boundaries for both normal and extreme flight conditions. This ensures that the aircraft structure can safely sustain all expected combinations of aerodynamic and gust-induced forces encountered during service.

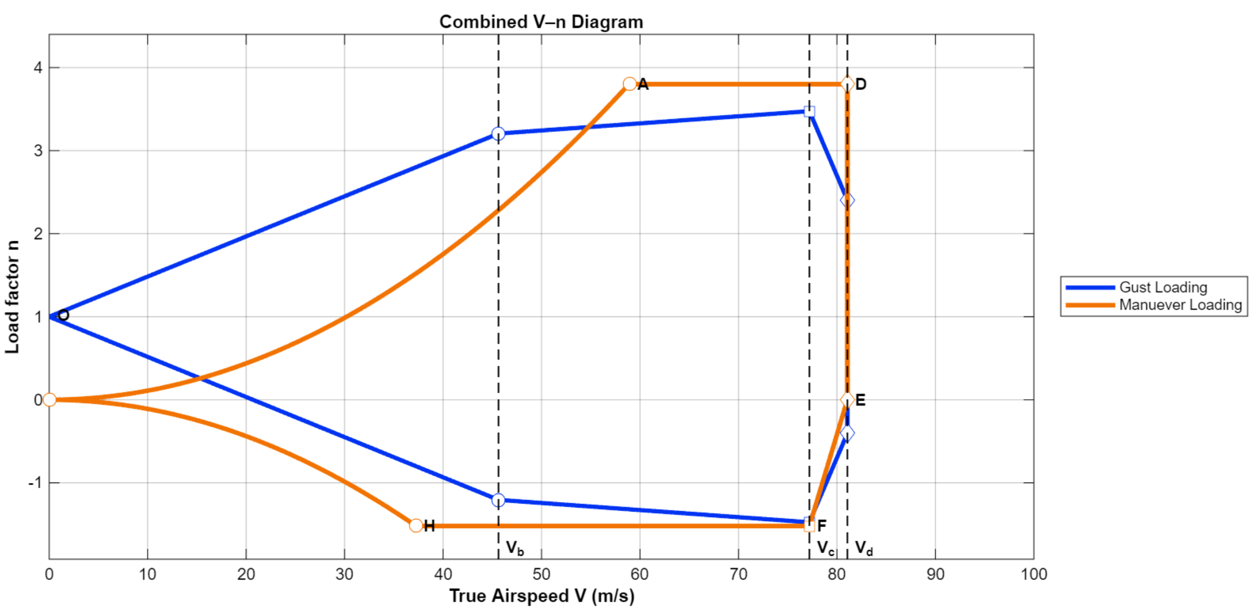

Figure 2.1: Combined Gust and Load Factor V-n Diagram

The O–A line represents the region where the aircraft's positive load factor increases from level flight to the maximum limit load. As the airspeed increases from stall speed, the lift generated by the wings grows with the square of the velocity. This curve is limited by the stall condition at low speeds and transitions to a constant limit at point A, where the structural load factor limit of the aircraft is reached. Beyond this point, additional speed no longer increases load factor because the aircraft structure cannot safely sustain higher loads.

The A–D segment defines the constant positive load limit of the aircraft. Here, the structure experiences the maximum allowable positive load factor (typically $n = +3.8$ for a normal-category aircraft). As speed continues to increase up to the dive velocity V_d, the aircraft is restricted to this same maximum load, creating a horizontal line on the V–n diagram. Point D marks the intersection of the positive limit load with the maximum operating speed and represents the upper-right boundary of the flight envelope.

The O–H curve corresponds to the negative stall region, where the aircraft can produce downward lift (negative load factor) at low speeds. Similar to the positive stall region, this portion is governed by the maximum negative lift the wing can produce before stalling in an inverted or nose-down condition. The line ends at point H, where the structural negative load limit (here $n = -1.52$) is first reached.

The H–F line indicates the constant negative load factor region. Between points H and F, the aircraft sustains the maximum permitted negative load factor. Increasing airspeed beyond this range does not increase the negative load, as the aircraft structure would be at its limit. Point F, located at the cruise velocity V_c, marks the end of this constant region.

Finally, the F–E line shows the recovery region of the negative envelope. As speed increases beyond the cruise velocity up to the dive velocity V_d, the allowable negative load factor is linearly reduced to zero at point E. This sloped line represents the gradual unloading of the aircraft structure as the aerodynamic loads decrease toward the boundary of safe operation. Points D and E together form the extreme ends of the maneuver envelope, beyond which flight is structurally unsafe.

The stall speed of the aircraft can also be identified directly from the maneuver envelope. In this diagram, point H occurs at an airspeed of 37.2 m/s, which corresponds to the speed at which the aircraft first reaches the negative structural limit load factor of –1.52. This indicates that, when operating in the negative-lift condition, the wing will stall at approximately 37.2 m/s, showing how the stall speed has increased slightly due to the higher load requirements at the negative limit.

The maximum design (limit) load used for structural sizing is taken as the larger of the maneuver and gust maxima, and the ultimate load is obtained by applying the safety factor of 1.5.

Therefore, the ultimate positive load factor is

$$N_{ult,+} = 1.5\, N_{\max} = 1.5 \times 3.8 = +5.70.$$

Similarly, for the negative side the governing limit is $N_{\min} = -1.52$ and the ultimate negative load is

$$N_{ult,-} = 1.5 \times (-1.52) = -2.28.$$

These ultimate load factors ($N_{ult,+} = +5.70$, $N_{ult,-} = -2.28$) are the values to be used in the Class-II structural weight estimation and component sizing

5.3 Tail Plane Geometry

In this section, the $\bar{V}$ method is applied to determine the initial sizing of the horizontal and vertical tail surfaces. The aircraft uses a conventional tail configuration, with the stabilizers attached to the rear fuselage section. The $\bar{V}$ method estimates the required tail dimensions by comparing the volume coefficients of similar general aviation aircraft, which share comparable aerodynamics and stability. This approach provides a practical first estimate of the tail area and moment arms needed to achieve adequate longitudinal and directional stability. While this method does not account for configuration-specific aerodynamics, it establishes the baseline geometry for the upcoming Class II weight estimation and scissor-plot stability analysis.

5.3.1 Horizontal Tail

The horizontal tail is sized using the $\bar{V}$ method, which relates the tail area, tail arm, and wing geometry through the horizontal tail volume coefficient. The coefficient is expressed as

$$\bar{V}_h = \frac{S_h\, l_h}{S\, \bar{c}} \qquad Eq.\ (3.1)$$

where S_h is the horizontal tail area, l_h is the tail arm measured from the wing aerodynamic center to the tail aerodynamic center, S is the wing area, and $\bar{c}$ is the mean aerodynamic chord.

To select an appropriate horizontal tail volume coefficient, similar four-seat general aviation aircraft were reviewed. These reference aircraft share comparable mission requirements and aerodynamic layouts, making them suitable for statistical comparison. The corresponding horizontal tail coefficients and surface areas are summarized in Table 3.1.

Aircraft	$\bar{V}_h$	$S_h\ (m^2)$
Cessna 182 Skylane	0.74	4.05
Cirrus SR20	0.78	4.20
Diamond DA40 NG	0.72	3.95
Mooney M20J	0.76	4.10

Table 3.1 Horizontal Tail Volume Estimation References

The average coefficient and tail area from these reference aircraft were adopted for this design. Using

$\bar{V}_h = 0.75$ and $S_h = 4.08\,\mathrm{m}^2$, along with the aircraft parameters $S = 14.52\,\mathrm{m}^2$ and $\bar{c} = 1.48\,\mathrm{m}$, the tail arm can be determined by rearranging Eq. (3.1):

$$l_h = \frac{V_h\, S\, \bar{c}}{S_h} \qquad Eq.\ (3.2)$$

$$l_h = \frac{0.75 \times 14.52 \times 1.48}{4.08} = 3.95\ \mathrm{m}$$

This results in a horizontal tail arm of approximately 3.95 m, which is consistent with typical tail placements for light, low-wing aircraft. The derived values ensure adequate longitudinal stability and provide a baseline for subsequent Class II weight estimation and stability analysis.

In addition to the tail arm and area sizing, other geometric characteristics must be established to define the complete horizontal stabilizer layout. The aspect ratio, taper ratio, sweep angle, and thickness ratio determine the aerodynamic efficiency and structural properties of the tail. For light general-aviation aircraft, an aspect ratio of approximately 6.0 provides a balance between lift effectiveness and structural stiffness. Using the previously calculated tail area $S_h = 4.08\,\mathrm{m}^2$ and aspect ratio $AR_h = 6.0$, the horizontal tail span is

$$b_h = \sqrt{AR_h\, S_h} \qquad Eq.\ (3.3)$$

$$b_h = \sqrt{6.0 \times 4.08} = 4.95\ \mathrm{m}$$

A taper ratio of $\lambda_h = 0.40$ is selected to reduce aerodynamic tip losses while maintaining structural simplicity. For a trapezoidal planform, the root and tip chords are related by

$$S_h = \frac{(c_{r,h} + c_{t,h})}{2}\, b_h \qquad Eq.\ (3.4)$$

$$c_{t,h} = \lambda_h\, c_{r,h} \qquad Eq.\ (3.5)$$

Solving for the root and tip chords yields

$$c_{r,h} = \frac{2S_h}{(1 + \lambda_h) b_h} = \frac{2 \times 4.08}{(1 + 0.4) \times 4.95} = 1.18\ \mathrm{m}$$

$$c_{t,h} = 1.18 \times 0.4 = 0.47\ \mathrm{m}$$

A quarter-chord sweep of 5° is applied to provide proper aerodynamic balance at higher speeds and is kept low since there won't be shock-induced separation to postpone at the low-speeds that our aircraft operates at. The thickness-to-chord ratio is chosen as $t/c = 0.11$, which balances sufficient structural depth while minimizing drag.

The elevator occupies roughly 25 percent of the horizontal tail area, giving an elevator surface of approximately $S_{elev} = 1.02\ \mathrm{m}^2$. The stabilizer is positioned slightly ahead of the vertical tail intersection to reduce interference between the two surfaces and to keep the control linkage compact.

The resulting horizontal-tail geometry defines a conventional low-tail configuration appropriate for a four-seat light aircraft. These parameters establish the baseline required for the subsequent weight, balance, and stability analyses.

5.3.2 Vertical Tail

Similar to the horizontal tail, the vertical tail is sized using the $\bar{V}$ method, which defines the relationship between tail area, tail arm, and wingspan through the vertical tail volume coefficient. This coefficient ensures that the aircraft maintains sufficient directional stability and yaw control throughout the flight envelope. The coefficient is expressed as

$$\bar{V_v} = \frac{S_v\, l_v}{S\, b} \qquad Eq.\ (3.6)$$

where S_v is the vertical tail area, l_v is the distance from the aircraft center of gravity to the aerodynamic center of the vertical tail, S is the wing area, and b is the wingspan.

To determine an appropriate vertical tail volume coefficient, data from reference general aviation aircraft were reviewed. These aircraft have similar configurations and mission requirements, making them suitable for comparison. The resulting coefficients and tail surface areas are summarized in Table 3.2.

Aircraft	$\bar{V_v}$	$S_v\ (m^2)$
Cessna 182 Skylane	0.045	2.00
Cirrus SR20	0.050	2.10
Diamond DA40 NG	0.040	1.95
Mooney M20J	0.047	2.05

Table 3.2 Vertical Tail Volume Estimation References

From the average values, $V_v = 0.046$ and $S_v = 2.03\ \mathrm{m}^2$ were selected for this design. Substituting $S = 14.52\ \mathrm{m}^2$ and $b = 10.43$ m into Eq. (3.6), the tail arm is determined as

$$l_v = \frac{\bar{V_v}\, S\, b}{S_v} \qquad Eq.\ (3.7)$$

$$l_v = \frac{0.046 \times 14.52 \times 10.54}{2.03} = 3.43\ \mathrm{m}$$

This yields a vertical tail arm of approximately 3.43 m, consistent with the placement of the horizontal tail and ensuring balanced directional stability. An aspect ratio of 1.7, taper ratio of 0.6, and quarter-chord sweep of 5° are applied to maintain structural strength while achieving sufficient aerodynamic control authority. The thickness-to-chord ratio is set at $t/c = 0.10$, and the rudder occupies approximately 25% of the total vertical tail area.

The remaining geometric parameters of the vertical tail are determined using the same relations as before:

$$b_v = \sqrt{AR_v S_v} \qquad \text{Eq. (3.8)}$$

$$C_{r,v} = \frac{2S_v}{b_v(1+\lambda_v)} \qquad \text{Eq. (3.9)}$$

$$C_{t,v} = \lambda_v C_r \qquad \text{Eq. (3.10)}$$

Substituting the known values gives a span $b_v = 1.86$ m, a root chord $C_{r,v} = 1.37$ m, and a tip chord $C_{t,v} = 0.82$ m. The mean aerodynamic chord is found from

$$\bar{c}_v = \frac{2}{3} C_r \frac{1 + \lambda_v + \lambda_v^2}{1 + \lambda_v} \qquad \text{Eq. (3.11)}$$

which gives $\bar{c}_v = 1.12$ m. These values provide a well-proportioned vertical stabilizer with adequate rudder depth and a realistic shape for a light general aviation aircraft.

These parameters define a conventional single-fin tail arrangement appropriate for a four-seat general aviation aircraft and provide the necessary yaw stability and control margins for later verification in the scissor plot analysis.

5.4 OEW Estimation using Class II Method

The Class II weight estimation builds on the geometric and aerodynamic data developed in previous sections. Unlike Class I methods, which rely solely on statistical trends and mission requirements, Class II methods use the actual dimensions and load factors of the aircraft to estimate individual component weights. This allows for a more accurate determination of the operational empty weight (OEW).

Raymer's Class II approach is adopted for this design. The method divides the aircraft into major structural and systems groups, allowing each to be estimated from its geometry, load factor, and material characteristics. These groups include the wing, horizontal tail, vertical tail, fuselage, landing gear, propulsion system, and aircraft systems. The sum of these groups provides the aircraft's total empty weight.

The following subsections apply the Class II weight estimation relations to each component group using the current design parameters and the ultimate load factor obtained in Section 2. The calculated OEW is then compared with the value obtained in the preliminary sizing stage to verify consistency within acceptable limits.

5.4.1 Wing Group Weight Estimation

The wing structural weight is estimated using Raymer's empirical expression for general aviation wings. The relation is

$$W_{wing} = 0.036\, S_w^{0.758}\, W_{fw}^{0.0035} \left(\frac{A}{\cos^2 \Lambda}\right)^{0.6} q^{0.006} \lambda^{0.04} \left(\frac{100\, t/c}{\cos \Lambda}\right)^{-0.3} (N_z W_{dg})^{0.49} \qquad \text{Eq. (4.1)}$$

where the variables are defined as in the Raymer notation. The following table lists the values available from Assignment 2 or from previous sections, converted to the units required by the empirical equation.

Variable	Symbol	Value	Units
Design takeoff weight	W_{dg}	13354	N
Ultimate load factor	N_z	5.70	-
Wing area	S_w	14.52	m^2
Aspect ratio	A	7.5	-
Dynamic pressure at cruise	q	2997.8	Pa
Taper ratio	λ	0.40	-
Thickness-to-chord ratio	t/c	0.12	-
Wing fuel weight	W_{fw}	2531	N
Quarter-chord sweep	Λ	-3.3	deg

Table 4.1: Wing weight variable values

The design parameters are converted to imperial units for consistency with Raymer's empirical constants: $S_w = 156.29\ \text{ft}^2$, $W_{dg} = 3{,}002$ lbf, $W_{fw} = 568.99$ lbf, and $q = 62.61\ \text{lb/ft}^2$. Substituting these values into Eq. (4.1) gives

$$W_{wing} = 0.036(156.29)^{0.758}(568.99)^{0.0035}\left(\frac{7.5}{(\cos(0))^2}\right)^{0.6}(62.61)^{0.006}(0.40)^{0.04}\left(\frac{100(0.12)}{\cos(0)}\right)^{-0.3}(5.70 \times 3002)^{0.49}$$

Evaluating this expression yields

$$W_{wing} = 315.8\ \text{lbf} = 1{,}404.7\ \text{N}$$

which corresponds to a structural wing weight of 143 kg.

This result represents the load-carrying structure of the wing, including the spars, ribs, and skin, but excluding the internal fuel system and carry-through structure. This value establishes the baseline for subsequent Class II component weight calculations in the operational empty weight estimation.

5.4.2 Horizontal Stabilizer Weight Estimation

The horizontal stabilizer structural weight is estimated using Raymer's empirical expression for general aviation aircraft. The relation is

$$W_{ht} = 0.016\,(N_z W_{dg})^{0.414}\, q^{0.168}\, S_{ht}^{0.896} \left(\frac{100\, t/c}{\cos \Lambda_{ht}}\right)^{-0.12} \left(\frac{A_{ht}}{\cos^2 \Lambda_{ht}}\right)^{0.043} \lambda_h^{-0.02} \qquad Eq.\ (4.2)$$

where the variables are defined as in Raymer's notation. The following table lists the values from Assignment 2 and previous sections, converted to the units required by the empirical equation.

Variable	Symbol	Value	Units
Design takeoff weight	W_{dg}	13354	N
Horizontal tail area	S_{ht}	4.08	m^2
Ultimate load factor	N_z	5.70	-
Dynamic pressure at cruise	q	2997.8	Pa
Aspect ratio	A_{ht}	6	-
Horizontal taper ratio	λ_h	0.40	-
Thickness-to-chord ratio	t/c	0.11	-
Quarter-chord sweep	Λ_{ht}	5	deg

Table 4.2: Horizontal tail variable values

The design parameters are converted to imperial units for consistency with Raymer's empirical constants: $S_{ht} = 43.92$ ft^2, $W_{dg} = 3{,}002$ lbf, and $q = 62.61$ lb/ft^2. Substituting these values into Eq. (4.2) gives

$$W_{ht} = 0.016(5.70 \times 3002)^{0.414}(62.61)^{0.168}(43.92)^{0.896}\left(\frac{100(0.11)}{\cos(5)}\right)^{-0.12}\left(\frac{6}{\cos^2 5}\right)^{0.043}(0.40)^{-0.02}$$

Evaluating this expression yields

$$W_{ht} = 44.34 \text{ lbf} = 197.2 \text{ N}$$

which corresponds to a structural horizontal-tail weight of 20.11 kg.

This result represents the load-carrying structure of the horizontal stabilizer, including spars, ribs, and skin, but excluding the control actuators and attachment fittings. The calculated weight serves as the baseline for the Class II component weight estimation in the overall operational empty weight analysis.

5.4.3 Vertical Stabilizer Weight Estimation

The structural weight of the vertical tail is estimated using Raymer's empirical equation for general aviation aircraft:

$$W_{vt} = 0.073(1 + 0.2\frac{H_t}{H_v})(N_z W_{dg})^{0.376} q^{0.122} S_{vt}^{0.873} (\frac{100\ t/c}{\cos \Lambda_{vt}})^{-0.49} (\frac{A}{\cos^2 \Lambda_{vt}})^{0.357} \lambda_{vt}^{0.039} \quad Eq. (4.3)$$

where the variables are defined as in Raymer's notation. The following table lists the parameters from previous sections and geometric data of the vertical tail:

Variable	Symbol	Value	Units
Design takeoff weight	W_{dg}	13354	N
Vertical tail area	S_{vt}	2.03	m^2
Ultimate load factor	N_z	5.70	-
Dynamic pressure at cruise	q	2997.8	Pa
Aspect ratio	A_{vt}	1.7	-
Vertical tail taper ratio	λ_h	0.60	-
Thickness-to-chord ratio	t/c	0.10	-
Quarter-chord sweep	Λ_{vt}	5	deg
Tail height ratio	H_t/H_v	1.0	-

Table 4.3: Vertical tail variable values

The parameters are converted to imperial units for substitution into Raymer's formula: $S_{vt} = 21.85$ ft^2, $W_{dg} = 3{,}002$ lbf, and $q = 62.61$ lb/ft^2. The quarter-chord sweep angle gives $\cos\ \Lambda_{vt} = \cos\ 5° = 0.996$. Substituting these values into Eq. (4.3) gives

$$W_{vt} = 0.073(1 + 0.2(1.0))(5.70 \times 3002)^{0.376}(62.61)^{0.122}(21.85)^{0.873}(\frac{100(0.10)}{\cos 5})^{-0.49}(\frac{1.7}{\cos^2 5})^{0.357}(0.60)^{0.039}$$

Evaluating this expression yields

$$W_{vt} = 32.18 \text{ lbf} = 143 \text{ N}$$

which corresponds to a structural vertical-tail weight of 14.57 kg.

This value represents the load-carrying structure of the fin and rudder assembly, including the primary spar and skin, but excluding the control actuators and attachment fittings. It provides the required directional stability and control authority for the aircraft configuration determined in Section 3.2.

5.4.4 Fuselage Structure Weight

The fuselage structural weight is estimated using Raymer's empirical equation for general aviation aircraft:

$$W_f = 0.052 S_f^{1.086} (N_z W_{dg})^{0.177} L^{-0.051} (L/D)^{-0.072} q^{0.241} + W_{press} \quad Eq. (4.4)$$

where W_f is the fuselage structural weight, W_{dg} is the design gross weight, N_z is the ultimate load factor, L is the fuselage length, S_f is the fuselage wetted area, L/D is the fuselage fineness ratio, q is the dynamic pressure, and W_{press} is the pressurization weight term (zero for this unpressurized aircraft).

The fuselage fineness ratio L/D was directly given as 7.5. Using this and the fuselage length, the external diameter D was computed as:

$$D = \frac{L}{L/D} = \frac{8.8}{7.5} = 1.17 \text{ m} \qquad Eq.\ (4.5)$$

The wetted surface area S_f was estimated assuming the fuselage behaves as a slightly tapered circular cylinder. The wetted area is approximated as:

$$S_f \approx 1.05\, \pi D L \qquad Eq. (4.6)$$

The 1.05 factor accounts for additional surface area due to nose and tail curvature. Substituting values:

$$S_f = 1.05\pi(1.17)(8.8) = 34.1 \text{ m}^2$$

The wing–body interference factor K_{ws} depends on the configuration type:

- 0.0–0.2 for high-wing aircraft,
- 0.2–0.35 for low-wing aircraft.

Because this aircraft uses a low-wing configuration, a value of $K_{ws} = 0.25$ is used.

Variable	Symbol	Value	Units
Design takeoff weight	W_{dg}	13354	N
Ultimate load factor	N_z	5.70	-
Fuselage length	L	8.8	m
Fuselage wetted area	S_f	34.1	m^2
Wing-body interference factor	K_{ws}	0.25	-
Fineness ratio	L/D	7.5	-
Dynamic pressure at cruise	q	2997.8	Pa

Table 4.4: Fuselage weight variable values

The parameters are converted to imperial units for substitution into Raymer's formula: $S_f = 34.1 \text{ m}^2 = 367.1 \text{ ft}^2$, $W_{dg} = 3{,}002$ lbf, and $q = 62.61 \text{ lb/ft}^2$. Substituting these values into Eq. (4.4) gives

$$W_f = 0.052(367.1)^{1.086}(5.70 \times 3002)^{0.177}(28.87)^{-0.051}(7.5)^{-0.072}(62.61)^{0.241}$$

Evaluating this expression yields

$$W_f = 351.7 \text{ lbf} = 1564.4 \text{ N}$$

which corresponds to a structural fuselage weight of 159.5 kg.

This result represents the load-carrying shell structure of the fuselage, including frames, stringers, and skin, but excluding interior furnishings and systems. It establishes the baseline for subsequent Class II component weight estimations used in the operational empty weight calculation.

5.4.5 Main Landing Gear Assembly Weight

The main landing gear weight is estimated using Raymer's empirical expression for non-retractable gear:

$$W_{main} = 0.095\,(N_l W_L)^{0.768}\left(\frac{L_m}{12}\right)^{0.409} \qquad Eq.\ (4.7)$$

where W_{main} is the main gear structural weight, N_l is the number of wheels, W_L is the landing weight, and L_m is the strut length (in inches). Separate calculations are performed for the main and nose landing gear assemblies.

Variable	Symbol	Value	Units
Number of main wheels	N_l	2	-
Landing weight	W_L	12019	N
Main shock strut length	L_m	0.508	m

Table 4.5: Main landing gear variable values

The parameters are converted to imperial units for substitution into Raymer's formula: $W_L = 12{,}019\text{ N} = 2{,}701.98\text{ lbf}$. $N_l W_L = 2 \times 2{,}701.98 = 5{,}403.96\text{ lbf}$. $L_m = 0.508\text{ m} = 20.0\text{ in}$, so $L_m/12 = 1.667$. Substituting these values into Eq. (4.7) gives

$$W_{main} = 0.095(5{,}403.96)^{0.768}(1.667)^{0.409}$$

Evaluating this expression yields

$$W_{main} = 86.14 \text{ lbf} = 383.1 \text{ N}$$

which corresponds to a structural main landing gear weight of 39.1 kg.

This value represents the complete main gear assembly including the shock struts, axle, and primary attachment fittings, but excluding the wheel fairings and braking system. The estimate provides a reasonable approximation for a light, non-retractable tricycle gear layout consistent with the geometry of the reference Diamond DA40 aircraft.

5.4.6 Nose Gear Assembly Weight

The structural weight of the nose landing gear is estimated using Raymer's empirical equation for non-retractable gear:

$$W_{nose} = 0.125(N_n W_L)^{0.566}(\frac{L_n}{12})^{0.845} \qquad Eq.\ (4.8)$$

where W_{nose} is the nose gear structural weight, N_n is the number of nose wheels, W_L is the landing weight, and L_n is the nose strut length (in inches).

Variable	Symbol	Value	Units
Landing weight	W_L	12019	N
Number of nose wheels	N_n	1	-
Nose shock strut length	L_n	0.33	m

Table 4.6: Main landing gear variable values

The parameters are converted to imperial units for substitution into Raymer's formula: $W_L = 12{,}019\ \text{N} = 2{,}701.98\ \text{lbf}$; $N_n W_L = 1 \times 2{,}701.98 = 2{,}701.98\ \text{lbf}$; $L_n = 0.33\ \text{m} = 13.0\ \text{in}$, so $L_n/12 = 1.0833$. Substituting these values into Eq. (4.8) gives

$$W_{nose} = 0.125(2{,}701.98)^{0.566}(1.0833)^{0.845}$$

Evaluating this expression yields

$$W_{nose} = 42.3\ \text{lbf} = 188.2\ \text{N}$$

which corresponds to a structural nose-gear weight of 19.2 kg.

This value represents the primary nose-gear structure, including the shock strut, fork, and axle, but excluding steering linkages, wheels, and brakes. It provides a realistic estimate for a tricycle-type gear layout typical of light, low-wing general aviation aircraft such as the Diamond DA40.

5.4.7 Installed Engine Weight

The total installed powerplant weight, including mounts, starter, and all related engine systems, is estimated using Raymer's empirical equation for general aviation aircraft:

$$W_{installed} = 2.575\ W_{en}^{0.922}\ N_{en} \qquad Eq.\ (4.9)$$

where $W_{installed}$ is the installed engine weight, W_{en} is the dry weight of a single engine, and N_{en} is the total number of engines installed on the aircraft.

For this aircraft, the selected engine from Assignment 2 is the Lycoming IO-390-A1A6, a four-cylinder, 210-hp, air-cooled piston engine. The dry weight for this engine is 324 lbs or 1,442 N.

Variable	Symbol	Value	Units
Engine dry weight	W_{en}	1442	N
Number of engines	N_{en}	1	-

Table 4.7: Installed engine group variable values

The parameters are converted to imperial units for substitution into Raymer's formula. $W_{en} = 1{,}442\text{ N} = 324\text{ lbf}$ and $N_{en} = 1$. Substituting these values into Eq. 4.7 gives

$$W_{installed} = 2.575(324)^{0.922}(1)$$

Evaluating this expression yields

$$W_{installed} = 531.5\text{ lbf} = 2{,}364\text{ N}$$

which corresponds to a total installed powerplant structural weight of 241 kg.

The value from Raymer's equation is higher than expected for a single piston engine installed on a light aircraft. Roskam's method provides a more appropriate estimate for piston engine installations because it reflects the weight of the mounts, accessories, and systems. For this reason, Roskam's installation rule is used for the final engine group weight in this design.

$$W_e = K_p P_{TO} \qquad Eq. (4.10)$$

In this relation, W_e is the installed engine weight, K_p is the installation factor for piston engines, and P_{TO} is the required takeoff power in horsepower.

$$W_e = (1.8)(188) = 342\text{ lbf} = 1{,}521\text{ N}$$

which corresponds to a total installed powerplant structural weight of 156 kg. This provides a much more feasible engine weight estimation.

This value represents the combined installed engine assembly, including the engine mounts, starter, cowling, and accessory systems. It provides a complete estimate of the powerplant installation mass used in the Class II operational empty weight calculation.

5.4.8 Fuel System Weight

The fuel system weight is estimated using Raymer's empirical equation for general aviation aircraft:

$$W_{fuel\,system} = 2.49\, V_t^{0.726} \left(\frac{1}{1 + \frac{V_i}{V_t}} \right)^{0.363} N_t^{0.242} N_{en}^{0.157} \qquad Eq.\ (4.11)$$

where $W_{fuel\,system}$ is the total fuel system weight, V_t is the total fuel tank volume, V_i is the integral tank volume, N_t is the total number of fuel tanks, and N_{en} is the number of engines.

The aircraft stores all mission fuel in integral wing tanks, so $V_i = V_t$, which simplifies the equation since $\frac{V_i}{V_t} = 1$. The equation then becomes:

$$W_{fuel\,system} = 2.49\, V_t^{0.726} \left(\frac{1}{2} \right)^{0.363} N_t^{0.242} N_{en}^{0.157}$$

Variable	Symbol	Value	Units
Total fuel volume	V_t	0.36	m^3
Number of fuel tanks	N_t	2	-
Number of engines	N_{en}	1	-

Table 4.9: Fuel system variable values

The total fuel volume of 0.36 m³ was obtained from the aircraft's wing fuel-storage analysis, which determined that a mission fuel mass of 258 kg (2,530 N) corresponds to a volume of approximately 0.36 m³ at a fuel density of 0.72 kg/L, with all fuel stored in two integral wing tanks.

The value of V_t is converted to cubic feet for substitution into Raymer's empirical formula:

$$V_t = 0.36\,\text{m}^3 \times 35.315 = 12.82\,\text{ft}^3$$

Substituting these values into Eq. (4.11) gives

$$W_{fuel\,system} = 2.49(12.82)^{0.726} \left(\frac{1}{2} \right)^{0.363} (2)^{0.242} (1)^{0.157}$$

Evaluating this expression yields

$$W_{fuel\,system} = 13.96\,\text{lbf} = 62.1\,\text{N}$$

which corresponds to a total fuel system structural weight of 6.3 kg.

This weight includes the tanks, fuel lines, valves, and fuel pumps integrated into the wing structure. Since all fuel is stored in integral wing tanks, the design minimizes additional system mass while maintaining compliance with FAR 23.963 fuel-system safety and accessibility requirements.

5.4.9 Flight Control Group Weight

The flight control group weight is estimated using Raymer's empirical equation for general aviation aircraft:

$$W_{flight} = 0.053L^{1.536}B_w^{0.371}(N_z W_{dg} \times 10^{-4})^{0.80} \qquad Eq.\ (4.12)$$

where W_{flight} is the total flight control group weight, L is the flight deck length, B_w is the cabin beam width, N_z is the ultimate load factor, and W_{dg} is the design gross weight.

Variable	Symbol	Value	Units
Flight deck length	L	1.10	m
Cabin beam width	B_w	1.27	m
Ultimate load factor	N_z	5.70	-
Design gross weight	W_{dg}	13354	N

Table 4.10 Flight control variable values

The flight deck length and cabin beam width are taken from the cabin geometry parameters. These values are converted to imperial units for substitution into Raymer's empirical formula: $L = 1.10$ m $= 3.61$ ft, $B_w = 1.27$ m $= 4.17$ ft, and $W_{dg} = 13{,}354$ N $= 3{,}002.1$ lbf. Substituting into Eq. (4.12):

$$W_{flight} = 0.053(3.61)^{1.536}(4.17)^{0.371}(5.70 \times 3002.1 \times 10^{-4})^{0.80}$$

Evaluating this expression yields

$$W_{flight} = 0.99 \text{ lbf} = 4.42 \text{ N}$$

which corresponds to a flight control group structural weight of 0.45 kg.

This result represents the weight of the primary flight control systems, including the control surfaces, linkages, and actuation mechanisms. It provides a statistical approximation of the structure necessary to transmit pilot inputs while maintaining stiffness and reliability during all flight conditions.

5.4.10 Avionics and Instrumentation Weight

The avionics and instrumentation weight is estimated using Raymer's empirical equation for general aviation aircraft:

$$W_{avionics} = 2.117\, W_{uav}^{0.933} \qquad Eq.\ (4.13)$$

where $W_{avionics}$ is the installed avionics weight and W_{uav} is the uninstalled avionics weight.

Variable	Symbol	Value	Units
Uninstalled avionics weight	W_{uav}	25.0	lbf

Table 4.10: Avionics and instrumentation variable values

A representative value of 25 lbf was adopted based on Raymer's general aviation database and comparable four-seat aircraft such as the Cessna 182 and Diamond DA40. This value corresponds to the typical uninstalled mass of communication, navigation, and flight instruments prior to installation.
Substituting into Eq. (4.13):

$$W_{avionics} = 2.117(25.0)^{0.933}$$

$$W_{avionics} = 2.117(20.17) = 42.78\ \text{lbf} = 190.3\ \text{N}$$

which corresponds to a total avionics and instrumentation weight of 19.4 kg.

This weight includes the installed avionics systems, wiring, mounting racks, and electrical connections. It provides a representative estimate for a modern four-seat general aviation aircraft equipped with standard navigation and communication systems.

5.4.11 Hydraulic Systems Weight

The hydraulic system weight is estimated using Raymer's empirical equation for general aviation aircraft:

$$W_{hydraulics} = 0.001\, W_{dg} \qquad Eq.\ (4.14)$$

where $W_{hydraulics}$ is the hydraulic system weight and W_{dg} is the design gross weight.

Variable	Symbol	Value	Units
Design gross weight	W_{dg}	13354	N

Table 4.11: Hydraulic system variable values

The design gross weight is converted to imperial units for substitution into Raymer's empirical formula:

$$W_{dg} = 13{,}354\ \text{N} = 3{,}002.1\ \text{lbf}.$$

Substituting into Eq. (4.14):

$$W_{hydr} = 0.001(3{,}002.1)$$

$$W_{hydr} = 3.00\ \text{lbf} = 13.36\ \text{N}$$

which corresponds to a total hydraulic system weight of 1.36 kg.

This value represents the installed hydraulic lines, pumps, reservoirs, and actuators used to operate flight control and braking systems. For this aircraft, the result is small due to the use of lightweight, compact general aviation hydraulic components. If electrically actuated systems are selected later in design, this value can be revised accordingly.

5.4.12 Electrical Systems Weight

The electrical system weight is estimated using Raymer's empirical equation for general aviation aircraft:

$$W_{elec} = 12.57\ (W_{fuel\,sys} + W_{avionics})^{0.51} \qquad Eq.\ (4.15)$$

where W_{elec} is the total electrical system weight, $W_{fuel\,sys}$ is the fuel system weight, and $W_{avionics}$ is the avionics system weight.

Variable	Symbol	Value	Units
Fuel weight system	$W_{fuel,system}$	13.96	lbf
Avionics system weight	$W_{avionics}$	42.78	lbf

Table 4.12: Electrical system variable values

The electrical system weight is dependent on the combined weights of the fuel and avionics systems. Substituting the known values into Eq. (4.15):

$$W_{elec} = 12.57(13.96 + 42.78)^{0.51}$$

$$W_{elec} = 12.57(7.53) = 94.60\ \text{lbf} = 420.7\ \text{N}$$

which corresponds to a total electrical system weight of 42.9 kg.

This value represents the installed electrical wiring, power distribution panels, battery, alternator, and circuit protection devices required for the aircraft's avionics, lighting, and system controls.

5.4.13 Furnishings Weight

The furnishings weight is estimated using Raymer's empirical equation for general aviation aircraft:

$$W_{furn} = 0.0582\ W_{dg} - 65 \qquad Eq.\ (4.16)$$

where W_{furn} is the furnishings weight and W_{dg} is the design gross weight.

Variable	Symbol	Value	Units
Design gross weight	W_{dg}	13354	N

Table 4.13: Furnishings weight variable values

The design gross weight is converted to imperial units for substitution into Raymer's empirical formula:

$$W_{dg} = 13{,}354\ \text{N} = 3{,}002.1\ \text{lbf}.$$

Substituting into Eq. (4.16):

$$W_{furn} = 0.0582(3{,}002.1) - 65$$

$$W_{furn} = 174.92 - 65 = 109.92\ \text{lbf} = 489.1\ \text{N}$$

which corresponds to a total furnishings weight of 49.8 kg.

This value includes the seats, interior panels, upholstery, floor coverings, and minor cabin fittings used in the aircraft. It provides a reasonable approximation for a four-seat, low-wing general aviation aircraft with a simple interior layout and minimal additional amenities.

5.4.14 Environmental Control, Air Conditioning, and Anti-Ice Weight

The environmental control, air conditioning, and anti-ice system weight is estimated using Raymer's empirical equation for general aviation aircraft:

$$W_{env} = 0.265\, W_{dg}^{0.52}\, N_p^{0.68}\, W_{avionics}^{0.17}\, M^{0.08} \qquad Eq.\ (4.17)$$

where W_{env} is the environmental control and anti-ice system weight, W_{dg} is the design gross weight, N_p is the number of passengers, $W_{avionics}$ is the installed avionics weight, and M is the cruise Mach number.

Variable	Symbol	Value	Units
Design gross weight	W_{dg}	13354	N
Number of passengers	N_p	3	-
Avionics weight	$W_{avionics}$	42.78	lbf
Cruise Mach number	M	0.23	-

Table 4.14: Environmental control, air conditioning, and anti-ice variable values

The design gross weight is converted to imperial units for substitution into Raymer's empirical formula:

$$W_{dg} = 13{,}354\ \text{N} = 3{,}002.1\ \text{lbf}.$$

Substituting into Eq. (4.17):

$$W_{env} = 0.265(3{,}002.1)^{0.52}(3)^{0.68}(42.78)^{0.17}(0.23)^{0.08}$$

$$W_{env} = 0.265(378.6) = 100.3 \text{ lbf} = 446.2 \text{ N}$$

which corresponds to a total environmental control, air conditioning, and anti-ice system weight of 45.5 kg. This value represents the installed systems that provide cabin ventilation, heating, defogging, and windshield anti-ice protection. The result is consistent with typical values for four-seat piston aircraft with basic environmental controls and no pressurization system.

5.4.15 Operational Empty Weight and Adjustment Factors

The operational empty weight (OEW) is obtained by summing the component weights calculated in Sections 4.1 through 4.14. These weights represent the structural and systems masses of the aircraft. The resulting values are listed in Table 4.15.

$$\text{OEW} = \sum W_i \qquad \textit{Eq. } (4.18)$$

Component	Weight (N)
Wing structural weight	1404.7
Horizontal tail structure weight	197.2
Vertical tail structure weight	143.0
Fuselage structure weight	1564.4
Main landing gear weight	383.1
Nose landing gear weight	188.2
Installed engine weight	1521.0
Fuel system weight	62.1
Flight control group weight	4.4
Installed avionics weight	190.3
Hydraulics system weight	13.4
Electrical system weight	420.7
Furnishings weight	489.1
Environmental/Anti-Ice weight	446.2
Total Operational Empty Weight (OEW)	7874.0

Table 4.15: Operational empty weight component summary

All component weights are expressed in both pounds-force and newtons for clarity. The summed OEW is 7,874.0 N, which corresponds to 1,770 lbf. Dividing by gravitational acceleration gives an equivalent empty weight mass of 803.0 kg. This value serves as the baseline configuration weight for subsequent performance and balance analysis.

Raymer recommends applying adjustment multipliers, often referred to as *fudge factors*, to account for material choice, construction methods, and system complexity. Typical multipliers include reductions for advanced composite structures and slight increases for conventional metallic construction. Representative factors are summarized in Table 4.16.

Category	Fudge Factor (Multiplier)
Conventional aluminum structure	1.00
Advanced composite wing	0.85
Advanced composite empennage	0.83
Simplified systems or reduced outfitting	0.95

Table 4.16: Raymer's recommended fudge factors for weight adjustment

Applying these multipliers allows refined OEW estimates for advanced configurations. For a baseline all-metal construction, a multiplier of 1.00 maintains the current value of 7,874 N. If composite materials are used in the wing and tail, an overall reduction of approximately seven percent is appropriate, resulting in an adjusted OEW of 7,323.2 N.

This adjusted value reflects expected savings achievable through advanced composite construction and lightweight interior systems. The final operational empty weight, whether using the baseline or adjusted value, establishes the foundation for payload-range and center-of-gravity calculations in subsequent analysis.

Compared to the OEW obtained during the preliminary sizing phase, the adjusted composite-based OEW is approximately 10% lower, which falls well within the expected refinement margin between early sizing methods and detailed component-based estimates. This close agreement indicates that the original weight targets were appropriate and that no major redesign or mass reallocation is required.

5.5 Center of Gravity Estimation

An important factor that contributes to the stable flight of an aircraft is the position of its center of gravity (CG). The longitudinal CG location determines the aircraft's stability, trim, and control characteristics, and is therefore a key parameter in the design process. The CG of a body is obtained by summing the product of each component's weight and its longitudinal arm from a defined reference point, divided by the total aircraft weight, as expressed in Equation 5.1.

$$COG = \frac{\sum W_{element} \times COG_{element}}{\sum W_{element}} \qquad Eq. (5.1)$$

It is important to note that not all weights on the aircraft remain fixed during operation. Movable items such as passengers, fuel, and baggage can shift the aircraft's overall CG. For this reason, the empty aircraft CG will first be computed, followed by analyses of different loading configurations in subsequent sections. These cases will evaluate the influence of payload and fuel distribution on the longitudinal CG travel to ensure that it remains within the acceptable limits for static stability and controllability.
The resulting OEW CG position will serve as the baseline reference for the loading diagrams and stability analysis that follow.

5.5.1 The Empty Aircraft

The operational empty weight (OEW) center of gravity was found by dividing the aircraft into three main structural groups: the fuselage group, the wing group, and the systems and services group. Each group includes components with similar functions and positions along the fuselage. The reference datum for all measurements is the aircraft nose, with positive x increasing toward the tail. Because the aircraft is symmetrical about its longitudinal axis, only the x-coordinate is required for the CG calculation.

Fuselage Group	Weight [N]	x (from nose) [m]
Fuselage structure	1564.4	5.2
Horizontal tail	197.2	8.5
Vertical tail	143	8.3
Nose landing gear	188.2	1.42
Furnishings	489.1	2.36
Total (Fuselage Group)	2582	-

Table 5.1: Fuselage Group Components

The fuselage group is dominated by the fuselage structure and tail surfaces, which shift the group CG aft relative to the nose-mounted equipment. The calculated fuselage group CG is located at approximately x = 4.81 m from the nose.

Wing Group	Weight [N]	x (from nose) [m]
Wing structure	1404.7	3.5
Engine assembly	1521.0	1.8
Main landing gear	383.1	3.6
Fuel system	62.1	3.6
Total (Wing Group)	3371.0	-

Table 5.2: Wing Group Components

The wing group contains the largest portion of total OEW. The CG of this group lies near x = 2.75 m, reflecting the combined influence of the wing box and forward-mounted engine.

Systems and Services	Weight [N]	x (from nose) [m]
Installed avionics	190.3	1.40
Hydraulic system	13.4	2.50
Electrical system	420.7	2.10
Environmental/Anti-Ice	446.2	1.60
Total (Systems Group)	1070.6	-

Table 5.3: Systems and Services Group Components

This group includes smaller distributed components located mostly in the forward fuselage, shifting its CG forward relative to the other groups with a calculated systems and services group CG of approximately x = 1.77 m.

Combining all components gives the overall operational empty weight center of gravity:

$$x_{CG,OEW} = \frac{\sum(W_i \cdot x_i)}{\sum W_i} \qquad Eq.(5.2)$$

$$x_{CG,OEW} = \frac{(2{,}582 \times 4.81) + (3371 \times 2.79) + (1{,}070.6 \times 1.77)}{2{,}582 + 3371 + 1{,}070.6} = 3.367 \text{ m from the nose.}$$

The estimated OEW CG is therefore x = 3.36 m aft of the nose. With a fuselage length of 8.8 m, this represents approximately 38% of the total length. When expressed relative to the wing mean aerodynamic chord (MAC = 1.48 m, LEMAC ≈ 3.0 m), the CG corresponds to 25% MAC, which falls within the typical 25–35% MAC range observed for light four-seat aircraft such as the DA40 and Cessna 182.

The center of gravity locations for the major aircraft components are shown in Figure 5.1. Each blue marker represents the longitudinal and lateral position of an individual component relative to the aircraft nose, which is located at the origin. The fixed landing gear, cabin structure, wings, tail surfaces, engine, and internal systems are all plotted according to their measured X positions from the geometric model. The red marker indicates the resulting operational empty weight center of gravity, which forms the reference point for the loading cases evaluated later in this section. The vertical line at the nose highlights the datum used for all X-distance measurements, and the dashed boundaries indicate the full span and height of the aircraft. This visualization provides a clear view of how the distributed component weights combine to establish the empty aircraft CG used in the stability and loading analysis.

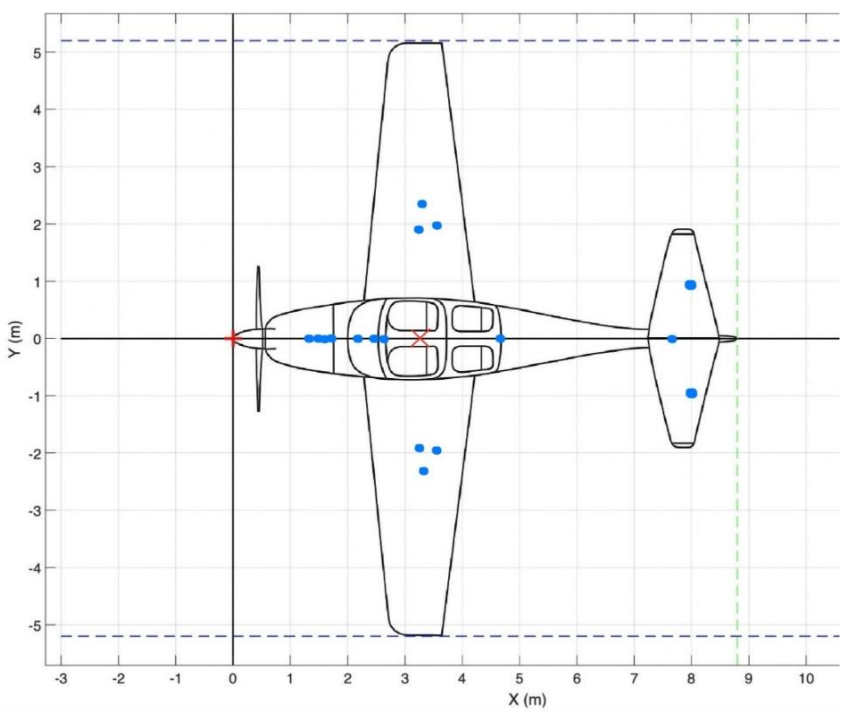

Figure 5.1: Aircraft component CG distribution

5.5.2 The Loading Diagram

After determining the empty-aircraft center of gravity, the next step is to evaluate how the CG varies when payload and fuel are added or removed, which therefore demonstrates the most forward and aft ward positions of the CG the aircraft would experience. This assessment verifies that the aircraft remains properly balanced throughout its mission and within the acceptable longitudinal limits defined by stability and control requirements. The analysis considered all variable load components: the pilot, 2 passengers, baggage, and usable fuel.

To construct the loading diagram, the CG is first set at the empty-aircraft value obtained in Section 5.1. From this baseline, the sequential effects of adding baggage, loading each occupant, and filling the fuel tanks are calculated. Each item contributes a moment proportional to its weight and its fuselage station, resulting in a corresponding shift of the total aircraft CG. The locations of the seats, baggage compartment, and fuel tanks are summarized in Table 5.2:

Item	X (m)	Weight (N)
Pilot	2.5	780
2 Passengers	3.8	1570
Cargo	4.7	300
Fuel	3.6, 3.9, 3.4	2500

5.5.2.1 Wing Configuration 1

In the neutral wing configuration (wing positioned at 3.6 m), the loading sequence begins with the cargo-loaded condition (red), which establishes the initial center of gravity at approximately 26% MAC. From this starting point, adding the pilot (yellow), who sits forward, shifts the CG slightly forward. The subsequent addition of the two passengers (green) produces the next aft movement, bringing the CG closer to the middle of the allowable envelope. Finally, loading the fuel (blue) increases the total weight substantially but results in only a moderate CG shift due to the fuel tanks being located close to the wing's aerodynamic center. The fully loaded configuration reaches approximately 29% MAC, giving a total CG travel of roughly 8% MAC across all loading steps. This limited and smooth CG excursion confirms that the neutral wing placement provides a well-balanced aircraft geometry in which all operational loading cases remain comfortably within longitudinal stability limits.

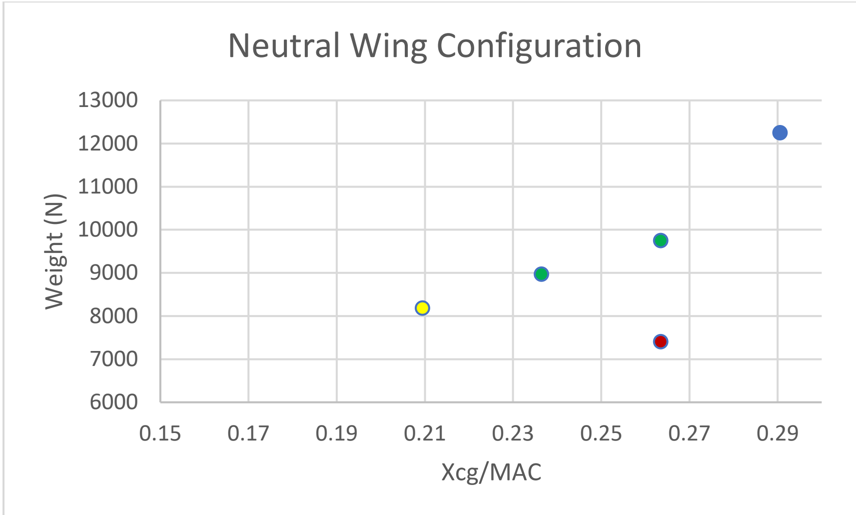

Figure 5.2.1: Neutral Wing Loading Diagram

5.5.2.2 Wing Configuration 2

In the aft wing configuration, shifting the wing rearward causes the MAC to move aft relative to the fuselage reference line, which places the initial cargo-loaded condition (red) extremely far forward on the MAC scale, at only about 6% MAC. Loading the pilot (yellow), who is positioned well ahead of the wing, keeps the CG near this forward region and produces only a minor shift. When the two passengers are added (green), the CG moves slightly farther aft but remains too forward due to the new location of the wing's aerodynamic center. Finally, loading the fuel (blue), which is carried near the wing, significantly increases the total aircraft weight but again results in only a small aft shift on the MAC scale, placing the fully loaded CG at roughly 13% MAC. Overall, the CG travels only a narrow range of about 12% MAC, but the entire envelope remains far forward of the typical acceptable CG band for stability. This indicates that an aft wing placement produces an undesirable forward-biased configuration requiring excessive tail-down force, reducing trim efficiency, and potentially causing controllability issues at low speeds. As a result, the aft-shifted wing arrangement is not suitable without major geometric or loading-limit adjustments.

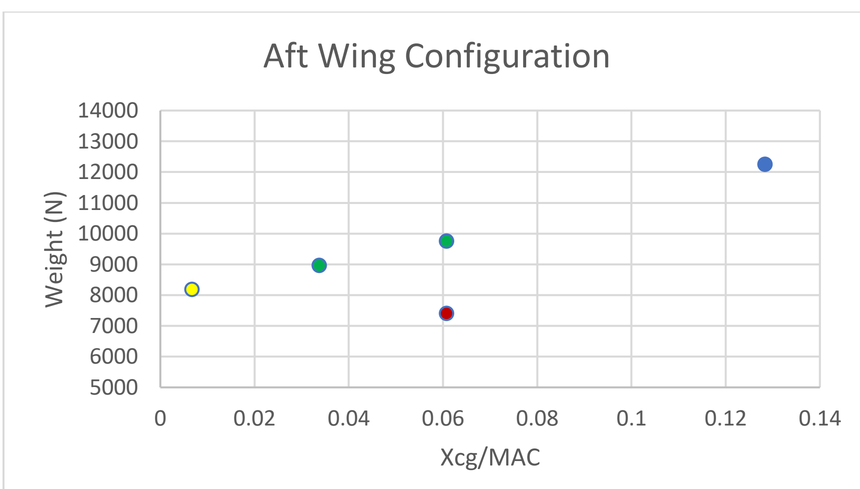

Figure 5.2.2: Aft Wing Loading Diagram

5.5.2.3 Wing Configuration 3

In the forward wing configuration, shifting the wing forward causes the MAC to translate forward along the fuselage, which makes the initial cargo-loaded condition (red) appear far aft on the MAC scale at approximately 40% MAC. Adding the pilot (yellow), whose seating position is forward relative to the cargo, pulls the CG slightly forward but still leaves it well aft of the desirable mid-range. Loading the two passengers (green) produces another modest aft shift, as their seats lie behind the aircraft's nominal CG reference but ahead of the cargo. Finally, adding fuel (blue) increases the total aircraft weight but shifts the CG only slightly due to the fuel tanks being located very close to the wing's aerodynamic center. The fully loaded configuration remains close to 40% MAC, giving a CG travel of roughly 4% MAC across the entire loading sequence. While the total CG change is small, the entire operating envelope is positioned near or beyond typical aft CG limits, which can degrade low-speed stability. Accordingly, this forward wing placement is also not favorable without imposing strict aft-loading restrictions or introducing geometric changes to fix the stability.

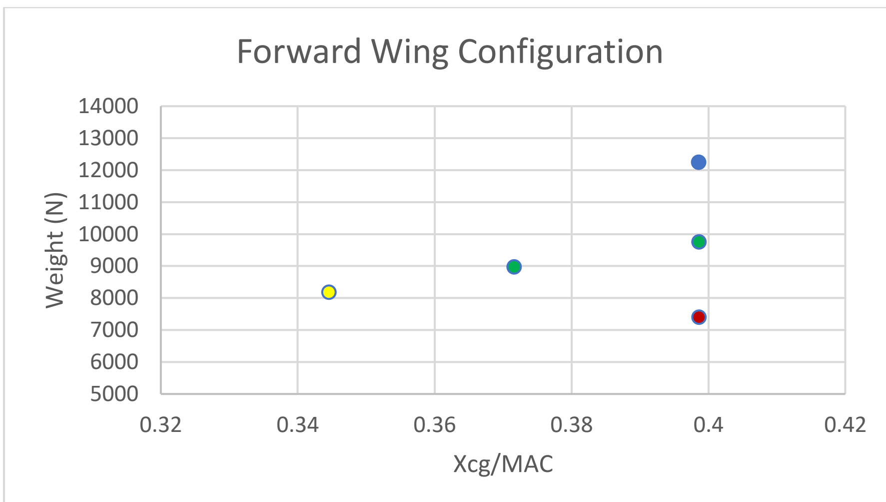

Figure 5.2.3: Forward Wing Loading Diagram

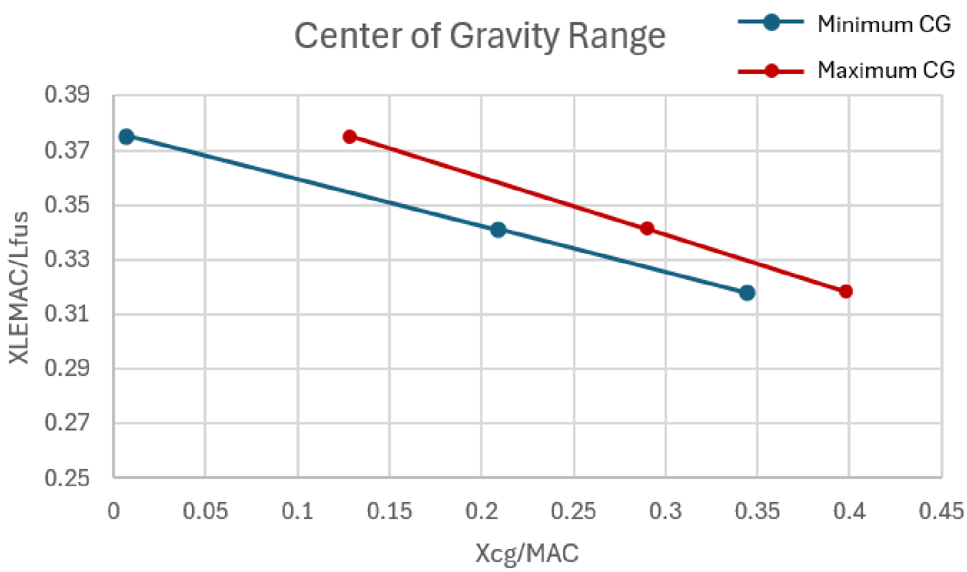

Figure 5.2.4: Range of Center of Gravity for Different Wing Locations

In figure 5.2.4, the minimum and maximum value for the different configurations are plotted together based on the leading edge of the MAC's position on the fuselage length. The top left points demonstrate the aft-winged configuration, while the bottom right points represent the forward-positioned wing configuration, and in the center is the neutral wing configuration demonstrating is balance between the two.

5.6 The Scissor Plot and Curves

This section establishes the horizontal tail size and wing reference location using a scissor plot. The analysis develops stability and controllability limits as functions of the tail area ratio $\frac{S_h}{S}$ and the allowable center of gravity travel. The resulting stability and control curves define the feasible design region, which provides the minimum horizontal tail area and the corresponding wing placement required to meet both criteria.

5.6.1 The Stability Curve

A longitudinally stable aircraft requires its center of gravity to lie ahead of the neutral point. The neutral point represents the location where the pitching moments from the wing and horizontal tail balance during small changes in angle of attack. Its nondimensional position is given by

$$\bar{x}_{np} = \bar{x}_{ac} + \frac{C_{L\alpha,h}}{C_{L\alpha,a}}\left(1 - \frac{d\epsilon}{d\alpha}\right)\frac{S_h l_h}{S\bar{c}} \qquad Eq.(6.1)$$

In this expression, $\bar{x}_{ac}$ is the aerodynamic-center position of the wing–fuselage group, $C_{L\alpha,h}$ is the lift-curve slope of the horizontal tail, $C_{L\alpha,a}$ is the lift-curve slope of the aircraft without the tail, $d\epsilon/d\alpha$ is the downwash gradient, S_h is the horizontal-tail area, S is the wing area, l_h is the tail moment arm, and $\bar{c}$ is the wing mean aerodynamic chord.

For this aircraft, $S = 14.52\ \mathrm{m}^2$, $S_h = 4.08\ \mathrm{m}^2$, $\bar{c} = 1.48\ \mathrm{m}$, and the tail arm is $l_h = 5.85\ \mathrm{m}$.

A statically stable aircraft requires the center of gravity to lie ahead of the neutral point. The margin between these two locations is the static margin, written as

$$S.M. = \bar{x}_{np} - \bar{x}_{cg}$$

A static-margin requirement of $S.M. = 0.05$ was selected to ensure stable and predictable handling qualities. Rearranging Eq. (6.1) leads to a useful design relation for the horizontal-tail size,

$$\frac{S_h}{S} = \frac{\bar{x}_{cg} - \bar{x}_{ac} - S.M.}{\frac{C_{L\alpha,h}}{C_{L\alpha,a}}\left(1 - \frac{d\epsilon}{d\alpha}\right)\frac{l_h}{\bar{c}}} \qquad Eq. (6.2)$$

This relationship forms the stability line that will appear in the scissor plot.

Next, the lift-curve slope of the horizontal tail must be evaluated. The DATCOM compressibility-corrected expression is used:

$$C_{L\alpha,h} = \frac{2\pi AR_h}{2 + \sqrt{4 + (AR_h\beta)^2(1 + \tan^2\Lambda_{\frac{1}{4}})}} \qquad Eq. (6.3)$$

with $AR_h = 6.0$, quarter-chord sweep $\Lambda_{1/4,h} = 5°$, and cruise Mach $M = 0.23$ giving $\beta = 0.973$, Eq. (6.3) yields a finite-wing tail slope of $C_{L\alpha,h} = 4.6012\ \mathrm{rad}^{-1}$. Applying the tail dynamic-pressure ratio $\eta = 0.85$ appropriate for a fuselage-mounted tail, the effective slope becomes $C_{L\alpha,h} = 3.9111\ \mathrm{rad}^{-1}$.

The aircraft lift-curve slope without the horizontal tail is required as well, using

$$C_{L\alpha,a} = C_{L\alpha,w} + C_{L\alpha,w}\left(\frac{S_{net}}{S}\right) \qquad Eq. (6.4)$$

Where $C_{L\alpha,w} = 5.622\ \mathrm{rad}^{-1}$ (from the clean-wing analysis) and the effective lifting area is $S_{net} = 14.03\ \mathrm{m}^2$. Equation (6.4) gives $C_{L\alpha,a} = 5.8201\ \mathrm{rad}^{-1}$.

The tail's stabilizing effect is reduced by the downwash produced by the wing. The downwash gradient is determined using the DATCOM formulation:

$$\frac{d\epsilon}{d\alpha} = K_{E\Lambda}K_{E\Lambda=0}\frac{C_{L\alpha,w}}{\pi AR}\left[\frac{r}{r^2 + m_{tv}^2} + \frac{0.4879}{\sqrt{r^2 + 0.6319 + m_{tv}^2}}\right]\left[1 + \left(\frac{r^2}{r^2 + 0.7915 + 5.0734m_{tv}^2}\right)^{0.3113}\left(1 - \frac{m_{tv}^2}{1 + m_{tv}^2}\right)\right] \qquad Eq. (6.5)$$

For this aircraft, $AR = 7.5$, wing sweep is small such that $K_{E\Lambda} = K_{E\Lambda=0} = 1.0$, the wingspan is $b = 10.44$, and the normalized geometry is $r = l_h/(b/2) = 1.1212$ and $m_{tv} = z_t/(b/2) = 0.0287$ with $z_t = 0.15$ m. Substituting these values into Eq. (6.5) gives a downwash gradient of $d\epsilon/d\alpha = 0.5524$.

The total aircraft lift-curve slope including tail effects is then

$$C_{L\alpha} = C_{L\alpha,a} + C_{L\alpha,h}\left(1 - \frac{d\epsilon}{d\alpha}\right)\frac{S_h}{S}\left(\frac{l_h}{\bar{c}}\right)^2 \qquad Eq.(6.6)$$

which quantifies the stabilizing contribution of the horizontal tail.

To complete the neutral-point calculation, the aerodynamic center of the wing–fuselage assembly is obtained from the DATCOM correction:

$$\left(\frac{x_{ac}}{\bar{c}}\right)_{wf} = \left(\frac{x_{ac}}{\bar{c}}\right)_{w} - \frac{1.8 b_f h_f + h_f l_{fn}}{C_{L\alpha,w} S \bar{c}} + \frac{0.273 b_f c_g (b - b_f)}{\bar{c}^2 (b + 2.15 b_f)} \tan \Lambda_{\frac{1}{4}} \qquad Eq.(6.7)$$

The wing aerodynamic center from the carpet plot is $(x_{ac}/\bar{c})_w = 0.24$. With fuselage width $b_f = 1.67$ m, fuselage height $h_f = 1.52$ m, wing-root distance from the nose $l_{fn} = 2.50$ m, geometric root chord $c_g = 1.988$ m, and wing quarter-chord sweep $\Lambda_{1/4} = -3.3°$, Eq. (6.7) gives

$$\left(\frac{x_{ac}}{\bar{c}}\right)_{wf} = 0.156$$

Since the aircraft has a single tractor engine and no nacelles, additional nacelle or jet effects do not apply. Thus, the aerodynamic-center location used in Eq. (6.1) is

$$\bar{x}_{ac} = \left(\frac{x_{ac}}{\bar{c}}\right)_{wf} \qquad Eq.(6.8)$$

$$\bar{x}_{ac} = 0.156$$

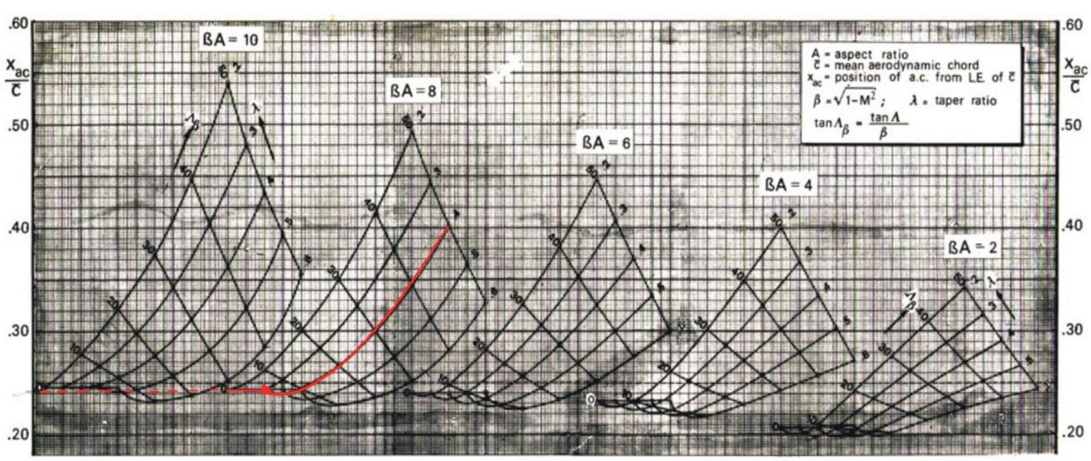

Figure 6.1: Carpet plot used to determine wing aerodynamic center

Substituting the computed values $C_{L\alpha,h} = 3.9111$, $C_{L\alpha,a} = 5.8201$, $d\epsilon/d\alpha = 0.5524$, and $V_h = (S_h l_h)/(S\bar{c}) = 1.1109$ into Eq. (6.1), the neutral point is found to be

$$\bar{x}_{np} = 0.4895$$

which corresponds to a physical distance of $x_{np} = 3.22$ aft of the nose.

5.6.2 The Controllability Curve

Tail sizing is crucial in aircraft control and becomes especially significant during low-speed phases such as landing and takeoff, where the wing produces increased nose-down pitching moments due to flap deployment. In these conditions, the horizontal tail must generate sufficient counteracting moment to allow the aircraft to trim at the most forward CG expected in operation. To evaluate this requirement, controllability is expressed as a relationship between nondimensional tail size and the CG location using the following equation:

$$\frac{S_h}{S} = \frac{\frac{C_{m,ac}}{C_{L\alpha-h}} + \left(\bar{x}_{cg} - \bar{x}_{ac}\right)}{\frac{C_{L\alpha h}}{C_{L\alpha}}\left(\frac{l_h}{\bar{c}}\right)} \qquad \textit{Eq. (6.10)}$$

In this expression, $C_{m,ac}$ is the pitching-moment coefficient about the wing aerodynamic center, $C_{L\alpha,h}$ is the landing-configuration lift-curve slope of the horizontal tail, $C_{L\alpha}$ is the aircraft lift-curve slope in landing, $\bar{x}_{cgL}$ is the nondimensional landing CG location, $\bar{x}_{ac}$ is the aerodynamic-center location from Eq. (6.8), and $l_h/\bar{c}$ provides the nondimensional tail moment arm. For this aircraft, the geometric parameters are 5.85 m, $\bar{c} = 1.48$ m, and $\bar{x}_{\mathrm{ac}} = 0.156$.

Several aerodynamic quantities differ from the cruise values used in the stability curve. With flaps deployed, the wing operates at a lower lift-curve slope than in the clean configuration, and the horizontal-tail effectiveness changes due to altered flow conditions. The finite-wing lift-curve slope of the horizontal tail in landing is determined using the DATCOM formulation

$$C_{L\alpha,h} = \frac{2\pi AR_h}{2 + \sqrt{4 + (AR_h\beta)^2(1 + \tan^2\Lambda_{1/4,h})}} \qquad Eq. (6.11)$$

where the geometry is $AR_h = 6.0$, $\Lambda_{1/4,h} = 5°$, and the landing Mach number is sufficiently low that $\beta = \sqrt{1 - M^2} = 0.973$. This gives us a finite-wing slope of 4.4768 rad^{-1}. Including the tail dynamic-pressure ratio $\eta = 0.85$ yields an effective landing configuration value

$$C_{L\alpha,h} = 3.8053\ \mathrm{rad}^{-1} \qquad Eq. (6.12)$$

The overall aircraft lift-curve slope in landing is evaluated using the same structural form as in Eq. (6.6), but with flap-modified wing data. This produces

$$C_{L\alpha} = 4.8763\ \text{rad}^{-1} \qquad Eq. (6.13)$$

The wing pitching-moment coefficient about its aerodynamic center is influenced by the fuselage and by flap deflection. Decomposing the total moment coefficient into its components gives

$$C_{m,ac} = C_{m,c} + \Delta_f C_{m,w} + \Delta_{fus} C_{m,w} \qquad Eq. (6.14)$$

Since the aircraft has no wing-mounted nacelles, there is no nacelle-moment contribution. A baseline clean-wing value of $C_{m,c} = -0.10$ is used, and the increase in nose-down moment from flap deployment is taken as $\Delta_f C_{m,w} = -0.05$, consistent with typical GA Fowler-flap behavior.

The change in pitching moment due to the fuselage is computed using the DATCOM expression

$$\Delta_{fus} C_{m,w} = -1.8\left(1 - 2.5\frac{b_f}{l_f}\right)\frac{\pi b_f h_f l_f}{4S\bar{c}}\frac{C_{L0}}{C_{L\alpha,w}} \qquad Eq. (6.15)$$

where $b_f = 1.67$ m and $h_f = 1.52$ m are the external fuselage width and height, $l_f = 8.8$ m is the fuselage length, C_{L0} is the landing lift coefficient at zero angle of attack, and $C_{L\alpha,w} = 5.622\ \text{rad}^{-1}$ is the clean-wing lift-curve slope. For this design, $C_{L0} = 1.155$ was used, consistent with the flap geometry.

Substituting these quantities into Eq. (6.15) gives

$$\Delta_{fus} C_{m,w} = -0.1587$$

The flap-induced pitching-moment increment is computed from

$$\Delta_f C_{m,w} = \frac{h_f}{\bar{c}}\left[k_1 C_L + k_2 (C_{Lmax} - C_L)\left(1 - \frac{S_{wf}}{S}\right)\right] + \frac{AR}{24}\Delta C_{Lmax} \tan\Lambda_{1/4,h}\left[c - \frac{2}{3}\left(\frac{x_{ac}}{\bar{c}}\right)\right] \qquad Eq. (6.16)$$

where k_1 and k_2 are empirical flap-effectiveness factors, ΔC_{Lmax} is the flap-induced change in maximum lift coefficient, and S_{wf} is the portion of the wing on which flaps act. Representative values for light Fowler flaps give $k_1 = 0.6$ and $k_2 = 0.3$, and for this aircraft $\Delta C_{Lmax} = 0.20$ was taken.

Substituting these values into Eq. (6.16) gives the resulting flap contribution of

$$\Delta_f C_{m,w} = -0.05$$

Combining the three contributions in Eq. (6.14) gives the total landing moment coefficient:

$$C_{m,ac} = -0.10 + (-0.05) + (-0.1587) = -0.3087$$

Finally, substituting $C_{m,ac} = -0.3087$, $C_{L\alpha,h} = 3.8053\ \text{rad}^{-1}$, $C_{L\alpha} = 4.8763\ \text{rad}^{-1}$, $\frac{l_h}{\bar{c}} = 3.9513$, and $\bar{x}_{ac} = 0.156$ into Eq. (6.10) produces the controllability curve.

This curve defines the minimum horizontal-tail area ratio required to trim the aircraft at its forward CG limit in the landing configuration. When plotted together with the stability curve from Section 6.1, the resulting scissor plot establishes the allowable CG envelope and confirms that the selected horizontal-tail geometry satisfies both stability and controllability constraints.

5.6.3 The Scissor Plot

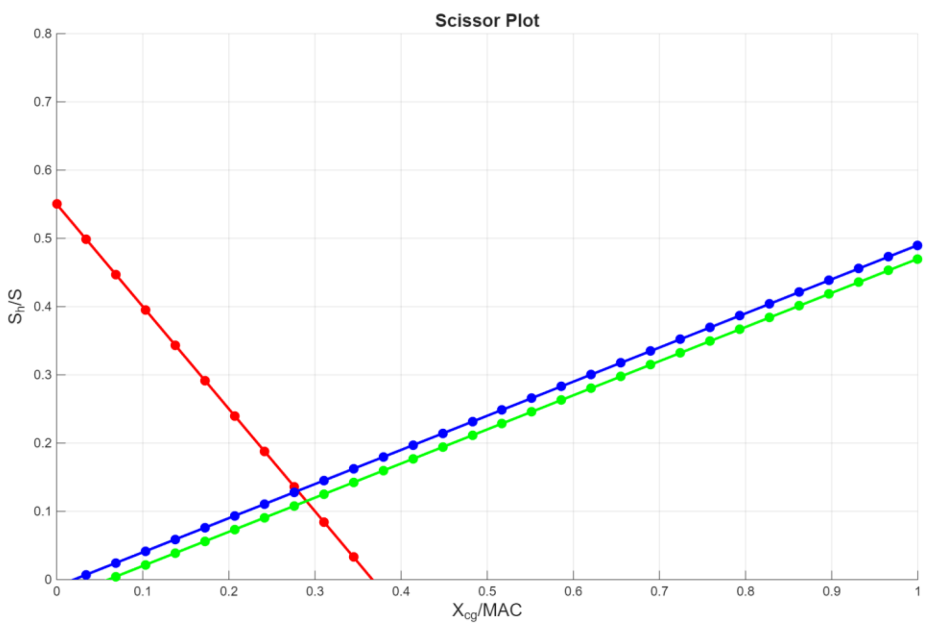

Figure 6.3.1: Calculated Scissor Plot

The final scissor plot in Figure 6.3.1 shows the controllability limit (red), the stick-fixed neutral-point line (blue), and the stability-margin line (green), each represented as straight lines defining the allowable CG range for the aircraft. The red line establishes the forward CG limit where the tail must provide enough authority for trim, while the blue and green lines define the aft CG boundary for neutral stability and the required static margin. The feasible operating region lies to the right of the red line and to the left of the green line. The smooth, gradual separation of the stability lines and the intersection points indicate that the aircraft's expected CG range fits comfortably within this allowable envelope, confirming that the selected tail sizing and wing placement provide an appropriate balance between controllability and static stability.

5.7 Revaluation of the Empennage

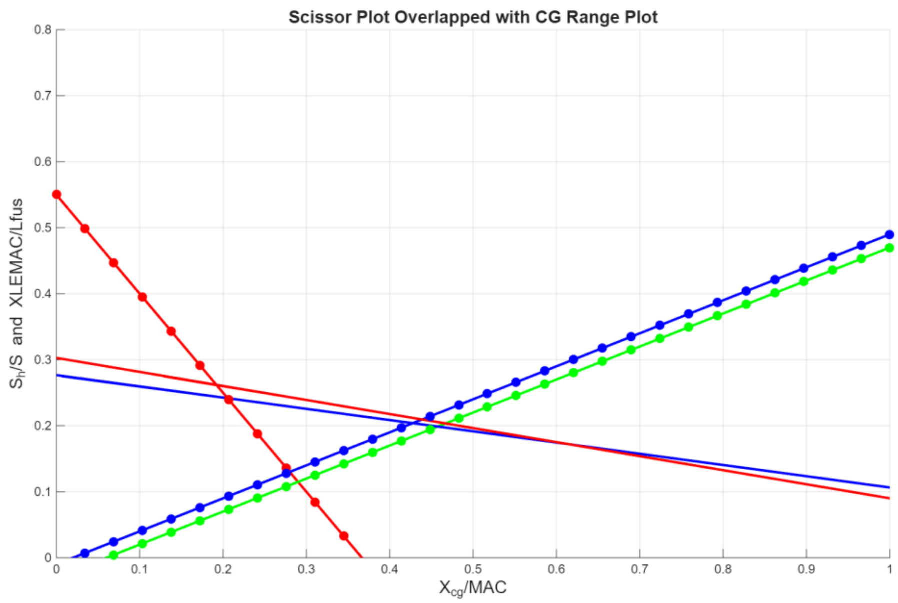

Figure 6.3.2: Scissor Plot Overlapped with CG Range Plot

Figure 6.3.2 overlays the scissor plot with the CG-range lines derived from the loading-diagram analysis, allowing direct comparison between the theoretical stability, control limits and the actual range of CG positions achievable by the aircraft. The two blue and two red CG-range segments represent the minimum and maximum CG locations obtained at different wing positions, extended to visualize their trends relative to the scissor boundaries. The region between the forward controllability limit and the aft stability line defines the acceptable tail-sizing and wing-position combinations, and the CG lines falling entirely within this envelope confirm that the selected tail size and longitudinal placement are appropriate. The value of X_{LEMAC}/L_{fus}obtained from our CG-range plot is within the tolerance typical of preliminary design, no iteration of the wing position or tail size is required. The goal of this stage is not to achieve exact coincidence between analytical and graphical results but to ensure that the aircraft's operational CG band lies safely between the stability and controllability limits which is satisfied here. This confirms that the current configuration maintains both adequate pitch authority at forward CG and static stability at aft CG without necessitating further geometric adjustments.

6 Improved Drag Prediction and Conceptual Design Review

6.1 Introduction

Following the completion of the aircraft's preliminary design, aerodynamic analysis, and stability evaluation in earlier assignments, this stage presents an improved estimation of the aircraft's drag characteristics. Each major component, including the wing, fuselage, empennage, nacelle, and pylon, is assessed individually to determine its contribution to overall drag. Using updated geometric and performance data at cruise conditions, a refined drag polar is developed and compared with the preliminary estimation from Assignment 2. The findings provide a more accurate representation of aerodynamic efficiency and support targeted recommendations for drag reduction and environmental performance enhancement.

6.2 Drag Estimation

In this section, the total drag is evaluated by analyzing the contribution of each major component to the overall aerodynamic resistance. The approach follows the same principle used in previous analyses, separating drag into two primary components: the zero-lift drag, $\boldsymbol{C_{D0}}$, and the lift-induced drag, $\boldsymbol{C_{DL}}$. The total drag coefficient is therefore expressed as

$$\boldsymbol{C_D = C_{D0} + C_{DL} \qquad Eq. (2.1)}$$

At the design cruise condition, the aircraft operates well within the subsonic regime, allowing drag estimation using incompressible aerodynamic relations. Each major airframe component—wing, fuselage, horizontal and vertical tail, engine installation, and landing gear—is evaluated individually to determine its contribution to the total zero-lift drag coefficient. The induced drag is then calculated based on the lift characteristics of the finite wing determined in Assignment 3.

For our aircraft, the analysis is performed at the cruise condition corresponding to Mach 0.23 and a flight altitude of 2,440 m. These conditions represent the dominant segment of the mission profile and are used to determine the improved drag polar for comparison with the preliminary results obtained in Assignment 2. The principal flight parameters at cruise are summarized in Table 2.1.

Symbol	Description	Value	Units
M	Cruise Mach number	0.23	-
V	Cruise velocity	77.2	m/s
$\boldsymbol{\rho}$	Air density	1.006	kg/m^3
$\boldsymbol{\mu}$	Dynamic viscosity	$\boldsymbol{1.789 \times 10^{-5}}$	kg/(m)(s)
$\boldsymbol{C_{L,cr}}$	Cruise lift coefficient	0.298	-

Table 2.1: Cruise flight conditions

The improved drag prediction integrates geometric data from Assignments 3 and 4, including the refined wing area of 14.52 m², an aspect ratio of 7.5, and tail surface dimensions determined through the V-bar method. Each surface's wetted area and Reynolds number are calculated using the mean aerodynamic chord and local flow conditions. Corrections for interference, surface roughness, and skin friction are applied using standard methods outlined in Raymer and Torenbeek.

The resulting component drag coefficients will be summed to obtain the total zero-lift drag coefficient, while the induced drag term will be calculated from the finite-wing lift distribution. The improved drag polar, combining both components, will then be compared against the initial results from the preliminary sizing phase to assess aerodynamic improvements achieved through the refined configuration.

6.2.1 Wing Contribution

The wing drag is determined by the combined effects of zero-lift drag and lift-induced drag, as expressed in Equation 2.1. The required parameters for the drag estimation were obtained from previous design stages and the CAD model. These include the wing's geometric characteristics, aerodynamic factors, and cruise-condition parameters. Table 2.1 summarizes the main variables used for estimating the wing drag.

Symbol	Description	Value	Unit
$\boldsymbol{L_{fus}}$	Fuselage length	8.80	m
$\boldsymbol{Re_{MAC}}$	Reynolds number (MAC, cruise)	$\boldsymbol{6.60 \times 10^6}$	-
$\boldsymbol{S}$	Wing planform area	14.52	m^2
$\boldsymbol{MAC}$	Mean aerodynamic chord	1.48	m
$\boldsymbol{b}$	Wingspan	10.43	m
$\boldsymbol{A_w}$	Aspect ratio of wing	7.5	-
$\boldsymbol{t/c_w}$	Wing thickness-to-chord ratio	0.12	-
$\boldsymbol{\lambda}$	Taper ratio	0.40	-
$\boldsymbol{S_{wet}}$	Wing wetted area	29.91	m^2
$\boldsymbol{C_{f,w}}$	Skin friction coefficient	0.00312	-
$\boldsymbol{FF_w}$	Profile form factor	1.20	-
$\boldsymbol{Q_w}$	Wing/fuselage interference factor	0.96	-
$\boldsymbol{L_f}$	Airfoil thickness parameter	1.2	-
$\boldsymbol{C_{L\alpha}}$	Wing lift gradient	5.44	1/rad
$\boldsymbol{C_{L,cruise}}$	Cruise lift coefficient	0.27	-
$\boldsymbol{M_{cruise}}$	Cruise Mach number	0.23	-
$\boldsymbol{e}$	Oswald efficiency factor	0.85	-
$\boldsymbol{C_{D0,w@M}}$	Estimated subsonic wing zero-lift drag coefficient	0.0076	-
$\boldsymbol{C_{D_i}}$	Estimated induced drag coefficient	0.0030	-
$\boldsymbol{C_{D,w}}$	Total estimated wing drag coefficient	0.0106	-

Table 2.1: Wing drag components

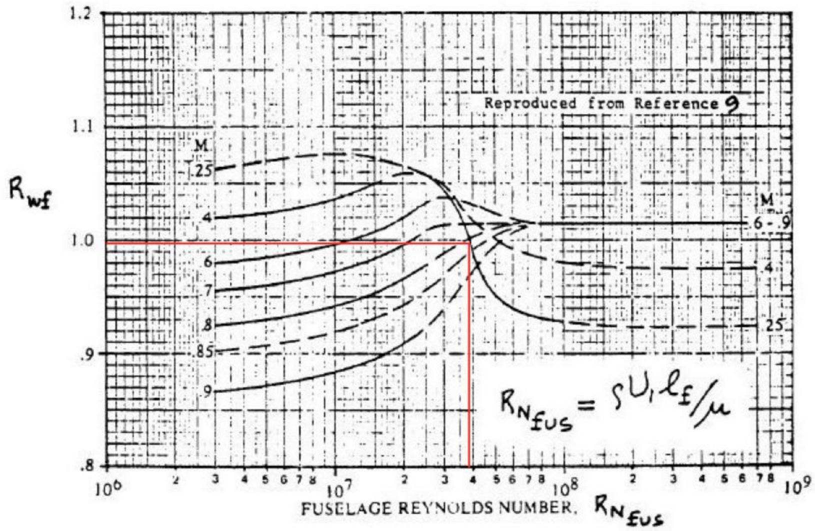

Figure 2.1: Wing interference factor used for $\boldsymbol{Q_w}$

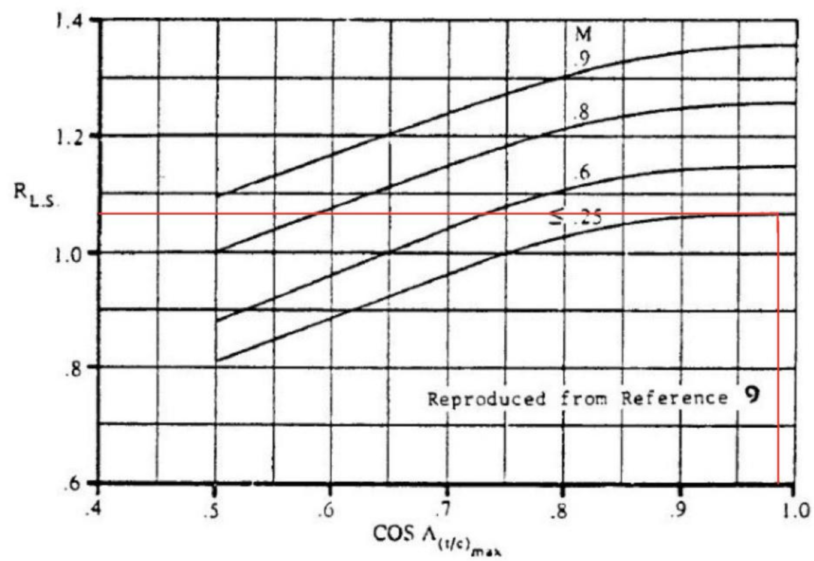

Figure 2.2: Lifting surface correction factor used for aerodynamic adjustments

The interference factor adjusts the drag for the wing and fuselage junction. The lifting surface correction factor adjusts the aerodynamic performance for the finite span. The form factor accounts for the airfoil thickness distribution. The wetted area comes from the geometric model. The friction coefficient depends on the Reynolds number at the mean aerodynamic chord.

The wing drag result comes from combining the zero lift contribution and the induced contribution for the cruise lift coefficient. These values form the wing portion of the total drag polar.

6.2.2 Fuselage Contribution

The fuselage drag is evaluated by finding the zero lift drag and the pressure drag at the cruise condition. The drag depends on the fuselage length, diameter, wetted area, and Reynolds number. The geometric inputs were taken from earlier design stages. The aerodynamic factors come from standard charts for skin friction and pressure drag. Table 2.2 lists the variables used in the fuselage drag calculation.

Symbol	Description	Value	Unit
L_{fus}	Fuselage length	8.80	m
Re_{fus}	Fuselage Reynolds number	3.9×10^7	-
S	Wing reference area	14.52	m^2
d_f	Maximum fuselage diameter	1.17	m
d_b	Base diameter	1.17	m
$S_{wet,fus}$	Fuselage wetted area	34.1	m^2
$C_{f,fus}$	Skin friction coefficient	0.002437	-
$C_{D,p}$	Pressure drag coefficient	9.15×10^{-4}	-
Q_w	Wing fuselage interference factor	1.00	-
$C_{D0,fus}$	Zero lift drag coefficient	0.00664	-

Table 2.2: Fuselage drag variables

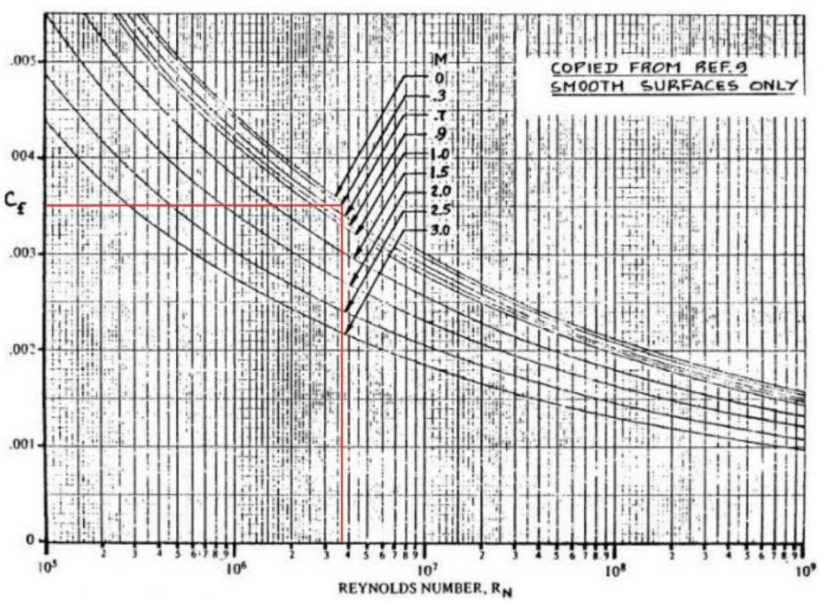

Figure 2.3: Skin-friction coefficient vs. Reynolds number for smooth surfaces

The skin friction coefficient uses the Reynolds number for the fuselage reference length. The pressure drag coefficient is adjusted for the fuselage shape and the base area. The wetted area is taken from the geometric model. The interference factor aligns the fuselage drag with the presence of the wing. The fuselage drag result provides one of the largest contributions to the aircraft zero lift drag at the cruise condition.

6.2.3 Empennage Contribution

The empennage drag is separated into the horizontal tail and vertical tail contributions. Each surface is evaluated using its own geometry, wetted area, and aerodynamic correction factors. The drag values depend on the Reynolds number, the tail planform shape, and the interference with the fuselage.

6.2.3.1 Horizontal Tail

The horizontal tail drag follows the same method used for the wing, with adjustments for tail geometry and surface placement. The drag depends on the horizontal tail area, aspect ratio, thickness ratio, and wetted area. Table 2.3.1 lists the variables used.

Symbol	Description	Value	Unit
S_{ht}	Horizontal tail area	4.08	m^2
A_{ht}	Horizontal tail aspect ratio	6.0	-
Re_{ht}	Horizontal tail Reynolds number	3.66×10^6	-
t/c_{ht}	Thickness to chord ratio	0.11	-
λ_{ht}	Taper ratio	0.40	-
$S_{wet,ht}$	Wetted area	8.364	m^2
$C_{f,ht}$	Skin friction coefficient	0.00355	-
FF_{ht}	Form factor	1.10	-
Q_{ht}	Interference factor	0.95	-
$C_{D0,ht}$	Zero lift drag coefficient	0.00214	-

Table 2.3: Horizontal tail drag variables

The horizontal tail contributes a small portion of the total drag. The aerodynamic behavior is influenced by the sweep, the thickness ratio, and the tail placement on the fuselage.

6.2.3.2 Vertical Tail

The vertical tail drag uses the same process without an induced drag term. The variables include the vertical tail area, aspect ratio, thickness ratio, and wetted area. Table 2.3.2 lists the variables used.

Symbol	Description	Value	Unit
S_{vt}	Vertical tail area	2.03	m^2
A_{vt}	Vertical tail aspect ratio	1.70	-
Re_{vt}	Vertical tail Reynolds number	4.95×10^6	-
t/c_{vt}	Thickness to chord ratio	0.10	-

λ_{vt}	Taper ratio	0.60	-
$S_{wet,vt}$	Wetted area	4.06	m^2
$C_{f,vt}$	Skin friction coefficient	0.00338	-
FF_{vt}	Form factor	1.20	-
Q_{vt}	Interference factor	0.95	-
$C_{D0,vt}$	Zero lift drag coefficient	0.00108	-

Table 2.4: Vertical tail drag variables

The vertical tail drag reflects the shape and location of the surface. Its drag contribution remains moderate and depends on the surface finish and leading edge sweep.

6.2.4 Landing Gear Contribution

The landing gear drag is evaluated at the cruise condition with the gear fixed in place. The drag depends on the frontal area of the gear, the shape of the struts, and the interaction with the fuselage and wing. The landing gear contributes to the zero lift drag and adds a steady profile drag component. Table 2.4 lists the variables used in the landing gear drag calculation.

Symbol	Description	Value	Unit
$\boldsymbol{A_{front,mg}}$	Main gear frontal area	0.090	m^2
$\boldsymbol{A_{front,ng}}$	Nose gear frontal area	0.045	m^2
$\boldsymbol{S_{wet,gear}}$	Wetted area of gear and struts	0.52	m^2
$\boldsymbol{C_{d,mg}}$	Main gear drag coefficients	1.15	-
$\boldsymbol{C_{d,ng}}$	Nose gear drag coefficients	0.90	-
$\boldsymbol{Q_{gear}}$	Interference factor	1.00	-
$\boldsymbol{C_{D0,gear}}$	Zero lift drag coefficient	0.0054	-

Table 2.5: Landing gear drag variables

The drag of the landing gear depends on the exposed wheels, the struts, and the mounting geometry. The interference factor accounts for the flow disruption caused by the gear location. The frontal area is obtained from the geometric model. The landing gear provides a significant fraction of the total zero lift drag for a fixed gear configuration.

6.2.5 Windshield Contribution

The windshield contributes to the zero lift drag through its curvature, surface finish, and junction with the fuselage. The drag depends on the frontal area of the glazing and the incidence of the flow at the cruise condition. The aerodynamic behavior is influenced by the smoothness of the transition between the windshield and the fuselage. Table 2.5 lists the variables used in the windshield drag calculation.

Symbol	Description	Value	Unit
$\boldsymbol{S_{ws}}$	Windshield frontal area	0.54	m^2

$C_{d,inc}$	Incidence drag coefficient	0.03	-
$C_{d,prof}$	Profile drag coefficient	0.03	-
$A_{fus,front}$	Forward fuselage reference area	1.08	m^2
$C_{D0,ws}$	Zero lift drag coefficient	0.00223	-

Table 2.6: Windshield drag variables

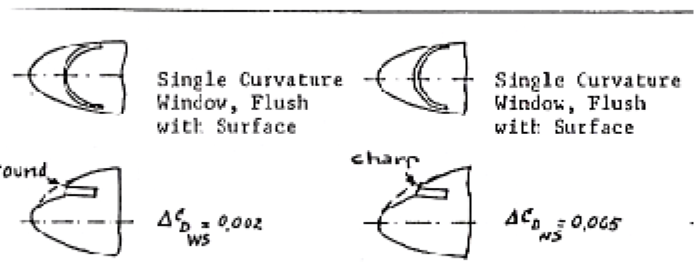

Figure 2.4: Windshield incidence

The windshield drag depends on its angle relative to the free stream, the curvature of the glazing, and the quality of the surface finish. The frontal area is taken from the geometric model. The incidence and profile coefficients are taken from standard aerodynamic data for light aircraft canopies. The windshield forms a modest part of the total zero lift drag.

6.2.6 Trim Contribution

The trim drag accounts for the aerodynamic forces required to balance the aircraft in steady flight. The horizontal tail provides the trimming force, which produces an additional drag component at the cruise condition. The trim drag depends on the tail surface area, the effective tail region, and the aerodynamic characteristics of the tail in the trimmed state. Table 2.6 lists the variables used in the trim drag calculation.

Symbol	Description	Value	Unit
S	Wing reference area	14.52	m^2
S_{ht}	Horizontal tail area	4.08	m^2
$\Lambda_{0.25,ht}$	Tail quarter chord sweep	0.0873	rad
$C_{L\alpha,ht}$	Horizontal tail lift gradient	4.69	1/rad
S_{ef}/S_{ht}	Effective tail area ratio	0.90	-
S_{ht}/S	Tail to wing area ratio	0.2810	-
$S_{ht,flap}$	Flapped tail area	1.02	m^2
$\Delta C_{D,trim}$	Trim drag increment	7.1×10^{-5}	-

Table 2.7: Trim drag variables

The trim drag arises from the pitching moment balance during steady flight. The tail generates a force that changes the drag of the aircraft. The variables listed above reflect the aerodynamic characteristics of the horizontal tail in the trimmed condition. This contribution is part of the total drag polar.

6.3 The Cl-Cd Graph

The drag contributions from the wing, fuselage, empennage, landing gear, windshield, and trim are combined to generate the aircraft drag polar. Each component adds to the total zero lift drag or to the lift dependent drag. The drag polar provides a more accurate representation of the aircraft performance than the initial estimates made during preliminary sizing.

The graph below shows the relationship between lift coefficient and drag coefficient for the full aircraft configuration. The individual section contributions are also included to show how each component affects the overall drag. This combined plot is used to assess the cruise condition and compare the updated drag values to the earlier design assumptions.

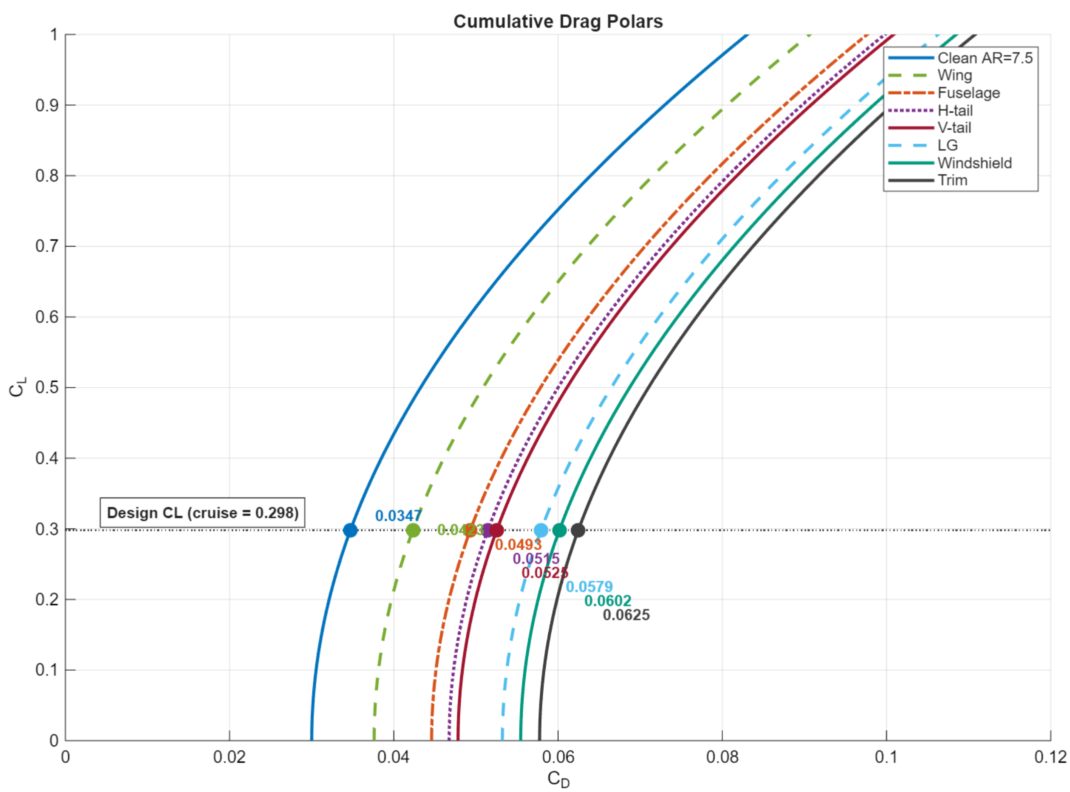

Figure 3.1: Cl-Cd graph for aircraft and component contributions

The refined drag polar developed in Assignment 5 therefore demonstrates significantly better aerodynamic performance than the preliminary Assignment 2 estimation, primarily due to improved parasite-drag modeling and slightly enhanced induced-drag characteristics. This confirmation validates the updated geometry and supports the aircraft's ability to meet cruise-efficiency and fuel-economy objectives more effectively than originally predicted.

6.4 Environmental Impacts

Several design changes improve the aerodynamic efficiency of the aircraft and reduce its environmental impact. Each improvement targets a source of drag or a feature that influences fuel use and noise.

One improvement is the refinement of the wingtip geometry. A small winglet or a tapered wingtip reduces lift induced drag and improves cruise performance without changing the primary wing structure. Another improvement is the addition of streamlined fairings around the fixed landing gear. These fairings lower the profile drag by reducing the exposed frontal area of the wheels and struts, which provides a direct benefit at the cruise condition.

The windshield and fuselage junction can also be improved by smoothing the transition between the two surfaces. A cleaner interface reduces local flow separation and lowers the drag generated at the cockpit area. Surface finish on the wing and tail surfaces is another factor. Smoother skins reduce the skin friction drag and support more efficient flight, which depends on material selection and manufacturing quality.

Finally, optimizing the cooling inlets at the nose reduces the form drag produced by the propulsion installation. A cleaner inlet shape improves the airflow entering the cowling and limits disturbances that increase drag. Together, these improvements lower the drag of the aircraft and support reduced fuel use and emissions.

6.5 Conceptual Design Review

This section evaluates whether the proposed aircraft configuration satisfies the operational requirements and design constraints identified in Assignments 1–4. Requirements describe what the aircraft must achieve to be considered successful. Constraints represent limitations that guided the design process, including physical, regulatory, structural, operational, and environmental boundaries.

Compliance is indicated as follows:

- C – Complies
- PC – Partially complies
- NC – Does not comply

Where partial or non-compliance exists, a corrective action or path to compliance is suggested.

6.5.1 Requirements Table

Requirement	Target Value	Compliance	Where Demonstrated / Comments
Range requirement	1600 km	PC	Assignment 2 cruise sizing showed design range ≈ 1382 km with full payload; compliant range achieved when payload reduced by one passenger. Path to compliance: increase fuel capacity or drastically improve aerodynamic efficiency.
Cruise speed	150 KTAS (77.2 m/s)	C	Assignment 3 wing design meets cruise CL = 0.298 at 77.2 m/s. Propulsion sizing matches required power loading.

Takeoff distance	410 m	C	Assignment 2 WP–WS diagram shows TO distance ≤ required using $CLmax_{TO} \approx 2.0$ with flaps.
Landing distance	410 m	C	Assignment 3 high-lift device sizing yields $C_{Lmax} \approx 2.4$. Landing distance is satisfied according to W/S sizing.
4 occupants + baggage	1 pilot + 3 passengers	PC	Assignment 2 MTOW analysis shows full 4-occupant payload creates range limitations. Aircraft operates safely but with reduced mission capability.
Stability and control	Meet static margin and controllability limits	C	Assignment 4 scissor plot shows intersection region exists; horizontal tail sized using V-bar satisfies stability and trim margins.
Short-field capability	Operations from small regional airports	C	Takeoff, landing, stall speed, power loading all meet GA short-field criteria in Assignments 2–3.

6.5.2 Constraint Table

Requirement	Description / Basis	Compliance	Where Demonstrated / Comments
Regulatory: FAR Part 23	Light aircraft structural, stability, and controllability requirements	C	Assignment 4 V-n diagram, ultimate load factor, and stability analyses all follow Part 23 methods.
Manufacturability	Simple fixed gear, unswept wing, composite fuselage	C	Configurations chosen in Assignments 1–3 avoid high sweep, complex mechanisms, retractable gear.
Weight limits (MTOW 1361 kg)	Structural weight must remain below GA class limits	PC	Assignment 2 weight estimation shows MTOW ~1361 kg is feasible but near upper GA boundary. Small margin remains.
Payload-range trade	Must stay within GA performance class	PC	With full payload, range reduces (Assignment 2). Path to compliance: optional extended-range tanks or lighter structures.
Engine availability	Must use certified piston engine	C	Lycoming IO-390 selected; meets power requirements (Assignment 2 engine sizing).
Aerodynamic efficiency	Must support low drag for cruise efficiency	C	Assignment 3 drag polars and CL/CD show good cruise performance at Re = 6.6×10^{6}.
Structural safety factor (1.5)	Required by regulations	C	Assignment 4 uses $N_{ult} = 1.5 \cdot N_{limit}$ with gust and maneuver loads.
Cabin size and ergonomics	4-seat layout with required width/height	C	Assignment 1 fuselage layout meets dimensional constraints and matches reference aircraft like DA40.

Takeoff rotation geometry	Must allow rotation without tail strike	C	Assignment 4 CG and gear placement ensure safe rotation envelope.
Budget / simplicity constraint	Avoid complex high-lift devices or retractable systems	C	Double-slotted flaps replaced with simpler Fowler flaps + slats; non-retractable gear maintained.
Sustainability / fuel economy	Must stay within typical 210-hp piston fuel consumption	PC	Cruise economy meets expectations, but range shortfall exists at max payload. Improvements possible through minor aerodynamic refinements.

The review shows that the proposed configuration meets the key requirements for cruise speed, takeoff and landing performance, stability, and controllability. The design also operates within the structural, regulatory, and geometric limits set for a four-seat general aviation aircraft. Our aircraft falls short in two categories that affect the sustainability constraint: the payload-range trade-off along with the MTOW. These can be addressed through modest aerodynamic refinements such as varied airfoil testing to determine most suitable mechanically and practically, small increases in fuel capacity by potentially decreasing baggage/cargo area to compensate for fuel needs, or mission-based payload adjustments (i.e. decreased payload based on mission requirements). Overall, the aircraft demonstrates a sound balance between performance, simplicity, and feasibility at this stage of conceptual design, with a clear path to resolve the remaining partial compliance items in later design iterations.

Appendix 1: Aircraft parameters table

Characteristic/Parameters	Value	Unit
Aircraft Wing		
Wingspan	10.43	m
Wing Area	14.52	m^2
Aspect ratio	7.5	
Wing Sweep Angle (LE)	0	degrees
Wing Sweep Angle (0.25c)	-3.3	degrees
Wing Sweep Angle (0.5c)	-6.5	degrees
Wing Sweep Angle (1c)	-12.9	degrees
Cabin Parameters		
Cabin Length	3.5	m
Cabin Usable Length	2.5	m
Tail Cone Length	3.2	m
Nose Cone Length	2.54	m
Cabin Height	1.27	m
Cabin Width	1.27	m
Aisle Width	0.25	m
Wall Thickness	0.04	m
Fineness	7.5	m
Nose Fineness	2.0	m
Tail Fineness	2.5	m
Chair Width	0.44	m
Chair Pitch	0.77	m
Over nose Angle	12	m
Overside Angle	36	m
Grazing Angle	32	m
Upward Angle	18	m
Divergence Angle	17	m
Flight Deck Length	1.1	m
Fuselage total Length	8.8	m
Fuselage Width	1.67	m
Fuselage Height	1.52	m
Weights and Loading		
Empty Weight	925	Kg
Maximum Take-off Weight	1361	Kg
Aircraft Weight (MTOW x g)	13345	N
Wing Loading W/S	920	N/m^2
Power Loading W/P (based on 210 hp)	0.093	N/W
Estimated Thrust-to-weight at take-off	0.21	
Fuel mass (available/full tanks)	258	kg

Payload Mass (full fuel)	263	kg
Useful load	521	kg
Performance Parameters		
Cruise Altitude	2440	m
Cruise Speed	77.2	m/s
Cruise lift coefficient	0.293	
Maximum lift coefficient (take-off)	2.0	
Maximum lift coefficient (landing)	2.2	
Take-off ground roll	410	m
Landing Distance	450	m
Range	1382	km

Appendix 2: Aircraft technical drawings

Drawings are on the following page

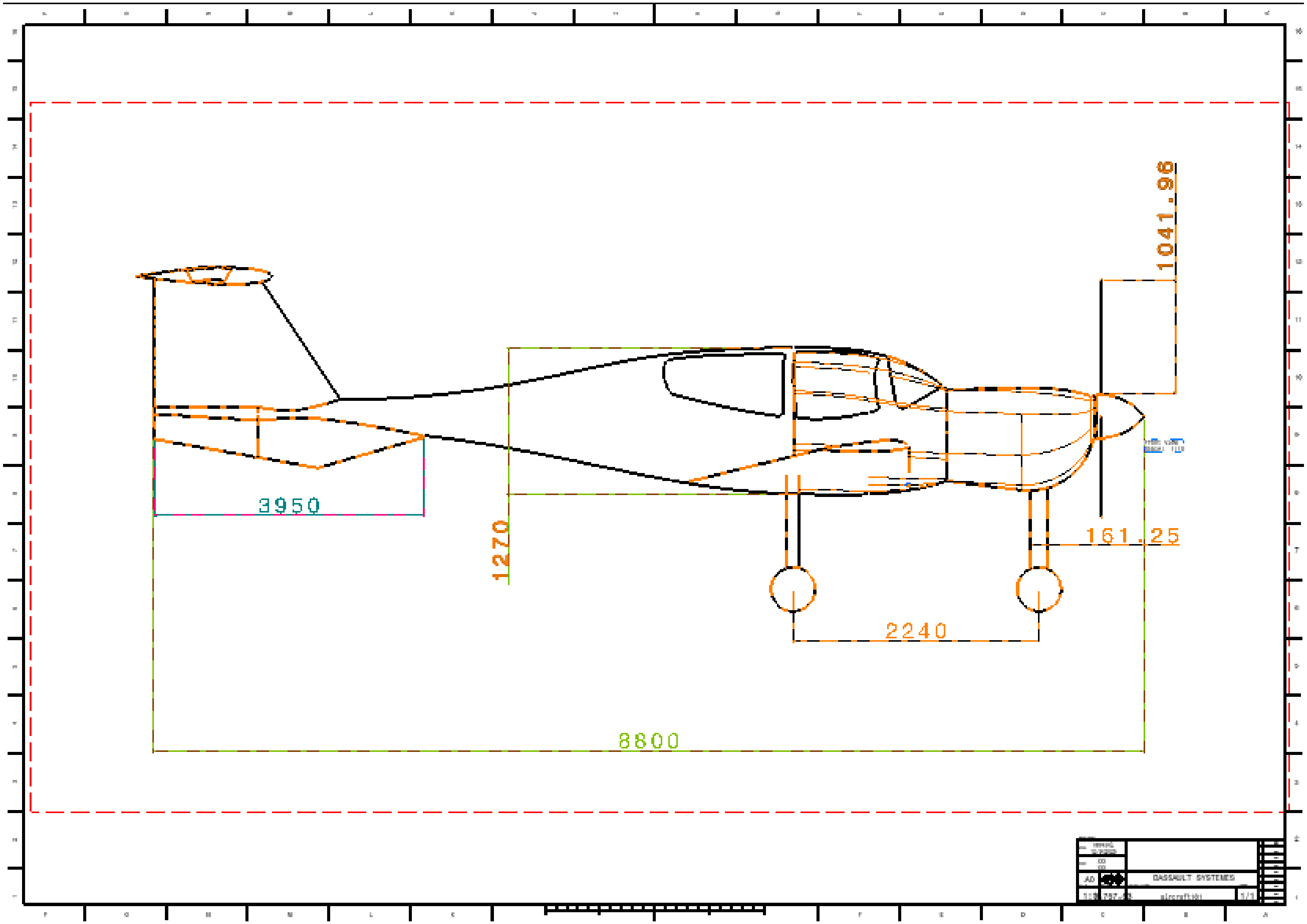
1041.96
3950
1270
161.25
2240
8800
DASSAULT SYSTEMES

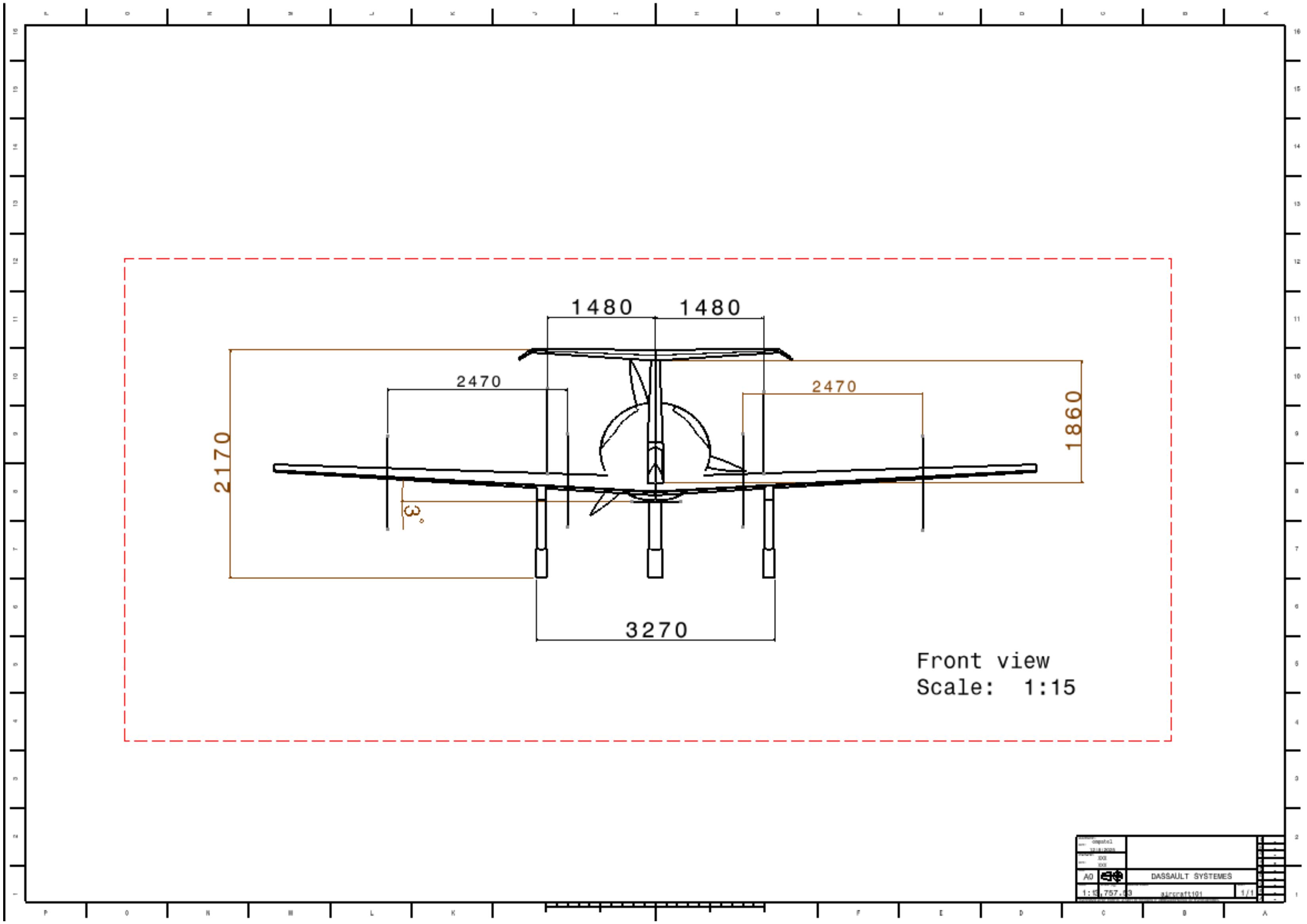
1480
1480
2470
2470
1860
2170
3°
3270
Front view
Scale: 1:15
DASSAULT SYSTEMES

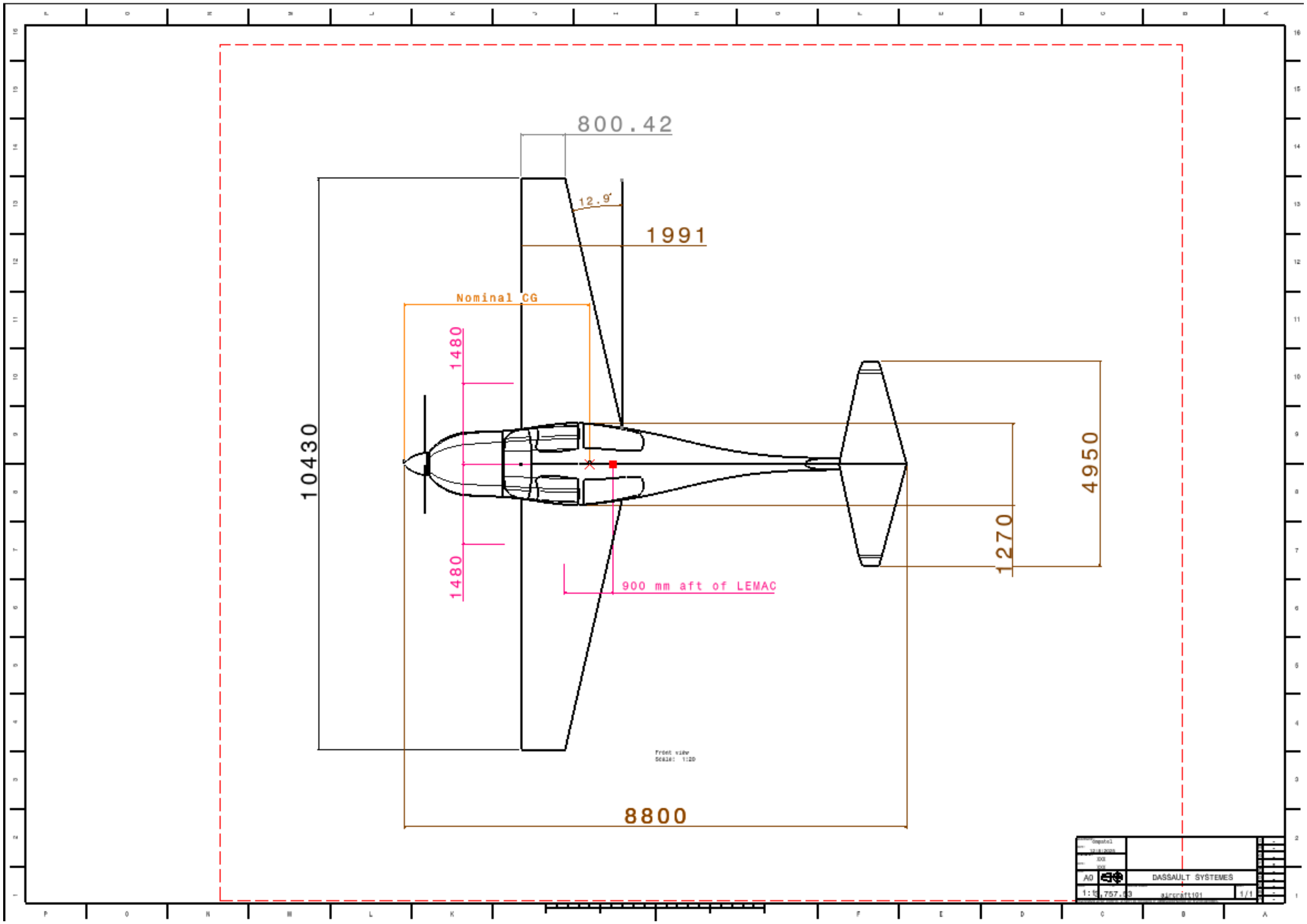
800.42
12.9°
1991
Nominal CG
1480
1480
10430
4950
1270
900 mm aft of LEMAC
8800
DASSAULT SYSTEMES

Appendix 3: W/P – W/S Diagram

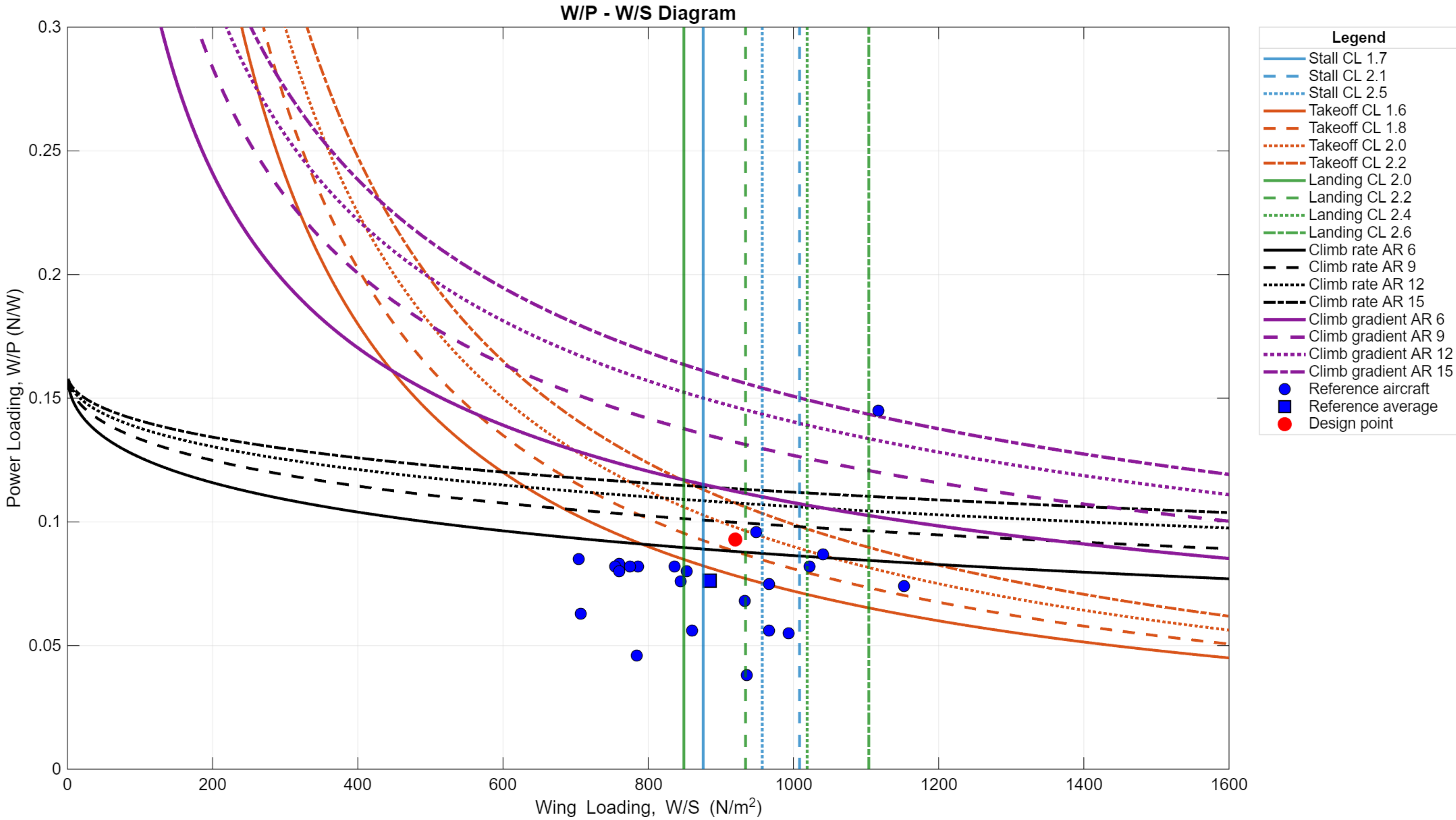

Appendix 4: Table of Reference Aircraft

Aircraft Name	A/C Type	Payload (kg)	Range (km)	Cruise Speed (m/s)	Cruise Altitude (m)	Length (m)	Wingspan (m)	MTOW (kg)	Take off Length (sea level) (m)	Landing field length at max landing weight (m)
101	GA	435	1600	80	2438	8	11	1361	408	408
Cessna 182 Skylane	GA	719	1722	75	2438	8.84	11	1406	461	411
Cirrus SR20	GA	664	1704	80	2438	8	12	1386	620	650
Mooney M20J	GA	540	1852	80	2286	7.5	7.52	1243	472	470
Diamond DA40 NG	GA	759	1741	79	3658	8.13	11.9	1310	370	343
Cessna 172 Skyhawk	GA	418	1204	63	914	8.28	11	1158	509	407
Piper Archer LX	GA	316	963	66	1524	7.32	10.8	1158	506	472
Beechcraft Bonanza G36	GA	788	1704	90	1829	8.38	10.21	1656	809	762
Diamond DA42 Twin Star	GA	971	1760	80	1829	9.6	13.42	2000	955	914
Piper PA-28R Arrow	GA	408	1620	72	1524	7.32	10.7	1134	420	396
Piper Cherokee 180	GA	395	2100	64	1524	7.32	10.7	1089	444	395
Piper Arrow III	GA	522	1750	70	1524	7.32	10.7	1247	514	488

Piper Comanche 250	GA	558	1760	77	1829	8.63	11.15	1316	521	488
Cessna Cardinal 177RG	GA	576	1480	75	1524	7.93	11.28	1270	511	488
Cessna 210 Centurion	GA	959	1700	82	1829	8.86	11.2	1725	701	650
Beechcraft Musketeer A23	GA	431	1950	62	1524	7.82	9.75	1111	463	427
Beechcraft Sierra C24R	GA	581	1150	72	1829	8.38	10.21	1316	542	503
Mooney M20F Executive	GA	508	1425	80	2286	7.5	7.52	1243	503	470
Mooney M20F Ovation	GA	763	1480	87	3048	8	9.98	1527	686	640
Socata TB-20 Trinidad	GA	601	1480	77	2438	7.82	11.71	1401	585	548
Robin DR400/180	GA	372	1667	66	1524	7.02	8.72	1089	457	430
Piper PA-28-235 Dakota	GA	612	1300	72	1524	7.5	10.97	1315	532	503
Piper PA-28R-201 Arrow IV	GA	522	1440	72	1524	7.32	10.7	1247	526	488
Piper PA-32 Cherokee SIx	GA	735	1612	73	1829	9.75	11.02	1542	543	503
				AVERAGE	1943	8.02	10.63	1343.8		